КРИСТАЛЛОГРАФИЯ

SOVIET PHYSICS

Crystallography

VOLUME 2 NUMBER 2

A Translation

of the journal

Crystallography

of the

Academy of Sciences of the USSR

(RUSSIAN ORIGINAL VOL. 2, NO. 2)

Published by the

AMERICAN INSTITUTE OF PHYSICS

INCORPORATED

SOVIET PHYSICS

Crystallography

A translation of the journal "Crystallography" of the Academy of Sciences of the USSR

A publication of the
AMERICAN INSTITUTE OF PHYSICS

Governing Board

FREDERICK SEITZ, *Chairman*

Members

WALTER S. BAIRD
JESSE W. BEAMS
RAYMOND T. BIRGE
R. H. BOLT
J. W. BUCHTA
J. H. DILLON
VERNET E. EATON
HERBERT A. ERF
IRVINE C. GARDNER
S. A. GOUDSMIT
C. KITTEL
WINSTON E. KOCK
R. BRUCE LINDSAY
WALTER C. MICHELS
G. E. PAKE
R. RONALD PALMER
JOSEPH B. PLATT
RALPH A. SAWYER
H. D. SMYTH
JOHN STRONG
GEORGE E. UHLENBECK

Officers and Staff

ELMER HUTCHISSON
Director
HENRY A. BARTON
Associate Director
WALLACE WATERFALL
Secretary and Treasurer
EDWARD P. TOBER
Mgr., Production and Distribution
THEODORE VORBURGER
Advertising Manager
RUTH F. BRYANS
Publication Manager
KATHRYN SETZE
Assistant Treasurer
ALICE MASTROPIETRO
Circulation Manager
EUGENE H. KONE
Director of Public Relations

American Institute of Physics Advisory Board on Russian Translations

ROBERT T. BEYER, *Chairman*

FREEMAN DYSON, DWIGHT GRAY, MORTON HAMERMESH, DAVID HARKER, VLADIMIR ROJANSKY, HARRISON F. WEAVER

Advisory Editor, Soviet Physics – Crystallography: DAVID HARKER, Protein Structure Project, Polytechnic Institute of Brooklyn, Brooklyn 2, New York

"Soviet Physics – Crystallography" is published by the American Institute of Physics, with the cooperation of the American Crystallographic Association, for the purpose of making available in English reports of current Soviet research in crystallography as contained in the journal "Crystallography" of the Academy of Sciences of the USSR. The translation begins with the 1957 issues.

Transliteration of the names of Russian authors follows the system employed by the Library of Congress.

This translating and publishing project was undertaken by the Institute in the conviction that dissemination of the results of research everywhere in the world is invaluable to the advancement of science. The National Science Foundation of the United States encouraged the project initially and is supporting it in large part by a grant. Translation and printing are being handled by Consultants Bureau, Inc.

The American Institute of Physics and its translators propose to translate faithfully all of the scientific material in the "Crystallographic Journal of the Academy of Sciences of the USSR" appearing after January 1, 1957. The views expressed in the translated material, therefore, are intended to be those expressed by the original authors, and not those of the translators nor of the American Institute of Physics.

One volume is published annually. The volume numbering coincides with that of the original Russian journal.

Subscription Prices:

Per year (6 issues), starting with Vol. 2, No. 1

General: United States and Canada	$25.00
Elsewhere	27.00
Libraries of non-profit academic institutions:	
United States and Canada	10.00
Elsewhere	12.00
Back numbers, all issues	3.00

Subscriptions should be addressed to the American Institute of Physics, 335 East 45th Street, New York 17, New York.

Copyright by American Institute of Physics 1958

SOVIET PHYSICS

Crystallography

VOLUME 2, NUMBER 2 MARCH-APRIL, 1957

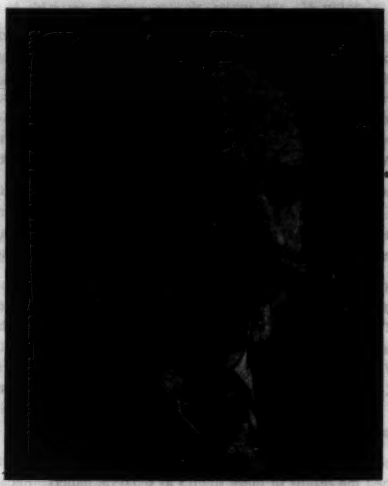

MEMORIAL TO VIKTOR IVANOVICH MIKHEEV

Viktor Ivanovich Mikheev, one of our leading crystallographers, died suddenly at the age of 45 on December 12, 1956, while working with his students at the Leningrad Institute of Mines.

V. I. Mikheev was born on February 11, 1912 in Petrograd, to the family of a printer. From 1918 to 1928 he attended a secondary school. In 1928 he entered the Leningrad Institute of Mines, from which he was graduated in 1932.

At the Institute, Viktor Ivanovich showed a very lively interest in crystallography, which was taught then by the well known professor Anatolii Kapitonovich Boldyrev. Boldyrev recognized his student's talents and introduced him to research work in the department. This led to Mikheev's specialization in crystallography.

After graduation, Mikheev remained at the Institute as a graduate student and laboratory assistant in crystallography.

In March of 1936, the young scientist successfully defended his dissertation on "Standard Powder Photographs of Refractory Minerals," and was awarded the degree of candidate of geological and mineralogical sciences. In the same year he became a lecturer in the department of crystallography and gave courses in

general and structural crystallography. Except for the war years, his entire scientific and pedagogical career was connected with the Institute of Mines, until death found him at his post.

In September of 1939 came war with Finland. Victor Ivanovich was called up, and participated in action as commander of a detachment of army engineers. After demobilization, in November of 1940, he returned to the Institute of Mines, but for a short time only. In June of 1941 German Fascists attacked our land, and Mikheev was again called into the army. He saw action on the Leningrad and Karelian fronts and in the Esthonian SSR.

When war ended in April of 1946, Mikheev returned to the Institute to continue his scientific and pedagogical work as a lecturer.

From 1936 he was in charge of the x-ray laboratory at the Institute of Mines. During the war and the blockade of Leningrad this laboratory had been completely destroyed. It required exceptional energy on Mikheev's part to create it anew.

Mikheev's scientific activity began when he was a student. His first work, on the "Causes of layering in oversaturated solutions," was published in the Proceedings of the Mineralogical Society in 1930. He was eighteen at this time. Since then he has published over 75 scientific papers. In addition he wrote 56 reports on individual minerals and mineral groups for various scientific-industrial organizations. The majority of these works were on x-ray investigation of minerals. Mikheev developed his own methods of investigation of minerals and chemical compounds. Since x-ray diffraction data give the most important constants of a substance, he, together with his teacher, A. K. Boldyrev, used these data as the basis for a new determinative method.

The Debye-Scherrer method was selected as the most suitable for analyzing mixtures and identifying minerals. The coincidence of the lines on a powder photograph of an unknown mineral with those of a known one on the reference photograph identifies the unknown or indicates its presence in a mixture. Coincidence of lines is established by comparison of interplanar distances computed from the photographs.

In order to make this method practical, it was necessary to collect and arrange in definite order the data computed from powder photographs of known minerals. This was accomplished in the "Key for the determination of minerals by x-rays." The first part of this work contains data for 142 minerals; the second, for 146. Shortly before his death, Mikheev sent to press a large third part with data for 905 minerals. He also prepared for publication a fourth part of the "Key." Mikheev was the most active participant in this work. The title page of the first part of the "Key" bears his name as co-author with A. K. Boldyrev; the second part was prepared by him with the help of V. N. Dubinina; the third and main part is his own entirely; and in the preparation of the fourth part he was assisted by E. P. Sal'dau.

While engaged in the enormous task of preparing the "Key," Mikheev made x-ray analyses of minerals and mineral groups and published the results of these studies as separate papers. Because of his labors, x-ray analysis of minerals is widely used in our country, and the publication of the fourth part of the "Key" will undoubtedly greatly increase the usefulness of the method.

Mikheev's investigation of arseno-sulvanite, a new mineral discovered by A. G. Betekhtin, deserves notice. This work will occupy an honored place in the history of Soviet crystallography, since it contains one of the earliest determinations of fine structure made in our country.

Beginning in 1950, a series of articles by Mikheev devoted to the problem of crystal homology began to appear in crystallographic and mineralogical journals. This research resulted in a large monograph, "Crystal Homology," which Mikheev defended brilliantly as a doctoral dissertation in 1952. The Academy of Science of the USSR honored this work by awarding the E. S. Fedorov Prize to its author.

In his work on homology, in addition to the usual elements of symmetry, Mikheev introduces planes, axes and inversion axes of homology. A plane of homology is a plane of oblique reflection. An axis of homology is an axis of circular or elliptic rotation. Thus the elements of symmetry are only special cases of the elements of homology. Mikheev's elements of homology are intimately related to Fedorov's affine deformations (shifting and stretching). The complete three-dimensional combinations of the elements of homology, or classes of homology, are derived from the 32 symmetry classes by the operation of shifting or stretching in oblique, parallel or perpendicular direction with respect to the symmetry elements.

As the result of solution of this problem, Mikheev derived 218 classes of homology. One hundred and eighty six of these classes are in the systems of lower symmetry. Therefore, classes of homology permit a much more exact classification of crystals with low symmetry. With their aid the packing of ellipsoids in parallel position and the symmetry of the resulting structure were derived for the first time. Such packing of ellipsoids is characteristic of crystals of low symmetry. The science of homology gave a practical solution of the problem of indexing powder photographs of substances of low symmetry. The new method of indexing takes account of the multiplicity of lines on a powder photograph for crystals of low symmetry as compared with those of cubic and hexagonal crystals.

Enough has been said to make clear the exceptional depth and orginality of Mikheev's ideas, which have opened completely new and wide horizons in crystallography.

In 1953.V. I. Mikheev was appointed Professor of Crystallography. In recent years he published a number of remarkable x-ray studies of chlorites, garnets, spinels, micas, etc., in which important relationships are established,permitting precise determination of the components of an isomorphous series.

Mikheev's works are widely recognized among Soviet mineralogists and crystallographers. His "Key for the determination of minerals by x-rays" is well known abroad as well. Mikheev was on the editorial board of "Crystallography" and the "Proceedings of the All-Union Mineralogical Society," and he edited the collection entitled "Crystallography" published by the Leningrad Institute of Mines.

Mikheev was a man of high principles, and exacting both in scientific work and in life.

While still a student, Mikheev joined the Komsomol; and in 1940, while in the Red Army, he was accepted into membership in the Soviet Communist Party.

V. I. Mikheev was awarded the orders of "The Red Star" and "Merit" and the medals "For Valor," "For Victory in the National War," "For the Defense of Leningrad" and "For Devotion to Work."

The memory of Viktor Ivanovich Mikheev will live in the hearts of those who knew him.

I. I. Shafranovskii and N. N. Stulov

SYMMETRY OF SCALARS, VECTORS, AND TENSORS OF SECOND RANK

I. S. Zheludev

The symmetry of polar and axial tensors is determined on the basis of the superposition of the elements of their symmetric and antisymmetric parts. The results obtained in this way agree with the corresponding ones for those cases which have previously been treated analytically. A new symmetry group is found for an antisymmetric axial tensor; it is shown that this tensor defines a polar vector and has its symmetry $(\infty \cdot m)$. A new symmetry group $\overline{4}$ is found, obtained as a result of the superposition of the symmetry elements of a polar and axial tensor of definite form. It is established that the number of groups of polar and axial tensors and their combinations is 17.

1. INTRODUCTION

In mathematics and physics (particularly in crystallophysics) one often has to deal with scalar, vector and tensor quantities. In treating these quantities most attention is usually paid to scalars of the first kind (or simply, scalars), polar vectors (or simply, vectors) and polar tensors (or simply, tensors), and less to scalars of the second kind (pseudoscalars), axial vectors (pseudovectors), and axial tensors (pseudotensors).

Without going into detail in examples of scalars, vectors and tensors, we note that one may think of a scalar by considering, for instance, overall (hydrostatic) compression, which is characterized by a single number; one may think of a pseudoscalar by considering equal rotation of the plane of polarization for all directions; one may think of a polar vector by considering the displacement of a body under the influence of a force; of an axial vector by considering the rotation of a body under the action of a force couple; of a polar tensor by considering the stressed state of a solid under the action of two equal but opposite forces (tension or compression); of an axial tensor by considering the stressed state of a solid under the action of two equal force couples whose moments are equal but opposite (twisting).

In tensor calculus scalar and vector quantities are usually treated as tensors of zeroth and first rank, respectively. The difference between scalars and pseudoscalars, polar and axial vectors, and polar and axial tensors is expressed analytically by the fact that their components transform differently on going from one coordinate system to another. The fundamental characteristics of polar and axial tensors of the second, first, and zeroth rank are shown in Table 1.

In the transformation formulas for pseudoscalars, axial vectors, and axial tensors (see Table 1) the positive sign on the cosines c_{ik} of the angles between the new and old axes is taken when the old and new coordinate system have the same sign, being either left or right handed systems, and the minus sign is taken when the sign of the coordinate system changes (a left handed system is transformed to a right handed one, or vice versa).

2. SYMMETRY OF TENSORS OF SECOND RANK*

By treating scalars and vectors as special cases of tensors of second rank, we can define their symmetry in the same way as for tensors. A tensor is usually said to have one or another symmetry [1-3] if the application

* In the present work we consider only affine orthogonal tensors.

TABLE 1

Fundamental Characteristics of Scalars, Vectors, and Tensors of Second Rank

Terminology	Notation	Number of independent coefficients	Transformation formulas for the components	Tensor rank
Scalar	a	1	$a \equiv a$	0
Pseudoscalar	A	1	$A = \pm A$	0
Polar vector	$\mathfrak{a}$	3	$a_i = c_{ik}a'_k$ $a'_i = c_{ki}a_k$	1
Axial vector	$\mathfrak{A}$	3	$A_i = \pm\, c_{ik}A'_k$ $A'_i = \pm\, c_{ki}A_k$	1
Polar Tensor	(a)	9	$a_{ik} = c_{il}c_{km}a'_{lm}$ $a'_{ik} = c_{li}c_{mk}a_{lm}$	2
Axial tensor	(A)	9	$A_{ik} = \pm\, c_{il}c_{km}A'_{lm}$ $A'_{ik} = \pm\, c_{li}c_{mk}A_{lm}$	2

of the appropriate symmetry transformation transforms all of its components into themselves. The symmetry of polar and axial tensors of second rank has been treated by Shubnikov [1]. We here propose a new method for determining tensor symmetries. This method, it seem to us, is quite simple and clear, and leads to more precision in the previously obtained results on symmetries of tensors of second rank, as well as to several new results.

As is well known, the symmetry of a symmetric polar tensor

$$\begin{vmatrix} a_{11} & a_{12} & a_{13} \\ a_{12} & a_{22} & a_{23} \\ a_{13} & a_{23} & a_{33} \end{vmatrix} \qquad (1)$$

is determined by the number of its different diagonal components. The number of these different components can always be found, since an arbitrary symmetric tensor can be transformed by a coordinate transformation to one of the following three diagonal forms:

$$\begin{vmatrix} a_{11} & 0 & 0 \\ 0 & a_{11} & 0 \\ 0 & 0 & a_{11} \end{vmatrix}; \quad \begin{vmatrix} a'_{11} & 0 & 0 \\ 0 & a'_{11} & 0 \\ 0 & 0 & a'_{33} \end{vmatrix}; \quad \begin{vmatrix} a'_{11} & 0 & 0 \\ 0 & a'_{22} & 0 \\ 0 & 0 & a'_{33} \end{vmatrix}. \qquad (2)$$

The coordinate system in which a symmetric tensor appears in diagonal form is called the principal coordinate system.

It turns out that in the case in which all the diagonal elements are equal ($a_{11}=a_{22}=a_{33}$), a symmetric polar tensor has the symmetry of one of the limiting point symmetry groups, namely that of a sphere with symmetry planes, which Shubnikov denotes $\infty/\infty\cdot m$. This tensor is completely specified by a single number, its form is independent of the coordinate system, and any symmetry operation can be performed on it, so that it possesses the symmetry of a scalar $\infty/\infty\cdot m$. When two of the diagonal elements are equal (for instance $a_{11}=a_{22}\neq a_{33}$), the tensor possesses the symmetry $m\cdot\infty : m$, or that of an ellipsoid of revolution; when the three diagonal elements are unequal, the symmetry is $m\cdot 2 : m$ or that of an ellipsoid with three unequal axes. It is interesting to note that from the point of view of symmetry it is irrelevant if one of the diagonal elements of a symmetric polar tensor vanishes (that is, if the tensor is not complete).

An antisymmetric polar tensor ($a_{ik} = -a_{ki}$)

$$\begin{vmatrix} 0 & -a_{12} & a_{13} \\ a_{12} & 0 & -a_{23} \\ -a_{13} & a_{23} & 0 \end{vmatrix}, \tag{3}$$

defines an axial vector, as is well know, which possesses the symmetry $\infty : m$ (an axis of order infinity and a symmetry plane perpendicular to it). A geometric model of an axial vector, according to Shubnikov, is a directed line element. According to a theorem of Shubnikov [1], it is always possible to perform a coordinate transformation which will bring an antisymmetric tensor into the simplest form:

$$\begin{vmatrix} 0 & -a_{12} & 0 \\ a_{12} & 0 & 0 \\ 0 & 0 & 0 \end{vmatrix}. \tag{4}$$

In this case the X_3 axis coincides with the ∞ axis, and we shall call this the principal axis of the antisymmetric polar tensor (or axial vector).

A general polar tensor (asymmetric) can always be resolved into the sum of two tensors, one of which is symmetric and the other antisymmetric. One may assume that the symmetry of a general tensor is given by the superposition of the symmetry elements of its symmetric and antisymmetric parts (the Curie symmetry principle). As will be shown later, this assumption is valid even if only because the results obtained by the method suggested are not in contradiction with those obtained analytically (for those cases which have been previously considered).

Let us determine the symmetry of an asymmetric tensor by proceeding in the following way. First, by a coordinate transformation, let us bring the symmetric part of the tensor into the form given by its principal coordinate system* and its antisymmetric part to the simplest form given by (4). In doing this, the following two cases may arise: 1) the principal axis of the axial vector (antisymmetric part of the tensor) coincides with one of the principal axes of the symmetric part of the tensor, and 2) two such axes do not coincide. In both cases the symmetry of the asymmetric tensor is defined as the largest common subgroup of the symmetry groups of both parts for the given distribution of the symmetry elements of the groups $\infty/\infty \cdot m$, $m \cdot \infty : m$ or $m \cdot 2 : m$ and the group $\infty : m$.

For the first case, the forms of the asymmetric tensor obtained as a result of adding the transformed symmetric and antisymmetric parts (which we shall call canonical forms) are

$$\begin{vmatrix} a_{11} & -a_{12} & 0 \\ a_{12} & a_{11} & 0 \\ 0 & 0 & a_{11} \end{vmatrix}; \quad \begin{vmatrix} a_{11} & -a_{12} & 0 \\ a_{12} & a_{11} & 0 \\ 0 & 0 & a_{33} \end{vmatrix}; \quad \begin{vmatrix} a_{11} & -a_{12} & 0 \\ a_{12} & a_{22} & 0 \\ 0 & 0 & a_{33} \end{vmatrix}; \quad \begin{vmatrix} a_{11} & -a_{12} & 0 \\ a_{12} & a_{22} & 0 \\ 0 & 0 & a_{33} \end{vmatrix}.$$

It is easily seen that the symmetry groups of these tensors, according to the Curie symmetry principle, are $\infty : m$; $\infty : m$; $2 : m$ and $2 : m$, respectively.

In the second case we shall consider the tensor to be in canonical form when it is written in the principal coordinate system of the symmetric part. It is clear that in this case the axial vector will not be written in simplest form. Examples of canonical forms of such tensors are

$$\begin{vmatrix} a_{11} & -a_{12} & a_{13} \\ a_{12} & a_{11} & -a_{23} \\ -a_{13} & a_{23} & a_{33} \end{vmatrix}; \qquad \begin{vmatrix} a_{11} & -a_{12} & a_{13} \\ a_{12} & a_{22} & -a_{23} \\ -a_{13} & a_{23} & a_{33} \end{vmatrix}.$$

In this case the general symmetry element of a symmetric tensor and an axial vector will be just the symmetry center, so that these tensors belong to the symmetry group 2.

*We note that any arbitrary coordinate system may be taken as the principal one of a tensor for which $a_{11}=a_{22}=a_{33}$ (that is, a scalar), whereas for a tensor for which $a_{11}=a_{22} \neq a_{33}$, only the direction of the X_3 axis is fixed.

TABLE 2

Canonical Forms and Symmetries of Polar Tensors of Second Rank

Terminology	Canonical form of tensor	Tensor symmetry	Orientation of the axes
Scalar	$\begin{matrix} a_{11} & 0 & 0 \\ 0 & a_{11} & 0 \\ 0 & 0 & a_{11} \end{matrix}$	$\infty/\infty \cdot m$	Axes arbitrarily oriented
Polar tensor	$\begin{matrix} a_{12} & 0 & 0 \\ 0 & a_{11} & 0 \\ 0 & 0 & a_{33} \end{matrix}$	$m \cdot \infty : m$	The ∞ axis coincides with the X_3 axis
	$\begin{matrix} a_{11} & 0 & 0 \\ 0 & a_{22} & 0 \\ 0 & 0 & a_{33} \end{matrix}$	$m \cdot 2 : m$	The 2 axis coincides with the X_1, X_2, X_3 axes
Axial vector	$\begin{matrix} 0 & -a_{12} & 0 \\ a_{12} & 0 & 0 \\ 0 & 0 & 0 \end{matrix}$	$\infty : m$	The ∞ axis of the axial vector coincides with the X_3 axis
Combination of scalar and axial vector	$\begin{matrix} a_{11} & -a_{12} & 0 \\ a_{12} & a_{11} & 0 \\ 0 & 0 & a_{11} \end{matrix}$		The ∞ axis of the axial vector coincides with the X_3 axis
Combination of polar tensor and axial vector	$\begin{matrix} a_{11} & -a_{12} & 0 \\ a_{12} & a_{11} & 0 \\ 0 & 0 & a_{33} \end{matrix}$	$\infty : m$	The ∞ axes of the polar tensor and of the axial vector coincide with the X_3 axis
	$\begin{matrix} a_{11} & -a_{12} & 0 \\ a_{12} & a_{22} & 0 \\ 0 & 0 & a_{33} \end{matrix}$	$2 : m$	The ∞ axis of the polar tensor coincides with the X_1 axis; the ∞ axis of the axial vector coincides with the X_3 axis
	$\begin{matrix} a_{11} & -a_{12} & 0 \\ a_{12} & a_{22} & 0 \\ 0 & 0 & a_{33} \end{matrix}$		The 2 axes of the polar tensor coincide with the X_1, X_2, X_3 axes; the ∞ axis of the axial vector coincides with X_3 axis
	$\begin{matrix} a_{11} & -a_{12} & a_{13} \\ a_{12} & a_{11} & -a_{23} \\ -a_{13} & a_{23} & a_{33} \end{matrix}$	$\bar{2}$	The ∞ axis of the polar tensor coincides with the X_3 axis; the ∞ axis of the axial vector coincides with no other axis
	$\begin{matrix} a_{11} & -a_{12} & a_{13} \\ a_{12} & a_{22} & -a_{23} \\ -a_{13} & a_{23} & a_{33} \end{matrix}$		The 2 axes of the polar tensor coincide with the X_1, X_2, X_3 axes; the ∞ axis of the axial vector coincides with no other axis

These considerations show that the determination of the symmetry of a general polar tensor reduces to the determination of the symmetry of a scalar (which is a special case of a symmetric tensor), a symmetric tensor (which is all that should properly be called a tensor), and an axial vector, plus the determination of the symmetry of their combinations. The total number of symmetry groups for a polar tensor is six: $\infty/\infty \cdot m$; $m \cdot \infty : m$; $m \cdot 2 : m$; $\infty : m$; $2 : m$; $\bar{2}$. All these groups are centrally symmetric. The canonical forms and symmetries of polar tensors of second rank are presented in Table 2.

3. SYMMETRY OF AXIAL TENSORS OF SECOND RANK

As has been mentioned above, the components of an axial tensor $\{A_{ik}\}$ transform according to

$$A_{ik} = \pm c_{il}\ c_{km}\ A'_{lm}, \qquad (5)$$

which coincides with the transformation equation for a polar tensor

$$a_{ik} = c_{il}\ c_{mk}\ a'_{lm}$$

for the case in which the coordinate transformation reduces to a single proper rotation (or, reflections are excluded). In dealing with the symmetry of polar tensors, we used several theorems of tensor algebra (the possibility of bringing a symmetric tensor to diagonal form and an antisymmetric tensor to simplest form; the possibility of resolving a general tensor into its symmetric and antisymmetric parts, etc.). It should be noted that there is no loss of generality in these theorems if the only coordinate transformations we consider are those which are connected to proper rotations. We may thus assert that by using only proper rotations (when the transformation formulas for polar and axial tensors are identical) a symmetric axial tensor can be brought to diagonal form, an antisymmetric one to simplest form, and a general axial tensor (asymmetric) can be resolved into its symmetric and antisymmetric parts.

As has been shown by Shubnikov [1], from the point of view of symmetry there exist four different kinds of axial tensors with only diagonal nonzero components (and therefore symmetric), namely

$$\begin{vmatrix} A_{11} & 0 & 0 \\ 0 & A_{11} & 0 \\ 0 & 0 & A_{11} \end{vmatrix}, \quad \begin{vmatrix} A_{11} & 0 & 0 \\ 0 & A_{11} & 0 \\ 0 & 0 & A_{33} \end{vmatrix}, \quad \begin{vmatrix} A_{11} & 0 & 0 \\ 0 & A_{22} & 0 \\ 0 & 0 & A_{33} \end{vmatrix}, \quad \begin{vmatrix} A_{11} & 0 & 0 \\ 0 & -A_{11} & 0 \\ 0 & 0 & 0 \end{vmatrix},$$

and these belong to the symmetry groups ∞/∞; $\infty:2$; $2:2$ and $\bar{4}\cdot m$, respectively. A tensor, all of whose diagonal elements are equal, has the same form in all coordinate systems. The forbidden symmetry operations for this tensor are any inversions (according to its symmetry formula). Thus this tensor, since it is defined by a single number and changes its sign on reflection, has all the properties of a pseudoscalar, which means that a pseudoscalar has the symmetry ∞/∞. The remaining three symmetric tensors may properly be called axial tensors.

Geometric models of these tensors are a sphere with its radii twisted equally in a given direction (∞/∞), a sphere twisted equally along two mutually perpendicular directions and differently along the third ($\infty:2$), a sphere twisted unequally along three mutually perpendicular directions ($2:2$), and a sphere twisted equally along two mutually perpendicular directions, but in the opposite sense ($\bar{4}\cdot m$).

Let us go on to a determination of the symmetry of an antisymmetric axial tensor. Since the proper symmetry of a tensor (which is what we are discussing in this paper) is independent of the coordinate system in which it is represented, we shall consider an antisymmetric axial tensor in its simplest form:

$$\begin{vmatrix} 0 & -A_{12} & 0 \\ A_{12} & 0 & 0 \\ 0 & 0 & 0 \end{vmatrix}. \tag{6}$$

We shall prove that this tensor possesses the symmetry $\infty\cdot m$, or that of a polar vector [2]. It is not necessary to prove that this tensor has a symmetry axis ∞ coinciding with the X_3 axis, since the antisymmetric polar tensor of similar form (axial vector) has the same kind of a symmetry axis, and under proper rotations about the X_3 axis (which is the kind of rotation that corresponds to the ∞ axis) the transformation laws for axial and polar tensors are the same. It is easily verified that the tensor shown in (6) has no symmetry plane perpendicular to the X_3 axis, but has an infinite number of symmetry planes passing through this axis. Indeed, the matrix of the direction cosines corresponding to reflection in the plane perpendicular to the X_3 axis is

$$\begin{matrix} 1 & 0 & 0 \\ 0 & 1 & 0. \\ 0 & 0 & -1 \end{matrix}$$

and according to (5) the components of (6) under such a coordinate transformation (multiplied by minus one) are

$$A'_{11} = A'_{22} = A'_{33} = A'_{13} = A'_{31} = A'_{23} = A'_{32} = 0;$$
$$A'_{12} = A_{12}; \quad A'_{21} = -A_{12}.$$

But before transformation we had

$$A_{12} = -A_{12}; \quad A_{21} = A_{12}.$$

This shows that such a transformation is allowable from the point of view of symmetry only if $A_{12} = A_{21} = 0$, so that (6) has no symmetry plane perpendicular to the X_3 axis.

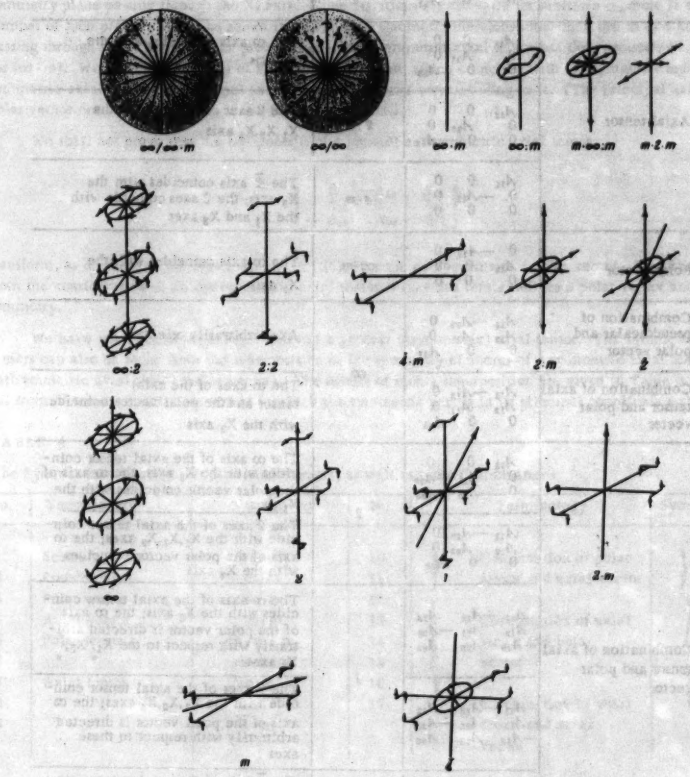

Fig. 1. Geometric models of scalars, vectors and tensors of second rank.

The matrix of direction cosines corresponding to reflection of the coordinate system in some plane passing through the X_3 axis and making an angle α with the X_1 axis is

$$\begin{matrix} \cos 2\alpha & \sin 2\alpha & 0 \\ \sin 2\alpha & -\cos 2\alpha & 0 \\ 0 & 0 & 0 \end{matrix}$$

TABLE 3

Canonical Forms and Symmetries of Axial Tensors of Second Rank

Terminology	Canonical form of tensor	Tensor symmetry	Orientation of the axes
Pseudoscalar	$\begin{matrix} A_{11} & 0 & 0 \\ 0 & A_{11} & 0 \\ 0 & 0 & A_{11} \end{matrix}$	∞/∞	Axes arbitrarily oriented
Axial tensor	$\begin{matrix} A_{11} & 0 & 0 \\ 0 & A_{11} & 0 \\ 0 & 0 & A_{33} \end{matrix}$	$\infty:2$	The ∞ axis coincides with the X_3 axis
	$\begin{matrix} A_{11} & 0 & 0 \\ 0 & A_{22} & 0 \\ 0 & 0 & A_{33} \end{matrix}$	$2:2$	The 2 axes coincide with the X_1, X_2, X_3 axis
	$\begin{matrix} A_{11} & 0 & 0 \\ 0 & -A_{11} & 0 \\ 0 & 0 & 0 \end{matrix}$	$\overline{4}\cdot m$	The $\overline{4}$ axis coincides with the X_3 axis; the 2 axes coincide with the X_1 and X_2 axes
Polar vector	$\begin{matrix} 0 & -A_{12} & 0 \\ A_{12} & 0 & 0 \\ 0 & 0 & 0 \end{matrix}$	$\infty\cdot m$	The ∞ axis coincides with the X_3 axis
Combination of pseudoscalar and polar vector	$\begin{matrix} A_{11} & -A_{12} & 0 \\ A_{12} & A_{11} & 0 \\ 0 & 0 & A_{11} \end{matrix}$	∞	Axes arbitrarily oriented
Combination of axial tensor and polar vector	$\begin{matrix} A_{11} & -A_{12} & 0 \\ A_{12} & A_{11} & 0 \\ 0 & 0 & A_{33} \end{matrix}$		The ∞ axes of the axial tensor and the polar vector coincide with the X_3 axis
Combination of axial tensor and polar vector	$\begin{matrix} A_{11} & 0 & 0 \\ 0 & A_{11} & -A_{23} \\ 0 & A_{23} & A_{33} \end{matrix}$	2	The ∞ axis of the axial tensor coincides with the X_3 axis; the ∞ axis of the polar vector coincides with the X_1 axis
	$\begin{matrix} A_{11} & -A_{12} & 0 \\ A_{12} & A_{22} & 0 \\ 0 & 0 & A_{33} \end{matrix}$		The 2 axes of the axial tensor coincide with the X_1, X_2, X_3 axes; the ∞ axis of the polar vector coincides with the X_3 axis
	$\begin{matrix} A_{11} & -A_{12} & A_{13} \\ A_{12} & A_{11} & -A_{23} \\ -A_{13} & A_{23} & A_{33} \end{matrix}$	1	The ∞ axis of the axial tensor coincides with the X_3 axis; the ∞ axis of the polar vector is directed arbitrarily with respect to the X_1, X_2, X_3 axes
	$\begin{matrix} A_{11} & -A_{12} & A_{13} \\ A_{12} & A_{22} & -A_{23} \\ -A_{13} & A_{23} & A_{33} \end{matrix}$		The 2 axes of the axial tensor coincide with the X_1, X_2, X_3 axes; the ∞ axis of the polar vector is directed arbitrarily with respect to these axes
	$\begin{matrix} A_{11} & A_{12} & 0 \\ A_{12} & -A_{11} & 0 \\ 0 & 0 & 0 \end{matrix}$	$2\cdot m$	The $\overline{4}$ axis of the axial tensor coincides with the X_3 axis; the ∞ axis of the polar vector coincides with the X_3 axis
	$\begin{matrix} A_{11} & -A_{12} & A_{13} \\ A_{12} & -A_{11} & -A_{13} \\ -A_{13} & A_{13} & 0 \end{matrix}$	m	The symmetry plane makes an angle of 45° with the axes X_1 and X_2

Using this matrix, we obtain an expression for the components of (6) in the new coordinate system. Performing the calculations, we obtain

$$A'_{11} = A'_{22} = A'_{33} = A'_{13} = A'_{31} = A'_{23} = A'_{32} = 0;$$
$$A'_{12} = -A_{12}; \quad A'_{21} = A_{12}. \tag{7}$$

Thus, under this transformation, the tensor components transform into themselves, and this shows that (6) has a symmetry plane passing through the X_3 axis. Since Equations (7) are valid for arbitrary α, there is an infinite number of such planes. It can be shown that (6) has no symmetry elements other than the ∞ axis and the planes passing through it. It has thus been proven that an antisymmetric axial tensor has the symmetry of a polar vector ($\infty \cdot m$). We shall call the axis of the coordinate system which coincides with the symmetry axis of an antisymmetric axial tensor the principal axis of the polar vector corresponding to it. (The principal axis of the polar vector corresponding to the tensor (6) is the X_3 axis.)

We shall not prove that the components of a general antisymmetric axial tensor

$$\begin{vmatrix} 0 & -A_{12} & A_{13} \\ A_{12} & 0 & -A_{23} \\ -A_{13} & A_{23} & 0 \end{vmatrix},$$

transform, as do those of the tensor shown in (6), like the components of a polar vector. The final conclusion from the consideration of an antisymmetric axial tensor is that this tensor defines a polar vector and has its symmetry.

We have yet to consider the symmetry of a general (asymmetric) axial tensor. The symmetry of such tensors can also be found from the superposition of the symmetry elements of a symmetric axial tensor and an antisymmetric axial tensor (polar vector). The results of such a superposition are given in Table 3. The canonical form of tensors in this case is that in which the symmetric part is in its principal coordinate system.

TABLE 4

The Symmetries of Scalars, Vectors, and Tensors, as well as some Combinations

No.	Terminology	Symmetry	No.	Terminology	Symmetry
1	Scalar	$\infty/\infty \cdot m$	10	Combination of polar tensor and axial vector	$2:m$
2	Pseudoscalar	∞/∞	11		$\bar{2}$
3	Polar vector	$\infty \cdot m$	12	Combination of axial tensor and polar vector	∞
4	Axial vector	$\infty:m$	13		2
5	Polar tensor	$m \cdot \infty : m$	14		1
6	" "	$m \cdot 2 : m$	15		$2 \cdot m$
7	Axial tensor	$\infty : 2$	16		m
8	" "	$2:2$	17	Combination of axial tensor and axial vector	$\bar{4}$
9	" "	$\bar{4} \cdot m$			

As is seen from the Table, there exist only ten symmetry groups for axial tensors: ∞/∞, $\infty:2$, $2:2$, $\bar{4} \cdot m$, $\infty \cdot m$, ∞, 2, 1, $2 \cdot m$, m, of which only the groups $\infty:2$; $2:2$ and $\bar{4} \cdot m$ are symmetry groups for proper axial tensors, while ∞/∞ is the symmetry group of a pseudoscalar and $\infty \cdot m$ is the symmetry group of a polar vector. The other groups ∞; 2, 1, $2 \cdot m$ and m result from the superposition of the above groups. None of the symmetry groups of axial tensors presented contains among its elements a center of symmetry. We note, finally, that the axial tensor of the form

$$\begin{vmatrix} 0 & 0 & 0 \\ 0 & 0 & 0 \\ 0 & 0 & A_{33} \end{vmatrix},$$

has the same symmetry (∞ : 2) as the tensor

$$\begin{vmatrix} A_{11} & 0 & 0 \\ 0 & A_{11} & 0 \\ 0 & 0 & A_{33} \end{vmatrix},$$

and has not been treated separately (just as we have not given a separate treatment for a polar tensor having vanishing diagonal elements, which has the same symmetry as one with no vanishing diagonal elements).

It is interesting to note that combinations of polar and axial tensors may occur which belong to a new symmetry group which is not among the symmetry groups of polar and axial tensors alone, namely $\bar{4}$. This group is obtained as a result of combining an axial tensor with symmetry $\bar{4} \cdot m$, and an axial vector with symmetry $\infty : m$ on the condition that the $\bar{4}$ axis of the axial tensor coincides with the ∞ axis of the axial vector.

Thus in general the symmetry of polar tensors is described by six groups, and the symmetry of axial ones by ten groups, and, in addition, combinations of these tensors can lead to another different group ($\bar{4}$). The total number of symmetry groups of polar and axial tensors and their combinations is thus 17. Table 4 presents the symmetry groups corresponding to scalars, vectors, and tensors, as well as groups corresponding to several of their possible combinations which lead to new symmetry groups (new, that is, with respect to the symmetry groups of the scalars, vectors, and tensors themselves).

In Figure 1 we present geometric models corresponding to the symmetry of these 17 groups.

The author expresses his gratitude to Academician A. V. Shubnikov for discussing several of the questions dealt with in the present work.

LITERATURE CITED

[1] A. V. Shubnikov, "On the Symmetry of vectors and tensors," Izv. AN SSSR, Ser. Fiz. 13, 3, 347-375 (1949).

[2] A. V. Shubnikov, "Symmetry and the geometric interpretation of two-dimensional polar tensors," Izv. AN SSSR, Ser. Fiz. 13, 3, 376-391 (1949).

[3] A. V. Shubnikov, Piezoelectric Textures [In Russian] (1946).

Crystallography Institute
Academy of Sciences, USSR

Received January 21, 1957

X-RAY DIFFRACTION STUDY OF SODIUM AND POTASSIUM OXYGEN VANADIUM BRONZES $Me_{0.33}V_2O_5$

R. P. Ozerov, G. A. Gol'der and G. S. Zhdanov

An x-ray diffraction study of the structure of sodium and potassium vanadium bronzes $Me_{0.33}V_2O_5$ has been made. Positions of atoms in the structure recently determined by Wadsley have been refined by the use of sections of the electron density function. Crystallochemical similarity between the bronzes and the higher vanadium oxides has been established.

An investigation of vanadico-vanadates, or more correctly, vanadium bronzes [1], with a formula usually written $m \cdot Me_2O \cdot nV_2O_4 \cdot pV_2O_5$ (Me—an alkali metal, m, n, p—integers) or $Me_xV_2O_5 (0 < x < 1)$ is interesting from both theoretical and practical points of view. A number of points were not clear in the crystal chemistry of these compounds, e.g., the valence of vanadium ions in the structure, the unusual properties of the vanadium bronzes, their high electrical conductivity, metallic luster, chemical inertness and others. Of practical interest is the clarification of the role of the bronzes in the vanadium catalysts and in the making of sulfuric acid. Entirely contradictory views exist in the literature on this problem. Canneri [2] believes that vanadium bronzes are the active components in vanadium catalysts. If vanadium exists in these compounds in an intermediate valence state and is therefore easily reduced or oxidized, then his opinion is reasonable. But an opposite view is held by G. K. Boreskov [3], who believes that formation of the vanadium bronzes causes thermal poisoning of the catalysts. Until now it had not been definitely established which of these views is correct.

The first step toward the solution of these problems is the determination of the structure of vanadium bronzes and to this the present paper is devoted.

Sodium and potassium vanadium bronzes were obtained during investigation of the contact process of preparation of sulfuric acid, i.e., of systems containing V_2O_5 and sodium and potassium sulfates and vanadates [4, 5, 6]. The bronzes form long, black, flat acicular crystals with bluish metallic luster. Their composition is $(K, Na)_2O \cdot V_2O_4 \cdot 5V_2O_5$ or $(K, Na)_{0.33}V_2O_5$. The crystals have a fairly large number of faces. The simple forms are the pinacoids $\{102\}$, $\{101\}$, $\{100\}$ and $\{001\}$. The development of different faces varies from crystal to crystal.

Structural analysis by the Laue method shows that the crystals are monoclinic and belong to the Laue class C_{2h}—2/m. The dimensions of the unit cell were determined from photographs taken with an RKOP camera and then refined from photographs taken with the 114.56 mm RKU camera, and $FeK\alpha$ radiation. The reflections 900, 902 and 5010 were used with θ = 67-75°.

The following values were obtained for the lattice period of $Na_{0.33}V_2O_5$ (λFeK_α = 1.93597 A):

$$a = 10.039 \pm 0.003\text{Å},$$
$$b = 3.605 \pm 0.003\text{Å},$$
$$c = 15.335 \pm 0.003\text{Å},$$
$$\beta = 109°12' \pm 3' = 109.20°$$

The period b was determined from the 020 reflection on a powder photograph of the sodium vanadium bronze. The volume of the unit cell is therefore 524.2 A^3.

Comparison of rotation photographs of sodium and potassium vanadium bronzes shows that their lattice periods are nearly identical. For this reason the above values were accepted for both vanadium bronzes.

The density of the potassium vanadium bronze was determined in a pycnometer as $\rho = 3.57$ g/cm^3. For this density and the formula $K_2V_{15}O_{39}$, the number of molecules in the unit cell is $\sim 1 (0.97)$. The value of density computed from the x-ray data is $\rho_{roent} = 3.60$ g/cm^3.

The extinctions observed in the photographs indicate x-ray group No. 6 [7]. This group contains three space groups: A 2/m, A/2 and Am. The choice of the correct space group was made by analyzing the dimensions of the unit cell and the symmetry of the oxides of vanadium, molybdenum, tungsten and of the tungsten bronzes. The structures of many of these oxides [8] and also of some of the alkali compounds of these metals [9] consist of layers of polyhedra one polyhedron in thickness. Most frequently the polyhedra are octahedra, sometimes trigonal dipyramids. In all cases the period corresponding to the height of the polyhedron ranges from 3.56 A to 4.10 A. With decrease in symmetry of the lattice, these periods increase; for the 2/m class they are 3.5-3.7 A, for $2_1/c$ – 4.0 to 4.1 A. In the vanadium bronzes this period is 3.60 A and they belong therefore to the highest symmetry class – A2/m. This indicates also that in the bronze structure, all atoms lie in the mirror plane that is, their y coordinate is either 0 or ½ (position 4 (i)), a fact confirmed by the absence of extra-structural reflections even in the much overexposed photographs.

That this choice of the space group is correct is confirmed by comparing reciprocal lattice photographs for alternating values of n: those for n equal to 0 or 2 are identical to those for n equal to 1 or 3, and this shows that they belong to the centrosymmetrical group – A 2/m.

The magnitude of the period b suggests also that the structure of the bronzes consists of octahedra or trigonal dipyramids; the compounds built of other polyhedra (tetrahedrons VO_4) have no periods comparable to 3.60 A [10, 11, 12].

The values of experimental structural amplitudes were determined from optical diffraction patterns. The total number of measured reflections was about 800 (MoK_α -radiation), which includes practically the entire region of reflections. The intensity of reflections was estimated by comparison with a standard intensity scale [13]. To determine F as exactly as possible photographs with different exposures were used. Only the usual intensity factors were considered (absorption was disregarded).

The first information about structure was obtained from the Patterson projection P (u, w) along [010]. The positions of the vanadium atoms in the unit cell were determined from the projection on the basis of published data on the structure of vanadium, molybdenum and tungsten oxides [8]. Wadsley's paper [14] with structural studies of the compound $Na_{3-x}V_6O_{15}$ (this is his formula for sodium vanadium bronze) appeared at this stage of our investigation. Wadsley determined the initial position of the vanadium atoms from an analysis of the interatomic vectors by the method of "superposition of images" [15]. The structure was determined by him from the projection of electron density along [010] by the use of about 250 nonzero structure amplitudes of h0l type.

The coordinates of atoms given by Wadsley are listed in Table 1, while Fig. 1, A, shows the structure proposed by him.

To check Wadsley's results we constructed, using his coordinates, analogous projections for both sodium and potassium vanadium bronzes. All projections are very similar.

When the structure of the vanadium bronze is projected along axis Y, three oxygen atoms are covered by vanadium atoms and this makes it difficult to determine their positions. Wadsley avoided this difficulty by making two projections of the function of electron density; the projection for determining the position of vanadium atoms was based on distant reflections ($2 \sin \theta/\lambda > 0.8$), while the position of the oxygen atoms was determined by the use of differential synthesis. However, a more exact determination of the structure can be obtained not by the method of projections but from sections of the function ρ (xyz). This was one of the reasons whey we continued our study of this structure although Wadsley had already published his results.

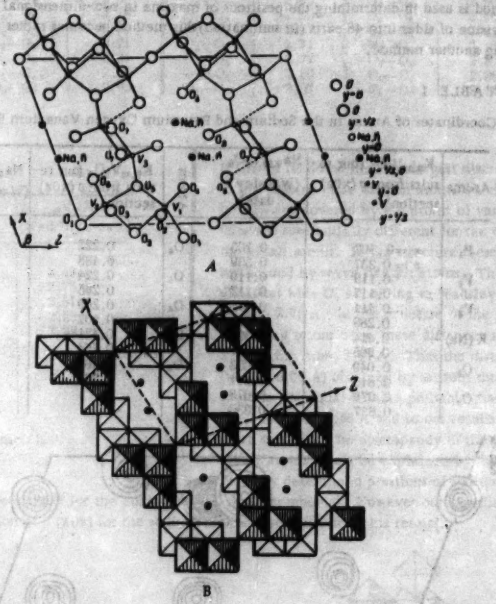

Fig. 1. Structure of sodium and potassium vanadium bronzes. A) Location of atoms in the structure; B) arrangement of polyhedra (⊗ – location of alkali atoms).

Another reason was that in the unit cell of the bronze, alkali atoms occupy only two of four available positions and this brings up the question of the distribution of the atoms and the "holes" in the structure. It was desired also to determine exactly the position of atoms in the potassium bronze, which was not studied by Wadsley.

These three circumstances made further investigations worthwhile in our opinion.

The section ρ (x0z) was constructed by the use of 800 reflections, it is shown in Fig. 2. Two new approaches were used in the construction of this section. First, in our case (for group A2/m all atoms lie in the mirror plane) the following relations hold almost exactly:

$$F(h0l) \cong M_3F(h2l) \cong M_4F(h4l) = \ldots$$
$$F(h1l) \cong M_3F(h3l) \cong M_4F(h5l) = \ldots$$

For this reason, to construct this section it is necessary only to use the amplitudes with k = 0 and 1. To diminish error in determination of reflection intensities we added also the amplitudes with k = 2 and 3. Second, at present Booth's method is used in determining the positions of maxima in two-dimensional synthesis. With large unit cells and division of sides into 48 parts (in summation) this method becomes rather crude. We avoided this difficulty by using another method.

TABLE 1

Coordinates of Atoms in the Sodium and Potassium Oxygen Vanadium Bronzes

Atoms	$K_{0.33}V_2O_5$ (our results from ρ (x0z) section)	$Na_{0.33}V_2O_5$ (Wadsley's data)	Atoms	$K_{0.33}V_2O_5$ (our results from ρ (x0z) section)	$Na_{0.33}V_2O_5$ (Wadsley's data)
V_1	$x = 0.103$	0.103	O_4	0.222	0.219
	$z = 0.337$	0.339		0.438	0.436
V_2	0.119	0.119	O_5	0.224	0.225
	0.117	0.117		0.265	0.264
V_3	0.411	0.411	O_6	0.269	0.271
	0.289	0.289		0.107	0.108
K (Na)	0.414	0.394	O_7	0.421	0.419
	0.995	0.007		0.754	0.750
O_1	0.049	0.053	O_8	0.464	0.467
	0.813	0.811		0.396	0.396
O_2	0.079	0.078			
	0.637	0.633			

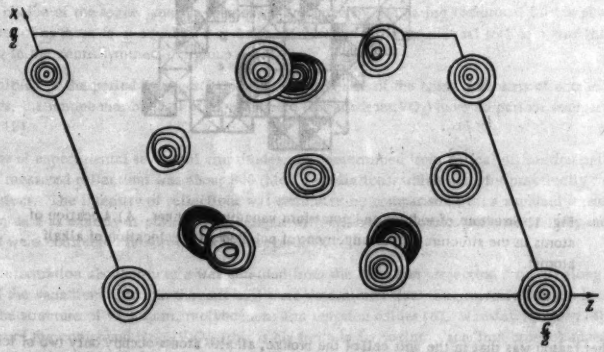

Fig. 2. Two-dimensional section of the function of electron density ρ (x0z) for $K_{0.33}V_2O_5$.

The coordinates of the atoms in potassium vanadium bronze determined by us and the ρ (x0z) sections are given in Table 1. Table 2 gives the corresponding interatomic distances.

Table 1 shows that our atomic coordinates agree well in almost all cases with those obtained by Wadsley.* * We compare the positions of atoms in the structures of analogous sodium and potassium compounds on the assumption that the positions of vanadium and oxygen atoms are practically identical in these compounds.

TABLE 2

Interatomic Distances (in A) in Potassium Vanadium Bronze

$V_1—O_4$	1.61	$V_2—O_6$	1.56	$V_3—O_8$	1.55
$V_1—O_3$	1.90	$V_2—O_9$	1.89	$V_3—O_7$	1.89
$V_1—O_2$	2.30	$V_2—O_1$	1.80	$V_3—O_7$	2.00
$V_1—O_5$	1.89	$V_2—O_6$	2.16	$V_3—O_5$	1.79
$V_1—O_9$	1.99	$V_2—O_3$	2.28	$V_3—O_9$	2.68
$O_2—O_3$	2.58	$O_3—O_3$	2.55	$O_7—O_7$	2.43
$O_2—O_5$	2.65	$O_6—O_6$	2.60	$O_8—O_5$	2.60
$O_3—O_5$	2.78	$O_9—O_9$	2.60	$O_5—O_9$	2.60
$O_4—O_5$	2.65	$O_1—O_9$	2.67	$O_8—O_7$	2.69
$O_4—O_3$	2.71	$O_1—O_6$	2.71	$O_7—O_5$	2.76
$O_2—O_9$	2.81	$O_3—O_9$	2.77	$O_7—O_9$	2.87
$O_2—O_4$	2.76	$O_1—O_6$	2.66	$O_8—O_7$	2.86
$O_3—O_4$	2.85	$O_1—O_3$	3.07	$O_8—O_7$	3.14

TABLE 3

Distance	$K_{0.33}V_2O_5$ ρ (x0z) section	$Na_{0.33}V_2O_5$ (Wadsley's data)
Me—O_8	2.50	2.46
Me—O_5	2.49	2.75
Me—O_4	2.56	2.51
Me—O_6	2.57	2.29
Me—Me	1.68	2.22
$O_4—O_6$	2.73	
$O_4—O_8$	3.06	
$O_6—O_8$	3.23	
$O_8—O_4$	3.35	
$O_8—O_8$	3.03	

Note: Me = an alkali metal.

It should be noted that the largest discrepancies occur in the case of those oxygen atoms which in the projection are covered by the atoms of vanadium. Our data are substantially different for the coordinates of the alkali atoms. In the structure these atoms are surrounded by seven oxygen atoms. The interatomic distances Me—O, according to Wadsley, range from 2.29 to 2.75 A. In the structure of the potassium bronze, according to our data, these distances are almost equal—2.49, 2.50, 2.56, 2.57 A. That the distances Me—O (within 0.06 A) obtained by us from three-dimensional sections are equal is more probable than that they differ by as much as 0.46 A and so our results appear to be more correct. The discrepancy in the position of the alkali atoms might be explained by the fact that Wadsley determined positions of sodium atoms in the sodium bronze while our results are for the analogous potassium compound. However, our coordinates for Na obtained from the projection of ρ (x0z) for the sodium bronze also differ from his results.

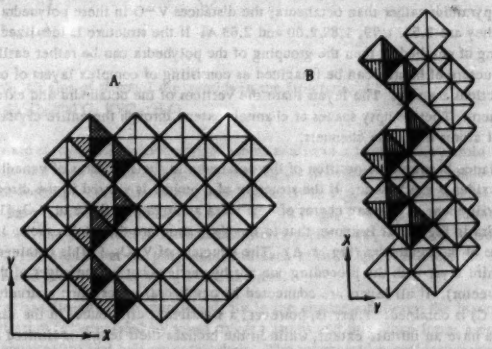

Fig. 3. Comparison of structures of vanadium pentoxide and vanadium bronze. A) grouping of polyhedra in V_2O_5; B) the grouping of polyhedra in $Me_{0.33}V_2O_5$.

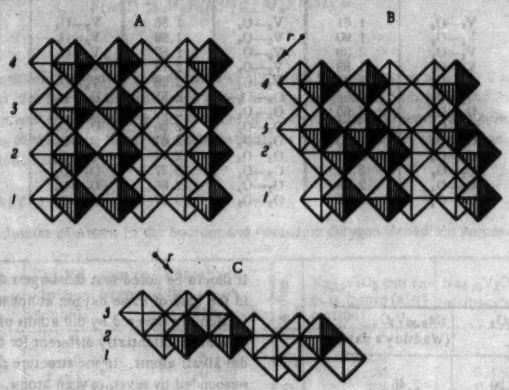

Fig. 4. The grouping of polyhedra in the structures. A) V_2O_5; B) $V_{12}O_{16}$ and C) $Me_{0.33}V_2O_5$.

The distance between two alkali atoms in $Na_{0.33}V_2O_5$ connected with each other by an axis of two-fold symmetry is 2.22 A according to Wadsley, but according to our data it is 2.02 A. The corresponding value for $K_{0.33}V_2O_5$ is 1.68 A.

Noteworthy are the shortened (as compared with the normal 1.7–1.8 A) distance V_1-O_4 (1.61 A), V_2-O_6 (1.56 A) and V_3-O_3 (1.55 A). In general this shortening is observed in some vanadium, molybdenum and other transition elements [17]; in our case, however, the shortening is always in the direction vanadium–oxygen–alkali metal.

As can be seen from Fig. 1, the structure of vanadium bronze consists of strongly deformed octahedra VO_6. This deformation is so great that some polyhedra, and especially those containing the V_3 atoms, could be considered trigonal dipyramids rather than octahedra; the distances V–O in these polyhedra differ considerably from each other; they are 1.55, 1.79, 1.89, 2.00 and 2.68 A. If the structure is idealized, that is, if it is considered as consisting of octahedra, then the grouping of the polyhedra can be rather easily visualized (Fig. 3, B). In this case the structure of bronze can be imagined as consisting of complex layers of octahedra infinitely extended in the directions $\underline{x}$ and $\underline{y}$. The layers share the vertices of the octahedra and extensive empty spaces are present between them. These empty spaces or channels extend through the entire crystal in the direction of the Y axis. The alkali atoms lie in the channels.

The resemblance between the position of the octahedra in the structures of vanadium bronzes and in the higher vanadium oxides is easily seen. If the structure of a bronze is viewed in the direction normal to the $\underline{xy}$ plane, the layers will apear as zig-zag chains of octahedra analogous to those in V_2O_5 [18]; to see this, compare the shaded octahedra in Fig. 3. It is known that in the V_2O_5 structure the chains shown in Fig. 3 are in contact only at the vertices of the octahedra (Fig. 4, A). The structure of $V_{12}O_{26}$ [19] is obtained from that of V_2O_5 by connecting each third layer with the preceding one not by vertices but by the edges of the octahedra (Fig. 4, B; $\underline{r}$ – displacement vector). If all layers are connected by octahedral edges, then a structure similar to that of $Me_2V_{12}O_{30}$ (Fig. 4, C) is obtained. There is, however, a significant difference: in the vanadium oxides the chains of octahedra have an infinite extent, while in the bronzes their length is limited to six octahedra.

All this is so if the structure is considered as consisting of ideal octahedra. But even if the actual polyhedra are considered the structures of the bronzes and the vanadium pentoxide have much in common.

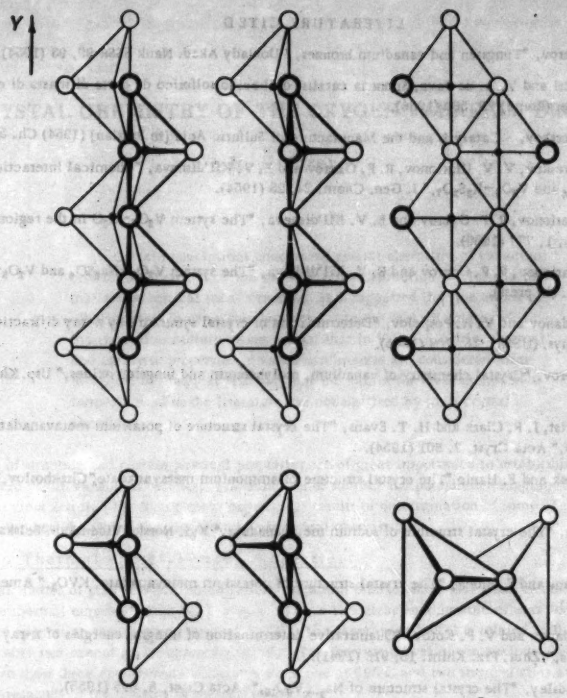

Fig. 5. Chains of trigonal dipyramids in the structure. A) V_2O_5; B) $Me_{0.33}V_2O_5$ and C) $KVO_3 \cdot H_2O$.

In V_2O_5, vanadium atoms are surrounded by five oxygen atoms and form a trigonal dipyramid. But this dipyramid is peculiar because its four vertices (four oxygen atoms) all lie in almost the same plane. Attached by their edges the dipyramids form special chains shown schematically in Fig. 5. In the bronzes similar chains of dipyramids stretch along the y axis joining the layers of octahedra (Figs. 1, A and 5, B). In the structure of another vanadium compound, the potassium metavanadate monohydrate $KVO_3 \cdot H_2O$ [9], vanadium atoms are also surrounded by five oxygen atoms and the polyhedra join each other in approximately the same way (Fig. 5, B) but the chains are different from those of V_2O_5 or the bronzes.

The alkali atoms, as has already been mentioned, lie in the channels between the layers of the octahedrons VO_6. Each alkali atom is surrounded by seven oxygen atoms and this group forms a polyhedron which is a combination of a trigonal prism and half an octahedron. The seven-fold coordination is rather rare but several occurrences of it are well known at present: the ion $(NaF_7)^{2-}$ has such a structure [20], and similar polyhedra are found in the structure of the intermetallic bismuth compound Bi_3Ni [20], etc.

This investigation of the structure of sodium and potassium vanadium bronzes $Me_{0.33}V_2O_5$ is the first step toward a crystallochemical study of these compounds.

LITERATURE CITED

[1] R. P. Ozerov, "Tungsten and vanadium bronzes," Doklady Akad. Nauk SSSR 99, 93 (1954).

[2] G. Canneri and V. A. de Pava, Spora la catalisi delli acido solforico da parte di masse di contatto al vanadio. Ann. Chim. (Rome) 26, 560 (1936).

[3] G. K. Boreskov, Catalysis and the Manufacture of Sulfuric Acid [in Russian] (1954) Ch. 5.

[4] G. K. Boreskov, V. V. Illarionov, R. P. Ozerov and E. V. Kil'disheva, "Chemical interactions in the system V_2O_5–K_2SO_4 and V_2O_5–$K_2S_2O_7$," J. Gen. Chem. 24, 23 (1954).

[5] V. V. Illarionov, R. P. Ozerov and E. V. Kil'disheva, "The system V_2O_5–K_2O in the region V_2O_5–KVO_3," Zhurn Neorg. Khim., 1, 777 (1956).

[6] V. V. Illarionov, R. P. Ozerov and E. V. Kil'disheva, "The system V_2O_5–Na_2SO_4 and V_2O_5–$NaVO_3$," Zhurn. Neorg. Khim. (in press).

[7] G. S. Zhdanov and V. A. Pospelov, "Determination of crystal symmetry by x-ray diffraction pattern," J. Expt.-Theoret. Phys. (USSR), 15, 709 (1945).

[8] R. P. Ozerov, "Crystal chemistry of vanadium, molybdenum and tungsten oxides," Usp. Khim. 24, 951 (1955).

[9] C. L. Christ, J. R. Clark and H. T. Evans, "The crystal structure of potassium metavanadate monohydrate, $KVO_3 \cdot H_2O$," Acta Cryst. 7, 801 (1954).

[10] V. Synecek and F. Hanic, "The crystal structure of ammonium metavanadate," Chekhoslov. Fiz. Zhurn. 4, 120 (1954).

[11] H. Sörum, "The crystal structure of sodium metavanadate," Kgl. Norske Videnskab. Selskabs. Fork., 16, 39 (1943).

[12] H. T. Evans and S. Block, "The crystal structure of potassium metavanadate, KVO_3," Amer. Mineralogist 39, 326 (1954).

[13] G. S. Zhdanov and V. P. Kotov, "Quantitative determination of integral energies of x-ray interference in structural analysis," Zhur. Fiz. Khim. 15, 918 (1941).

[14] A. D. Wadsley, "The crystal structure of $Na_{1-x}V_6O_{15}$," Acta Cryst. 8, 695 (1955).

[15] J. Clastre and K. Gay, J. phys. radium 11, 75 (1950).

[16] G. S. Zhdanov and V. A. Pospelov, "On the unequal lengths of the metals–oxygen bonds in some metal oxides and in the 'molecular structure' of ZnO," Doklady Akad. Nauk SSSR, 93, 97 (1953).

[17] A. Byström, K. A. Wilhelmi and O. Brotzen, "Vanadium pentoxide – a compound with five-coordinated vanadium atoms," Acta Chem. Scand. 4, 1119(1950).

[18] F. Aebi, "Phasenuntersuchungen in System Vanadium-Sauerstoff und die Krystallstruktur von $V_{12}O_{28}$," Helv. Chim. Acta 31, 8 (1948).

[19] J. L. Hoard, "Structure of complex fluorides," J. Am. Chem. Soc. 61, 1252 (1939).

[20] V. P. Glagoleva and G. S. Zhdanov, "Structure of superconductors. VII. X-ray structure determination of Bi_3Ni," J. Exptl.-Theoret. Phys. (USSR), 26, 337 (1954).

Ia. V. Samoilov Scientific Institute of Fertilizers and Insecti- and Fungicides

Received September 21, 1956

CRYSTAL CHEMISTRY OF THE OXYGEN VANADIUM BRONZES

R. P. Ozerov

Certain conclusions concerning crystal chemistry of vanadium bronzes are reached on the basis of x-ray diffraction studies and thermal and electrical measurements. It is suggested that the atoms of alkali metals in vanadium bronzes are in the metallic state, while the state of vanadium atoms is near that in V_2O_5. Electric, thermal and catalytic properties of vanadium bronzes are considered from this point of view. It is shown that the names for these compounds formerly used in the literature are not justified by their crystal chemistry.

Studies of structure and certain physical properties are of great importance in establishing the crystallochemical nature of the vanadium bronzes. The structure of sodium and potassium vanadium bronzes was described in a previous article [1]. The present paper gives results of determination of some of their physical properties and a number of conclusions concerning their crystal chemistry.

1. Certain Thermal and Electrical Properties

Thermal studies of pure sodium and potassium vanadium bronzes show that changes occur in them before melting. The thermal curves of $Na_{0.33}V_2O_5$ (Fig. 1, a) have two clear endothermic effects at 590° and at 738°C. Another effect appears on the cooling curves at 652°C. The reaction at 738°C is related to the melting of the bronzes; the other two cannot be interpreted a priori. The thermal curves of the analogous potassium compound (Fig. 1, b) also show three endothermic effects—a weak one at 395°C and two stronger ones at 472° and 520°C. The latter corresponds to the melting of the compound.

The occurrence of changes in crystalline substances before melting may be supposed to indicate polymorphic transitions. To check this, x-ray diffraction photographs were taken in the significant temperature ranges: at 20°, 620° and 700°C for the sodium compound, and at 20°, 450° and 500°C for the potassium compound. The photographs were obtained from single crystals by the method of oscillation in a high temperature camera. Comparison of the photographs shows that, precision of the experiment being taken into account, no changes occur in either compound besides thermal expansion. It may be supposed that thermal effects are related to finer structural changes which cannot be detected by the usual x-ray methods. We shall return to this question later.

An investigation of electrical conductivity is extremely important for the elucidation of the nature of the vanadium bronzes. The electrical conductivity of the bronzes was measured* on single crystals (at room temperature) and on powders (heated to fusion). The value of conductivity was measured with a double Wheatstone bridge.

The conductivity of the crystals of $Na_{0.33}V_2O_5$ was determined semiquantitatively. This was enough to establish the electrical anisotropy of the compound. The resistivities in the direction of the long axis of an acicular crystal $\rho_{\parallel}$ and normal to it $\rho_{\perp}$ are significantly different:

$$\rho_{\parallel} = 4.6 \cdot 10^{-3}\ \text{ohm} \cdot \text{cm};\ \rho_{\perp} = 29\ \text{ohm} \cdot \text{cm}.$$

* In collaboration with N. V. Noginov.

Their ratio is

$$\frac{\rho_{\perp}}{\rho_{\parallel}} = \frac{29}{4.6 \cdot 10^{-3}} = 630.$$

In other words, conductivity parallel to the length of the crystal is more than one hundred times as great as in the direction normal to the long axis of the crystal.

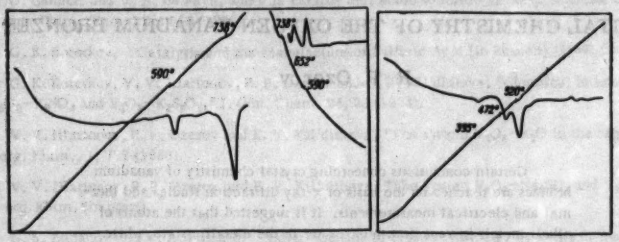

a b

Fig. 1. Thermal curves of sodium vanadium bronze (a) and potassium vanadium bronze (b).

Conductivity of powdered bronzes was measured in the apparatus shown in Fig. 2. The powder was placed in a porcelain tube approximately 3 mm long. Two electrodes were introduced into the ends of the tube and clamped by two long bolts and crosspieces; one of the electrodes was insulated from the crosspiece by mica. This device was placed in a quartz tube of 100 mm diameter. The tube was attached to a vaccum pump by means of an air-tight water-cooled cover and evacuated to 10^{-4} mm mercury. Electrical contacts and a thermocouple were inserted through the same cover. The quartz tube was placed in a vertical electric furnace.

The resistivity of the sodium vanadium bronze powder is about 10^{-2} ohm · cm. at room temperature. This agrees with known data [2]. Comparison with resistivities of crystals $\rho_{\parallel}$ and $\rho_{\perp}$ shows that the resistivity of powder is determined mainly by the conductivity along the axis.

The relation between resistivity of the sodium vanadium bronze and temperature is given in Fig. 3. In the interval from room temperature to 590°C the curve ρ (t°) is exponential, which is characteristic of semiconductors. At 590°C the curve ρ (t°) shows an inflection and resistivity decreases rapidly, but at 630°C it begins to increase somewhat, passes through a maximum at 667°C and increases again toward the melting point (738°C). It should be noted that slightly different curves were obtained in repeated tests but their general trend and the position of special points were invariably the same. The position of special points on the curves coincides with the thermal effects shown by thermal curves.

2. Structure and Properties of Vanadium Bronzes

The variation of resistivity with temperature and the strong electrical anisotropy of the crystals are evidently related to the peculiarities of crystal structure of vanadium bronzes. It is natural to suppose that the unusual properties of the vanadium bronzes which distinguish them from all other vanadium oxides (oxides, common vanadates, etc.) are due to the presence of the alkali metals in a special state and distribution in the structure.

X-ray diffraction studies of vanadium bronzes [1] show that the basic part of their structure is an oxygen framework consisting of layers of VO_6 octahedra united to each other in such a way that channels are left between them extending infinitely parallel to the Y axis. These channels contain atoms of the alkali metals, either sodium or potassium.

Since in the unit cell of a vanadium bronze there are only two alkali atoms for four positions, half of the positions remain unoccupied. How are these atoms and vacant places distributed in the structure ?

According to Wadsley [3] the distance between two sodium atoms lying in adjacent polyhedra and connected by a two-fold axis of symmetry is 2.22 A. This exceeds the sum of two ionic radii, but he believes that such a distribution is possible. Our data obtained from the ρ (x,z) projection for $Na_{0.33}V_2O_5$ give a smaller distance, 2.02 A. In $K_{0.33}V_2O_5$, instead of the expected larger distance, an even smaller one, 1.68 A, was measured, which is much smaller than the sum of ionic radii. This leads to the conclusion that two alkali atoms cannot be in two adjacent polyhedra connected by two-fold symmetry axes. This explains in part why a vanadium bronze of this structure cannot be obtained with $\underline{x}$ greater than 2/6 = 0.33.

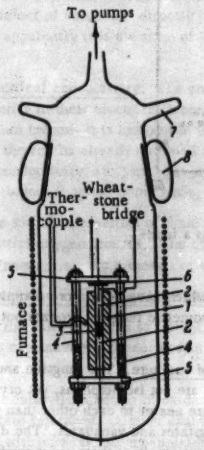

Fig. 2. An apparatus for measuring electrical resistivity of powdered bronzes at different temperatures: 1) porcelain tube; 2) brass electrodes; 3) sample; 4) bolts; 5) cross pieces; 6) mica insulation; 7) glass nipples for insertion of electrodes; 8) water tube for cooling of the cover.

There are three possible positions for the alkali atoms (Fig. 4): either they are located in the polyhedra above each other (along the Y axis), or in a zig-zag fashion, or at random, combining the first two positions. In the first two cases order may be attained within the limits of a single channel; in the absence of order throughout the volume of the crystal,* order is attained by random distribution of adjacent channels. This "disorder" retains the space group A2/m for the crystal as a whole, although for each unit cell the group is Am.

The three possible distributions of the alkali atoms, linear, zig-zag or random, are practically indistinguishable by x-ray analysis. However, different distributions of these atoms must result in entirely different physical properties of the crystals. Indeed, if by analogy with tungsten bronzes, it is supposed that in vanadium bronzes the neighboring alkali atoms have a metallic bond, then it follows that with linear distribution this bond is effective throughout the length of each channel. The presence of such metallic chains must necessarily affect electrical conductivity of the crystals and explain the sharp electrical anisotropy of vanadium bronzes. In the zig-zag arrangement of alkali atoms direct interaction among them is excluded and this must lead to reduced electrical conductivity in the direction of the long axis of the acicular crystals.

It may be assumed that the presence of alkali atoms with metallic bond in the channels of the oxygen framework is the cause of electrical anisotropy of the vanadium bronzes. At temperatures of 590°C and at about 650°C, these atoms are rearranged and this causes the anomalies appearing on the curves showing electrical conductivity of the powdered bronzes as a function of temperature; the absence of noticeable structural changes in this temperature interval does not contradict this hypothesis. There is, however, another important point to consider. Vanadium oxides, especially the higher ones, are typical semiconductors. Therefore the electrical properties of the vanadium bronzes are due to the combination of the semiconductor properties of the oxygen framework, consisting of VO_6 octahedra, with the metallic properties of the alkali atoms. Thus the interpretation of the function ρ (t°) becomes very difficult since it is affected by the electrical properties of the semiconductor framework and the metallic chains.

3. Terminology, Tungsten and Vanadium Bronzes

The term "vanadium bronze" was suggested by the author in an earlier paper [4] for the compounds known in the literature as "vanadico-vanadates" [5] or "vanadyl-vanadates" [2, 6], after comparing a number of their physical, chemical and structural characteristics with those of the tungsten bronzes. This term can be better justified now.

Are the older names for these compounds correct ? They imply the existence in these compounds of vanadium atoms with two different valences. According to this the compounds may be considered as salts of

* No extra-structural reflections were observed even in greatly overexposed photographs.

vanadico-vanadium acid $H_2O \cdot V^{4+}O_4 \cdot V^{5+}O_3$ or HV_2O_5. Structural analysis of $Me_{0.33}V_2O_5$ gives no reason to suppose that some of the vanadium ions (out of 12 in the unit cell) have different valence than others. It follows from this that names like "vandico-vanadate" and others are not justified by the crystal chemistry of these compounds.

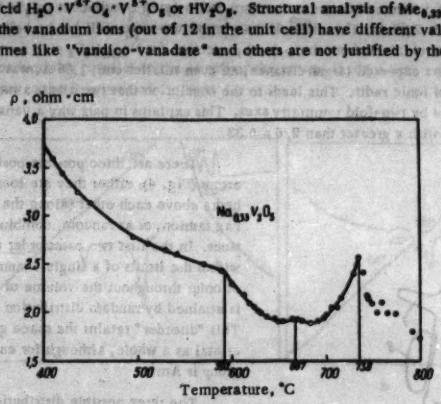

Fig. 3. Resistivity of the sodium vanadium bronze as a function of temperature.

These compounds have much in common with the tungsten bronzes, which have been more completely investigated (an especially close resemblance could be expected with nonisometric tungsten bronzes but there are few data on these at present). The resemblances are many.

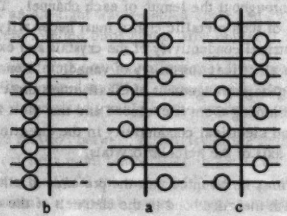

Fig. 4. Distribution of alkali atoms in the structure of vanadium bronzes, a) zig-zag; b) linear; c) random.

Similarity of structure. The tungsten and the vanadium bronzes are not isomorphous, yet crystallochemically they are nearer to each other than to the corresponding tungstates and vanadates. The difference between the structures of these compounds consists in the distribution and bonding of the oxygen polyhedra. In all known vanadates and tungstates the polyhedra in the crystal are not tied together continuously but are either isolated (as in scheelite, $CaWO_4$) or occur in separate chains (in metavanadates of the alkali metals, $MeVO_3$; see ref. in [1]). These structures exist only by virtue of electrostatic attraction between anions and cations; ionic bonds are essential to them.

In tungsten and vanadium bronzes the polyhedra MeO_6 (Me = W, V) form a stable framework with alkali atoms occupying empty spaces in it. In isometric tungsten bronzes this framework is preserved even after complete removal of the alkali atoms. The alkali atoms are in an entirely different state in the bronzes than in tungstates and vanadates since the ionic bonds between anions and cations are unimportant here. In tungstates and vanadates the cations are an integral part of the structure while in the bronzes the alkali cations are only "foreign inclusions" in the oxide framework. In this case the alkali atoms can use their valence electrons in different ways: when possible, they use them to form metallic bonds; in other words, they surrender them to the zone of conductivity. This is what makes bronzes such special compounds.

Chemical similarity. As has already been mentioned [4], the chemical formulas of the tungsten and vanadium bronzes are analogous. The formulas Me_xWO_3 and $Me_xV_2O_5$ are alike in containing tungsten and vanadium in their higest oxidation states.

It has been established [7] that tungsten is hexavalent in tungsten bronzes, as it is in WO_3. Evidently, in vanadium bronzes, vanadium is pentavalent (as in V_2O_5), which agrees with the metallic state of the alkali atoms in the structure.

Both kinds of bronzes are extremely inert chemically.

The color of the tungsten and vanadium bronzes. Is is known that the color of the tungsten bronzes does not depend on the type of the alkali atom (Na, K, Pb, etc.) but only on the average formal valence of tungsten [7]. If the color of tungsten bronzes is taken as a function of the defect of formal valence (maximum minus average valence), then the color of vanadium bronzes is also found to obey this rule. It is interesting to note that the defect of valence is directly related to the concentration of the electron gas in the compounds (to the value x); apparently it is the state of this gas that determines the color of the bronzes (as well as their metallic luster).

Electrical conductivity. The considerable structural difference between the two kinds of bronzes makes the similarity in their electrical properties less evident. Without a detailed investigation of these properties in vanadium bronzes it is impossible to make definite conclusions as to the state of the alkali atoms in them; however, the results already obtained (the difference in the values of $\rho_{\parallel}$ and $\rho_{\perp}$, the relatively large value of specific conductivity, etc.) make it probable, as was stated above, that the alkali atoms in the vanadium, as in the analogous tungsten compounds, are in the metallic state.

The specific properties of these tungsten and vanadium compounds make it possible to place them in one group, that of oxygen bronzes. The characteristic feature of these bronzes is the presence of alkali atoms with metallic bonds, i.e., the presence of electron gas, which gives these oxygen compounds their metallic properties.

4. The Role of Vanadium Bronzes in the Catalytic Oxidation of SO_2 to SO_3

On the basis of results so far obtained it is possible to make certain tentative conclusions on the catalytic properties of vanadium bronzes and, in particular, on their role in the contact process of preparation of sulfuric acid.

The catalytic reaction of oxidation of sulfur dioxide to sulfur trioxide is of the type which requires an intermediate substance. A good example of this reaction is the catalytic oxidation of orthoxylene to phthalic anhydride with pure vanadium pentoxide as the catalyst [8]. In this case the action of V_2O_5 is due to the partial reduction of vanadium and formation of an intermediate oxide $V_{12}O_{26}$. The mechanism of this reaction consists in formation, on the surface of the vanadium pentoxide crystals, of nearly two-dimensional films of $V_{12}O_{26}$; the very close resemblance between the structures of these two oxides [1, 8] makes it easy to visualize this process. This resemblance is responsible also for the partial reduction of V_2O_5 when melted in vacuum to the intermediate oxide $V_{12}O_{26}$.

Vanadium bronzes do not exhibit these phenomena. They are very stable compounds. All vanadium atoms in them have the valence of five, which excludes the possibility of change of valence of vanadium in the structure. This suggests that vanadium bronzes are catalytically inert. A study of the phase diagrams representing the action of vanadium catalysts with added sodium in the contact process [9] showed that the formation of the bronzes results not in activation but in thermal poisoning of the catalysts.

In conclusion it should be mentioned that recently Krylov [10, 11] synthesized certain new niobium compounds, suggested by the diagonal analogies of Mendeleev's periodic table, which physically and chemically resemble both tungsten and vanadium bronzes; he believes that similar titanium compounds may also be made. These compounds he called niobium bronzes. Vanadium does not lie on this diagonal, which suggests that there may exist in the periodic table a whole region of elements capable of forming oxygen bronzes. Among these are the elements with high and variable valence, such as tantalum, chromium, manganese, rhenium and others.

Further studies of structures, physical and physicochemical properties of similar compounds will undoubtedly give more complete information on their nature.

In conclusion the author wishes to express his gratitude to N. V. Noginov, V. F. Shramchenko and G. A. Kotov for their help in experimental work and to E. V. Kil'disheva for the synthesis of samples.

LITERATURE CITED

[1] R. P. Ozerov, G. A. Gol'der and G. S. Zhdanov, "Structure of the oxygen,sodium and potassium vanadium bronzes," Kristallografiia 2, 217-226 (1957).*

[2] H. Flood and H. Sörum, "Om vanadylvanadat, en ny type elektriske halvledere. 1. Systemet $Na_2O-V_2O_5$," Tidsskel Kjemi, Bergvesen Met. 3, 55 (1943).

[3] A. D. Wadsley, "The crystal structure of $Na_{2-x}V_2O_5$," Acta Cryst. 8, 695 (1955).

[4] R. P. Ozerov, "Tungsten and vanadium bronzes," Doklady Akad. Nauk SSSR, 99, 93 (1954).

[5] C. Canneri, "Sui vanadyco-vanadati," Gazz. chim. ital. 58, 6 (1928).

[6] W. Prandtl and H. Murschhauser, Ber. 38, 657, 1906; Z. anorg. allg. chem. 56, 173 (1908).

[7] R. P. Ozerov, "Crystal chemistry of vanadium, tungsten and molybdenum oxides," Usp. Khim. 24, 951 (1955).

[8] G. L. Simard, J. F. Steger, R. J. Arnott and L. A. Siegel," "Vanadium oxides as oxidation catalysts," Ind. Eng. Chem. 47, 1424 (1956).

[9] V. V. Illarionov, R. P. Ozerov and E. V. Kil'disheva," Phase diagrams of V_2O_5-Na_2SO_4 and V_2O_5-$NaVO_3$," Zhurnal Neorg. Khim. (in press).

[10] E. I. Krylov and A. A. Sharin, "Synthesis and properties of niobium bronzes," J. Gen. Chem. 25, 1680 (1954).

[11] E. I. Krylov, "The analogues of tungsten bronzes," Doklady Akad. Nauk SSSR 104, 246 (1955).

Ia. V. Samoilov Scientific Institute of Fertilizers and Insecti- and Fungicides

Received September 21, 1956

* Present issue, translation page 211.

X-RAY STUDY OF THE SYSTEM $PbTiO_3-BaSnO_3$

Iu. N. Venevtsev, A. G. Kapyshev, and Iu. V. Shumov

The existence of a continuous series of solid solutions in the system $PbTiO_3$-$BaSnO_3$ has been established and a phase diagram of the solid solution (Pb, Ba) (Ti, Sn)O_3 has been constructed. The Curie temperature in this system decreases with increase in $BaSnO_3$ content more sharply than in the system $PbTiO_3$-"$PbSnO_3$" with increase in "$PbSnO_3$."

INTRODUCTION

In the system under investigation the titanate of lead is polar [1-3] while the stannate of lead is nonpolar [2, 4, 5]. Both compounds have structures of the perovskite type [6-8] and it can be expected, therefore, that they would form solid solutions. Preparation and investigation of solid solutions between polar and nonpolar compounds is of great practical and theoretical interest. The change of composition of polar solid solutions is utilized for obtaining materials with required properties and for investigation of the mechanism of polarization. The investigation of the system $PbTiO_3$-$BaSnO_3$ in which isomorphous substitution of cations of both types occurs was undertaken also for the purpose of a more detailed study of the factors influencing phase transitions in polar compounds with the perovskite structure. There are no x-ray data on this system in the literature.

Characteristics of Samples and Methods of Study

Samples were prepared in the physical laboratory of the Institute of Crystal Chemistry AN SSSR. The variation of dielectric properties and of the coefficients of linear expansion with temperature were investigated in the same laboratory. The results of the above investigations and the technical details of the preparation of samples were described in [9].

The raw materials used were chemically pure $BaCO_3$, TiO_2 and SnO_2, and PbO of the reagent grade. The terminal heating temperature for all samples was 1250°C (held for about one hour). In the x-ray study at different temperatures, essentially the same technique was used as in [10, 11]. For computation of the identity periods and determination of symmetry of the unit cells of samples containing 0, 10, 20, 30, 60, 70 and 100 mole % $BaSnO_3$, photographs were taken with CuK_α radiation and in the case of the 40 mole % $BaSnO_3$, photographs were taken with Cr radiation. In the case of the samples photographed with copper radiation, the identity periods of the tetragonal modification were computed from α_1 and α_2 lines with indices 413 and 314; periods of the cubic modification, from α_1 lines with $\Sigma h^2 = 24$ and 26. Identity period of the sample with 40% $BaSnO_3$, photographed with Cr radiation, was computed from the group of lines α_1 with $\Sigma h^2 = 10$ (301, 103 and 310). The angle of reflection θ for these lines is about 65° and therefore the exactness of determination of the identity period for this sample is ± 0.003 A.

Results of Study of Samples at Room Temperature

The values for the identity periods of $PbTiO_3$ and $BaSnO_3$ agree well with those given in the literature [8]. Study of the photographs of samples with intermediate composition showed that the system has a continuous series of solid solutions. The samples near $PbTiO_3$ in composition, like the end-member, exhibit tetragonal distortion of the unit cell. With increase of $BaSnO_3$ content, distortion decreases and at 43 mole % $BaSnO_3$ it disappears completely. Solid solutions near $BaSnO_3$ have cubic unit cells.

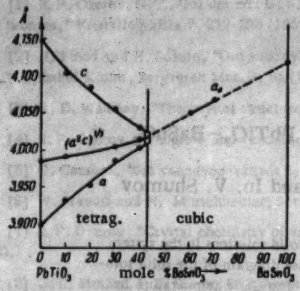

Fig. 1. Relation between identity periods and the composition of the solid solutions (Pb, Ba)-(Ti, Sn)O_3.

Figure 1 shows the relation between identity periods and the composition of the solid solutions (Pb, Ba) (Ti, Sn)O_3. The curve of variation in the ratio c/a with composition is given in Fig. 2, together with the curve for the solid solution Pb(Ti, Sn)O_3 [10,11]. The ratio c/a changes more rapidly in the former than in the latter. Extrapolating the ratio c/a to unity (interrupted line, Fig. 2) and taking into consideration that in changing from one modification to another the identity periods change abruptly [10], it may be concluded that the transition from tetragonal to cubic modification occurs approximately at 43 mole % $BaSnO_3$.

In the region of the cubic modification only three identity periods were measured (on samples with 60, 70, and 100 mole % $BaSnO_3$). Knowing these periods it is possible to draw a curve showing their change with composition for the entire region of the cubic modification (Fig. 1). The volume of the unit cell of the solid solution (Pb, Ba) (Ti, Sn)O_3 increases with increase in $BaSnO_3$ content (Fig. 3), which is to be expected, since the ionic radii of tin and barium are larger than those of titanium and lead [12].

The curve (Fig. 3) shows a break at the point of transition from the tetragonal to the cubic modification. No abrupt change in volume of the unit cell occurs although it could have been expected.

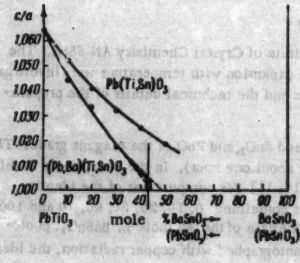

Fig. 2. Relation between c/a ratio and composition in the solid solutions (Pb, Ba) (Ti, Sn)O_3 and Pb(Ti, Sn)O_3 [10, 11].

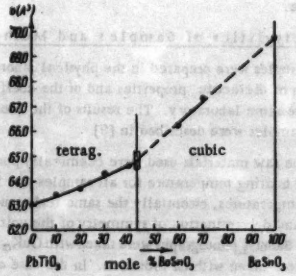

Fig. 3. Relation between the volume of the unit cell and composition for (Pb, Ba) (Ti, Sn)O_3.

Phase Diagram of the Solid Solution (Pb,Ba) (Ti, Sn)O_3

For construction of the phase diagram some samples were photographed not only at room temperature but at high and low temperatures. High temperature photographs of a sample with 30 mole % $BaSnO_3$ showed that the Curie temperature T_C = 190 ± 10°C, while for pure $PbTiO_3$ it is 490°C [13-15]. Therefore the Curie temperature of the system decreases with increase in $BaSnO_3$ content.

It has already been pointed out that at room temperature samples with $BaSnO_3$ content up to 43 % have

a tetragonally distorted lattice while those with more than 43% $BaSnO_3$ have cubic symmetry. This means that for the former the Curie point is above room temperature while for the latter it is below. For the sample with 43 mole % $BaSnO_3$ the Curie point is at room temperature.

Knowing the Curie point of three samples ($PbTiO_3$ and samples with 30 and 43 mole % $BaSnO_3$) it is possible to draw a curve showing its change with composition. In order to discover the shape of the curve in the low temperature region and look for any other possible modifications in the system, samples with 40 and 60 mole % $BaSnO_3$ were photographed at the temperature of liquid oxygen. The 40 mole % $BaSnO_3$ sample exhibited a tetragonally distorted lattice and that with 60 mole % $BaSnO_3$, a cubic lattice. Therefore, a sample with $BaSnO_3$ content between 40 and 60% must have the Curie point at -183°C.

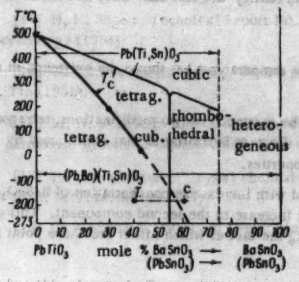

Fig. 4. Heavy lines – phase diagram of (Pb, Ba) (Ti, Sn)O_3; thin lines – phase diagram of Pb(Ti, Sn)O_3 according to the data in [10, 11, 17].

On the basis of the results obtained in the study of the system $BaTiO_3$-$PbTiO_3$ [16], which show that the second and third transition points are lowered sharply into the region of low temperatures with substitution of lead for barium in $BaTiO_3$, it may be supposed [10] that the unit cell of $PbTiO_3$ remains tetragonal from room temperature to 0° K. Since it has been established that at -183°C the unit cell of the sample with 40 mole % $BaSnO_3$ is tetragonally distorted, it can be expected that in the system $PbTiO_3$-$BaSnO_3$ there are no other modifications except cubic and tetragonal.

These data permit construction of a phase diagram of the solid solutions (Pb, Ba) (Ti, Sn)O_3 (Fig. 4). The phase diagram of the solid solutions Pb(Ti, Sn)O_3 [10, 11, 17] is given for comparison.

DISCUSSION OF RESULTS

As was shown earlier [10, 11, 17, 18], cations of A type ($t < 1$) fit loosely in the unit cells of compounds of $PbTiO_3$ and $BaSnO_3$. Therefore it is useful to compare the phase diagram of this system with diagrams of other systems in which $t < 1$, and first of all with the system $PbTiO_3$- "$PbSnO_3$."

As shown in Fig. 4 the Curie point in samples of solid solution with the end-member $PbTiO_3$ decreases more rapidly with increase in $BaSnO_3$ content than with increase in "$PbSnO_3$." This follows indirectly from comparison of the rate of decrease of the ratio c/a in the unit cells of (Pb, Ba) (Ti, Sn)O_3 and Pb(Ti, Sn)O_3 with increase in content of $BaSnO_3$ and "$PbSnO_3$," respectively (Fig. 2). It is known that the higher the ratio c/a, the higher the Curie point. Figure 2 shows that the curve for (Pb, Ba) (Ti, Sn)O_3 is below the curve for Pb(Ti, Sn)O_3.

According to the investigations of Myl'nikova [9], the curve showing variation of the Curie point with composition in the system $PbTiO_3$-$BaSnO_3$, drawn on the basis of her study of its dielectric properties, has a somewhat different form. In particular, this curve lies a little above that shown in Fig. 2. One reason for this may be that the curves were obtained from studies of different samples, even though these were prepared in a very similar way.

This difference does not change the conclusion that in the system $PbTiO_3$-$BaSnO_3$ the Curie point is lowered more rapidly than in the system $PbTiO_3$- "$PbSnO_3$" with increase in the content of the nonpolar component, for in both ours and Myl'nikova's curves the curve of variation of T_C for the solid solution (Pa, Ba)(Ti, Sn)O_3 lies considerably below the curve for Pb(Ti, Sn)O_3.

In the studies [10, 17] it was shown that for compounds ABO_3 with $t < 1$ the Curie point, other conditions being equal, rises with increase in polarizability of the cation A and with decrease in the identity periods of the lattice. The observed sharper drop in the Curie point in the system $PbTiO_3$-$BaSnO_3$ may be explained by the fact that in addition to the factors which cause this drop in the system $PbTiO_3$–"$PbSnO_3$," there are additional ones such as the lowering of mean polarizability of the polar ion of type A (polarization of the Ba ion, according to [19], is noticeably below that of Pb) and the fact that the introduction of a somewhat larger ion

Ba (R_{Ba} = 1.38 A) as compared with lead (R_{Pb} = 1.26 A), as well as introduction of large ions of tin for titanium, increases the dimensions of the unit cell of the solid solution (Pb, Ba) (Ti, Sn)O_3.

Comparison of phase diagrams of the solid solutions (Pb, Ba) (Ti, Sn)O_3 and Pb(Ti, Sn)O_3 shows that the former exists in only two modifications (tetragonal and cubic), while the latter occurs also in a rhombohedral modification. The explanation of this difference is as follows. It is known [10] that the change from tetragonal modification to rhombohedral and from the latter to pseudomonoclinic may occur for those components of a solid solution for which $t < 1$, the lowest value of t characterizing the pseudomonoclinic modification. Thus the appearance of the rhombohedral modification in Pb(Ti, Sn)O_3 is explained by the lowering of the factor t with increase in "$PbSnO_3$" content. In the case of (Pb, Ba),(Ti, Sn)O_3, t does not change with composition because the components of this solid solution have nearly equal values of t, which, according to the data from [10, 17], are .98 for $PbTiO_3$ and $1.01 \pm .03$ for $BaSnO_3$, and in reality are less than unity in both cases.

SUMMARY

1. An x-ray study of the system $PbTiO_3$-$BaSnO_3$ at different temperatures has shown the existence in the system of a continuous series of solid solutions.

2. A phase diagram of the system has been constructed. The existence of two modifications, tetragonal (polar) and cubic (paraelectric), has been established. The phase diagram is similar to that constructed by I. E. Myl'nikova on the basis of her measurements of dielectric properties.

3. The Curie point in the system $PbTiO_3$-$BaSnO_3$ is lowered with increase in concentration of $BaSnO_3$ more rapidly than in the analogous system $PbTiO_3$–"$PbSnO_3$" with increase in the second component. This confirms the correctness of the earlier conclusions [10, 17] concerning the factors which affect the Curie point in compounds with $t < 1$.

The authors express their gratitude to Doctor of Physicomathematical Sciences G. A. Smolenskii and to Candidate of Technical Sciences I. E. Myl'nikova for the loan of samples for x-ray analysis.

They are deeply grateful also to G. S. Zhdanov for his discussion of this work.

LITERATURE CITED

[1] G. H. Jonker and J. H. Santen, "Dielectric properties of titanates of perovskite type," Chem. Weekblad 43, 672-679 (1947).

[2] G. A. Smolenskii, "Polar properties of certain titanates and zirconates of bivalent metals with perovskite structure," J. Tech. Phys (USSR) 20, 2, 137 (1950); "New polar compound," Doklady Akad. Nauk SSSR 70, 3, 405 (1950); "Polar compounds with perovskite structure," (Dissertation) Trudy Fiz. Inst. Akad. Nauk SSSR (Moscow, 1954) [In Russian].

[3] S. Roberts, "Dielectric properties of lead zirconate and barium-lead zirconate, J. Am. Ceram. Soc. 33, 2, 63-66 (1950).

[4] G. A. Smolenskii, "Polarization and dielectric losses in zirconates, stannates, and certain titanates of bivalent metals," J. Tech. Phys. USSR 22, 1, 3-11 (1952).

[5] W. W. Coffeen, "Ceramic and dielectric properties of stannates," J. Am. Ceram. Soc. 36, 7, 207 (1953).

[6] S. S. Cole and H. Espenshied, "Lead titanate: crystal structure, temperature formation and specific gravity data," J. Phys. Chem. 41, 445 (1937).

[7] J. Naray-Szabo, Die structuren von Verbindungen ABO_3. "Schwesterstrukturen," Naturwissenschaften, 31, 466 (1943).

[8] H. D. Megaw, "Crystal structure of double oxides of the perovskite type," Proc. Phys. Soc. 58, 133 (1946).

[9] I. E. Myl'nikova, Investigation of Solid Solutions (Pb, Ba) (Ti, An)O_3 Possessing Polar Properties (Dissertation) Inst. Crystal Chem. Akad. Sci. L., (1955). [In Russian].

[10] Iu. N. Venevtsev, X-ray Investigation of Solid Solutions of Polar Compounds with Perovskite Structure (Dissertation) Moscow Physics and Engineering Institute (1955) [In Russian].

[11] Iu. N. Venevtsev, G. S. Zhdanov and T. N. Shendrik, "X-ray study of the system $PbTiO_3$-$PbSnO_3$," Crystallography 1, 6, 657-665 (1956).

[12] G. B. Bokii, Introduction to Crystal Chemistry [In Russian] (1954).

[13] G. Shirane, S. Hoshino and K. Suzuki, "Study of the phase transition in lead titanate," Phys. Rev. 80, 6, 1105 (1950).

[14] G. Shirane and S. Hoshino, "On the phase transition in lead titanate," J. Phys. Soc. Japan, 6, 4, 265 (1951).

[15] H. H. Rogers, Technical Report No. 56, Laboratory for Insulation Research, Massachusetts Institute of Technology (1953).

[16] G. Shirane and K. Suzuki, "On the phase transition in barium-lead titanate," J. Phys. Soc. Japan 6, 4, 775 (1951).

[17] Iu. N. Venevtsev and G. S. Zhdanov, "X-ray investigation of the solid solutions of polar compounds with perovskite structure," Izvest. Akad. Nauk SSSR, Ser. Fiz. 20, 2, 178 (1956).

[18] Iu. N. Venevtsev, "Crystal chemistry of polar compounds with perovskite structure," Izvest. Akad. Nauk SSSR, Ser. Fix. 21, 2 (1957).

[19] G. I. Skanavi, Physics of Dielectrics (1949) [In Russian].

L. Ia. Karpov Physico-Chemical Institute

Received November 16, 1956

THE CRYSTAL STRUCTURES OF TRANS-DIISOTHIOCYANOTETRAMMINE-NICKEL

E. K. Iukhno and M. A. Porai-Koshits

The structure of the monoclinic crystals of $Ni(NH_3)_4(NCS)_2$ is investigated. It is found that the structure is molecular; the hexacoordination octahedral complexes $[Ni(NH_3)_4(NCS)_2]$ have trans-structure. The linear thiocyanate groups are connected to the nickel atom through the nitrogen atom and are distributed along the lines of the Ni – N bond. The distances are Ni – N = 2.07 ± 0.03, Ni – NH_3 = 2.15 ± 0.02 kX. The distances in the thiocyanate groups are: N – C = 1.20 ± 0.05; C – S = 1.61 ± 0.04 kX. Insignificant distortions of valence angles were observed, which are caused by the packing conditions.

INTRODUCTION

The x-ray examination of $Ni(NH_3)_4(NCS)_2$ crystals was undertaken in order to determine the coordination number of the Ni atom in the given compound and consequently to ascertain the position of the acid radicals relative to this atom. An earlier examination of $NiPy_4Cl_2$ crystals [1] showed that the structural elements of this compound are the molecular octahedral complexes trans-$NiPy_4Cl_2$, in which all the bonds of the nickel-addendum, judging by the interatomic distances (Ni–Cl = 2.387, Ni–N = 2.00 kX), have a covalent character. The planes of all four pyridine rings are turned relative to the coordination square, formed by the N atoms around Ni, at a 45° angle in just one direction. The compound being described is isomorphic to the analogous cobalt compound $CoPy_4Cl_2$. Crystals of $Ni(H_2O)_4(CH_3COO)_2$ [3] also have a similar structure. The lack of structural investigations precludes drawing further conclusions as to how general is the hexacoordination octahedral structure of the complex in compounds of the NiA_4X_2 type.

The question of the structure of the thiocyanate group, its configuration, orientation in the complex and dimensions is also important. The existing x-ray data and microwave spectra data for the thiocyanogen ion $(NCS)^-$, covalently connected by the thiocyanate group and the isothiocyanate group, do not permit a final judgement as to the constancy or, on the contrary, the inconstancy of the interatomic distances N – C and C – S, nor, consequently, as to the character of the bond between the atoms.

The results obtained in separate examinations, both by the microwave spectra method [3-5] and the x-ray analysis method [6-8], differ significantly from one another. It is possible that these differences arose on account of inaccurate determination in one case or another. It is possible, however, that some differences are quite real, and the interatomic distances in the thiocyanate group would vary depending on whether it is connected with the central sulfur atom or the nitrogen atom, and also depending on the character and stability of this bond.

Synthesis and Character of the Crystals

Diisothiocyanotetrammine-nickel was obtained by Meizendorf [9] by dissolving nickel thiocyanate in an aqueous solution of ammonia and by evaporation of the resulting solution over a water bath. It is easier to

obtain this compound by the method described by Grossman [10]. A freshly prepared nickel hydroxide is dissolved in a boiling aqueous solution of ammonium thiocyanate, and to the solution filtered from the nondissolving hydroxide, containing $Ni(NCS)_2$ and NH_4SCN, an excess of concentrated ammonia is added. After cooling, coarse dark-blue crystals separate out from the solution. These crystals, left in the air, effloresce and turn sky-blue, and in water decompose with the formation of $Ni(OH)_2$ and ammonia.

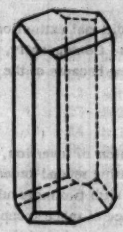

Fig. 1. Crystal of diisothiocyanotetrammine-nickel.

Quantitative analysis gave the following results: 24.09% Ni, 47.87% NCS, 27.97% NH_3; within the limits of experimental error this corresponds to the formula $Ni(NH_3)_4(NCS)_2$ (the compound $Ni(NH_3)_4(NCS)_2$ contains 24.15% Ni, 47.82% NCS and 28.04% NH_3).

The $Ni(NH_3)_4(NCS)_2$ crystals are prisms, elongated along axis c (Fig. 1). Optically the crystals are biaxial: $n_g = 1.674$, $n_m = 1.618$, $n_p = 1.561$ (in white light). The compound is paramagnetic, $\mu = 3.31$ Bohr magnetons,* which corresponds to the two uncoupled electrons of the Ni atom. Either tetrahedral enclosing of the Ni atom ($4s4p^3$-bonds) or octahedral ($4s4p^24d^2$-bonds) is therefore possible. The crystals show no piezoelectric effect.**

Nine crystals were measured on the goniometer. Owing to the efflorescence of the crystals, the surfaces of the faces quickly become dull, and this unfavorably affected the precision of the measurements. The results of the measurements are given in Table 1. On this basis, it was established that the crystals belong to the monoclinic crystal system, to the prismatic form of symmetry; for the axial units the ratios $a:b:c = 1.40:1:0.70$ were obtained, and for the monoclinic angle the value $\beta = 105°$.

TABLE 1

Results of Goniometric Measurements of $Ni(NH_3)_4(NCS)_2$ Crystals

Number	Simple forms	Symbol	ρ	φ	No. of ob.	Precision
1	Prism	110	90°00′	36°30′	9	± 10′
2	"	111	46°30′	48°30′	3	± 30′
3	Pinacoid	100	90°00′	90°00′	7	± 10′
4	"	001	15°00′	90°00′	9	± 30′
5	"	201	37°30′	270°00′	3	± 30′

The parameters of the lattice were determined by x-ray oscillation photographs along axes X, Y and Z, and also along directions [110] and [011], and made more precise by x-ray photographs taken in a camera photographing the reciprocal lattice, with NaCl-calibration: $\underline{a} = 11.46 \pm 0.02$, $\underline{b} = 8.18 \pm 0.02$, $c = 5.68 \pm 0.02$ kX; $\beta = 105°$. The ratio is $a:b:c = 1.401:1:0.694$ almost exactly coinciding with the goniometric data. According to the x-ray oscillation photograph along direction [110], it was found that the unit cell of the crystal was centered with respect to face (001).

* The magnetic susceptibility of $Ni(NH_3)_4(NCS)_2$ was determined by V. I. Belova at the Institute of General and Inorganic Chemistry, the Academy of Sciences, USSR.

** The measurement of the piezoelectric effect was made by V. A. Koptsik of Physics faculty of Moscow State University.

Determined by the pycnometric method, the density of the crystals is $d_n = 1.550$ g/cm^3; the number of molecules in the unit cell is

$$N = \frac{V \cdot d_n}{1.66 \cdot M} = \frac{514.3 \cdot 1.550}{1.66 \cdot 242.97} = 1.976 \approx 2;$$

the calculated density of the crystals is $d_x = 1.568$ g/cm^3.

The space group is not clearly determined by extinctions. None of the additional extinctions, except those specified by the centrosymmetry of the lattice, were observed on the prints. Consequently, three Fedorov groups are possible: C2, Cm, C2/m. According to the goniometric data, and also because of the absence of the piezoelectric effect, the most probable group is C2/m.

X-Ray Examination

In the C2/m space group there are four equivalent twofold positions in centers of inversion, five fourfold positions, of which two are in equivalent centers of inversion, two are at the rotating second-order axes and one is in the plane of symmetry, and finally there is the general eightfold position. With two molecules in the cell, the position of the nickel atoms is well-defined, even without regard to the choice of space group, since in all three cases the coordinates 000 and $^1/_2$ $^1/_2$ 0, can be ascribed to the nickel atoms, the origin of the cell coordinates having been selected in the appropriate way.

Thiocyanate groups naturally cannot occupy the twofold and the first of the fourfold positions, since for these positions points with symmetry 1 are required. The distribution of the thiocyanogen group at the rotating axes is discarded simply from considerations of space: period b is insufficient for the spacing of two linear groups of NCS [11] in line with the nickel atom. Only one possibility therefore remains: the NCS groups must be placed in the fourfold position in the mirror plane of symmetry. The general eightfold position is of course ascribed to the NH_3 groups.

For determining the structure, the zero and first five layer lines are unfolded by rotation of the crystal around axis Y and the zero layer line by rotation of the crystal around axis Z. X-ray photographs were taken by molybdenum emission in a camera for photographing the reciprocal lattice made at the NII of Physics, MGU. A visual appraisal of the intensity of the reflections was made with the help of a calibrated density scale. Structure amplitudes were calculated taking into account the polarization and Lorenz factors; the absorption factor was not taken into account. For the x-ray exposure, crystals having a nearly true hexagonal cross section were selected, and in that case taking account of absorption does not materially change the projection pictures [12]. The total number of reflections used during the calculation of the projections and the cross section equals 97 (for projection xz), 71 (for projection xy) and 394 (for the cross section). The structure amplitude values of $|F_o(hk[\ ])|$ when k = 0, 1, 2 are given in Table 2.

For obtaining preliminary data regarding the structure, projections of interatomic vector functions were constructed on planes uv and uw.

These projections are given in the curves in Fig. 2 and 3. Maxima located on axis u of projection uv are confirmation that the thiocyanate groups lie in one of the planes with the nickel atoms; these planes are oriented perpendicular to axis Y; the indicated maxima evidently should be ascribed to the ends of vectors Ni − N, Ni − C and Ni − S (the latter naturally is the most powerful). The distribution of maxima on the projection uv thus confirms the presence of mirror reflection planes (at least in relation to the Ni atoms and thiocyanate groups). The distances of maxima from the origin of the coordinates and from one another are less than the ordinary interatomic distances Ni − N, N − C and C − S, which is apparently the result of foreshortening. The form of the projection of the interatomic function on plane uw does not contradict this conclusion: strong maxima corresponding to Ni − S vectors are found on diagonal line of the "rhomb," the sides of which are a/2 and c.

The number of strong maxima on the projection uw, which can be ascribed to the ends of the Ni − S vectors, shows that the sulfur atoms from only one true system of periods and therefore are connected with one another not only by the planes of symmetry but by the rotating axes. Thus, group C2/m finds further confirmation here.

TABLE 2

Comparison of Experimental $|F_e|$ and Calculated F_c Structure Amplitudes

hkl	$\|F_e\|$	F_c	hkl	$\|F_e\|$	F_c	hkl	$\|F_e\|$	F_c	hkl	$\|F_e\|$	F_c	hkl	$\|F_e\|$	F_c
001	26	27	$\bar{6}05$	10	4	$\bar{1}4.03$	12	14	$\bar{1}1.12$	8	4	$\bar{6}22$	6	12
002	4	−11	$\bar{6}06$	10	15	$\bar{1}4.04$	13	8	$\bar{1}1.13$	16	19	$\bar{6}23$	45	45
003	47	37	607	9	4	110	37	44	13.10	9	9	$\bar{6}24$	10	−5
004	18	22	800	44	36	111	78	88	020	84	106	$\bar{6}25$	8	9
005	0	−2	801	13	−22	112	35	40	021	9	−6	$\bar{6}26$	12	22
006	16	23	802	25	15	113	0	0	022	15	15	820	55	45
007	13	14	803	41	30	114	38	33	023	71	68	821	0	−1
200	34	35	804	10	6	$\bar{1}11$	27	38	024	38	31	882	21	21
201	43	41	805	9	5	$\bar{1}12$	41	52	025	0	−8	823	20	21
202	82	82	806	14	8	$\bar{1}13$	19	19	026	15	12	842	9	−3
203	28	32	$\bar{8}01$	53	42	$\bar{1}14$	7	6	027	14	9	825	0	1
204	10	−21	$\bar{8}02$	18	14	$\bar{1}15$	30	38	220	6	−1	$\bar{8}21$	30	27
205	15	18	$\bar{8}03$	27	23	310	52	66	221	19	−19	$\bar{8}22$	10	10
206	15	19	$\bar{8}04$	29	33	311	59	59	222	62	52	$\bar{8}23$	7	11
$\bar{2}01$	96	121	$\bar{8}05$	8	13	312	8	14	223	53	43	$\bar{8}24$	34	36
$\bar{2}02$	44	−32	$\bar{8}06$	0	3	313	50	41	224	0	0	$\bar{8}25$	8	3
$\bar{2}03$	0	−4	10.00	0	−2	314	10	14	225	11	22	10.20	0	−9
$\bar{2}04$	62	53	10.01	15	11	$\bar{3}11$	0	7	226	13	13	10.21	20	16
$\bar{2}05$	20	29	10.02	28	17	$\bar{3}12$	39	28	$\bar{2}21$	110	125	10.22	21	25
$\bar{2}06$	0	0	10.03	0	−1	$\bar{3}13$	46	47	$\bar{2}22$	44	24	10.23	0	3
400	15	−17	10.04	0	4	$\bar{3}14$	22	20	$\bar{2}23$	11	14	10.24	0	1
401	82	78	10.05	10	12	$\bar{3}15$	0	9	$\bar{2}24$	26	36	$\bar{1}0.21$	11	23
402	75	71	$\bar{1}0.01$	60	44	510	39	38	$\bar{2}25$	13	11	$\bar{1}0.22$	18	16
403	0	−4	$\bar{1}0.02$	25	26	511	0	6	$\bar{2}26$	8	−5	$\bar{1}0.23$	13	2
404	29	19	$\bar{1}0.03$	0	−4	512	50	42	$\bar{2}27$	13	12	$\bar{1}0.24$	12	16
405	16	16	$\bar{1}0.04$	0	5	513	20	27	420	13	11	$\bar{1}0.25$	12	21
406	0	−4	$\bar{1}0.05$	16	19	$\bar{5}11$	40	40	421	54	49	12.20	9	6
$\bar{4}01$	15	−16	$\bar{1}0.06$	0	1	$\bar{5}12$	8	8	422	34	30	12.21	15	15
$\bar{4}02$	81	78	12.00	18	16	$\bar{5}13$	45	37	423	10	−14	12.22	0	3
$\bar{4}03$	8	11	12.01	29	22	$\bar{5}14$	30	37	424	15	23	$\bar{1}2.21$	0	−6
$\bar{4}04$	28	23	12.02	0	0	$\bar{5}15$	0	8	425	12	23	$\bar{1}2.22$	12	24
$\bar{4}05$	29	38	12.03	0	−2	710	0	−2	426	0	0	$\bar{1}2.23$	15	12
$\bar{4}06$	11	8	12.04	10	8	711	22	24	$\bar{4}21$	37	37	$\bar{1}2.24$	9	2
600	36	28	$\bar{1}2.01$	0	−1	712	20	26	$\bar{4}22$	102	91	14.20	14	12
601	49	40	$\bar{1}2.02$	22	21	711	45	40	$\bar{4}23$	12	6			
602	0	−4	$\bar{1}2.03$	0	3	$\bar{7}12$	46	41	$\bar{4}24$	0	−1			
603	53	34	$\bar{1}2.04$	0	−2	$\bar{7}13$	9	6	$\bar{4}25$	11	25			
604	41	29	$\bar{1}2.05$	12	10	$\bar{7}14$	24	23	$\bar{4}26$	9	11			
605	0	−3	$\bar{1}2.06$	13	15	910	21	20	620	60	60			
606	0	0	14.00	20	16	911	21	21	621	34	50			
607	14	6	14.01	8	6	$\bar{9}11$	10	7	622	10	−15			
601	6	−12	14.02	0	2	$\bar{9}12$	39	35	623	15	14			
602	42	31	14.03	10	7	$\bar{9}13$	20	22	624	16	20			
603	85	78	$\bar{1}4.01$	0	4	11.10	24	22	625	0	1			
604	14	5	$\bar{1}4.02$	0	−6	$\bar{1}1.11$	15	15	$\bar{6}21$	22	7			

The maxima of Ni − NH_3 are also allowed on both of the indicated projections. Is is apparent that their distribution corresponds to the octahedral enclosing of the nickel atoms by six addenda: four NH_3 groups and two thiocyanate groups, connected with the Ni atom through the nitrogen atom.

For refinement of the structure, 9 parameters had to be determined: coordinates $\underline{x}$ and $\underline{z}$ of the N, C and S atoms and coordinates $\underline{x}$, $\underline{y}$ and $\underline{z}$ of the NH_3 groups. In the projection of the interatomic vector functions

Fig. 2. Projection of interatomic vector functions on plane uv.

on plane uv all atoms are permitted (precisely the ends of the Ni-addendum vectors); therefore 5 parameters – coordinates x of the N, C, S atoms and x and y of the NH_3 groups – were determined simultaneously. In the projection of the structure on plane (010), the NCS groups, distributed approximately along the diagonal of the "rhomb" (with sides a/2 and c), superimpose on one another; over the N atom, which is located at height y = 0, lies the S atom at height y = 1/2 and vice versa; the C atoms also are superimposed on one another. An analogous superposition also occurs on the projection of the interatomic vector functions. Nevertheless in the first stages, the position of the corresponding maximum of the projection (010) was assumed as the coordinate z of the sulfur atom, in spite of the fact that as a result of superposition of the Ni – S and Ni – N vectors this maximum cannot be displaced.

Coordinates z of the N and C atoms were calculated on the basis of data in the literature on the interatomic distances C – S and N – C in the thiocyanate group [3, 4].

The coordinates of the atoms were refined primarily by means of successive approximations through projections of electron density on planes (001) and (010) (Fig. 4 and 5).

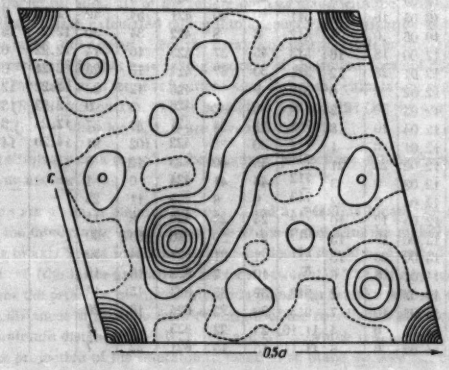

Fig. 3. Projection of interatomic vector functions on plane uw.

For obtaining final data for the coordinate z of the S, C and N atoms, a cross section was calculated for electron density ρ (x0z) (Fig. 6). Assumed as final were the coordinates x and z of the N, C and S atoms, obtained from cross sections, and coordinates x, y and z of the NH_3 groups, obtained from projections of electron density (see Table 3).

TABLE 3

Atoms	Coordinates of atoms					
	In fractions of unit cell			in kX		
	x	y	z	x	y	z
Ni	0	0	0	0	0	0
N	0.152	0	0.293	1.74	0	1.66
C	0.240	0	0.462	2.75	0	2.62
S	0.358	0	0.690	4.10	0	3.92
NH_3	0.083	0.188	0.834	0.95	1.54	4.74 (−0.94)

The structure amplitudes of reflections h0*l*, h1*l*, h2*l*, calculated according to these coordinates, are compared with the experimental in Table 2. The temperature correction constant B found by the usual method [13, 14] proved to equal 3.1 A^2. The value of the Reliability Coefficient proved to equal: for reflections hk0, 0.214; for reflections h0*l*, 0.242. If the absent $|F_{exp}|$ are not counted, then R is 0.176 and 0.210 correspondingly.

The calculation of the probable error in the determination of the coordinates of atoms according to the Vainshtein formula [15] for the three-dimensional case leads clearly to an overestimate of accuracy. This can be explained partly by the fact that under real conditions the termination of the Fourier series is not uniform along different directions so that the mean value $(\sin\vartheta/\lambda)_{max}$ does not reflect the actual parameters characteristic of the termination of the series.

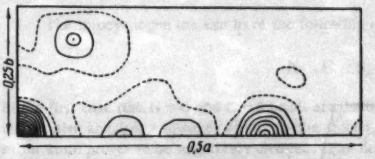

Fig. 4. Projection of electron density on plane (001). Curves are drawn with intervals 4 el/(kX)² beginning with level 2 el/(kX)² (broken line).

On the other hand, it would be incorrect to take a minimum value as $(\sin\vartheta/\lambda)_{max}$, i.e., a value which corresponds to the upper limit of index k. Actually, since coordinates x and z are obtained from a cross section parallel to plane (010), i.e., from the sum of the two-dimensional series with respect to h and *l*, the termination of the series with respect to k does not give a terminated wave, but an error wave; it forms part of the error in the values of the coefficients Φ_{hk}, and not in the limits of summation.

But in any case the error in the determination of coordinates from a cross section should be less than in the case of a projection. Therefore, in using the B. K. Vainshtein formula for a projection, we will in any case know the limits of the probable error.

The Vainshtein formula for the projection in the present case has the following form:

$$\Delta r_j = 0.114 \frac{b \cdot \sqrt{\sum_i Z_i^{1.33}}}{\sqrt{S \cdot Z_j^{1.33}}}$$

where b is the mean error in the determination of the amplitudes; Z_i and Z_j are the atomic numbers of the i and j atoms; S is the area of the corresponding face of the unit cell; coefficient 0.114 is obtained from coefficients 0.111 (for B = 3) and 0.143 (for B = 4), indicated by B. K. Vainshtein by linear interpolation.

According to this formula the values of probable errors were found to be: $\Delta r_S = 0.01$; $\Delta r_C = 0.04$; $\Delta r_N = 0.03$; $\Delta r_{NH_3} = 0.02$ kX.

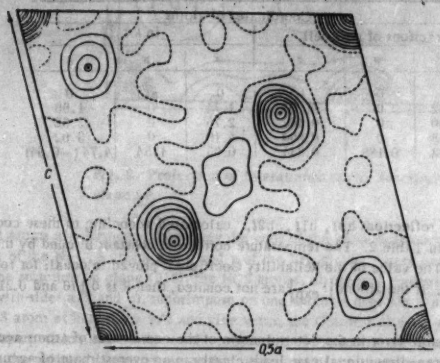

Fig. 5. Projection of electron density on plane (010). Curves are drawn with intervals 4 el/$(kX)^3$ beginning with level 2 el $(kX)^3$ (broken line).

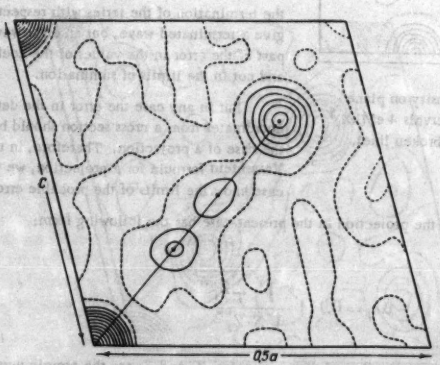

Fig. 6. Cross section of electron density along plane (010).

Description of the Structure

The crystal structure consists of the complex molecules $[Ni(NH_3)_4(NCS)_2]$, in which each Ni atom is enclosed by an octahedron of six nitrogen atoms. This confirms the suppositions of Shaw [16], based on the study of the slope of the curve of electrical conductivity of a solution of $(NH_3)_4(NCS)_2$ and NH_3, that complexes of $[Ni(NH_3)_4(NCS)_2]$ are formed in the solution. The distances in the complex are: Ni – NH_3 = 2.15 ± 0.02 kX,

Ni − N = 2.07 ± 0.03 kX. The octahedrons have insignificant distortions; the NH_3 molecules are not distributed in the form of a square, but form a rectangle having lengths of sides equal to 3.08 and 3.00 kX; the thiocyanate group, having a linear structure, is not distributed perpendicular to the plane of the rectangle of the four NH_3 groups, but deviates from the normal parallel to the shortest side of the rectangle by an angle of 1° 15'. All these deviations exceed only a little the errors in the estimated positions of the atoms.

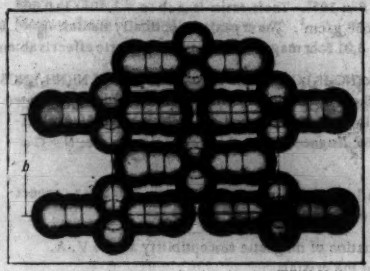

Fig. 7. Distribution of molecules in a layer parallel to plane $(\bar{2}01)$.

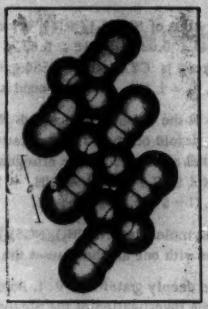

Fig. 8. Superposition of molecules in subsequent layers of the structure.

The thiocyanogen ion can have the following electron configurations:

$$\ddot{N}: :C: :\ddot{S}: \text{ and } :N: : :C: \ddot{S}:$$

In the first case (the N − C and C − S bonds are double) there is an odd electron and consequently the negative charge also acquires a nitrogen atom. In the second case (the N − C bond is triple, and C − S is ordinary) the sulfur atom proves to be negatively charged. The distances that we obtained in the thiocyanate group, N − C 1.20 ± 0.05 kX and C − S 1.61 ± 0.04 kX, indicate that the bond between nitrogen and carbon is intermediate between double and triple. However, the circumstance that the linear group NCS deviates only a little from the line of the Ni − N bond shows that in the N − C bond the triple and not the double bond predominates.* It may therefore be supposed that the sulfur atom carries the surplus of the negative charge. Judging by the interatomic distances, the bond of nitrogen with nickel is also intermediate between the purely ionic and the purely covalent.

The octahedral molecules are packed in layers in a close packed arrangement, parallel to plane $(\bar{2}01)$ of the crystal. One such layer is shown in Fig. 7. In the layers the molecules mesh with sulfur atoms and the NH_3 groups. The S atom adjoins the four NH_3- groups, which is in agreement with the conclusion concerning the surplus negative charge on the sulfur ion. Owing to the deviation of the thiocyanate group from the normal to to the plane of the rectangle formed by the ammonium groups around Ni, two NH_3 groups prove to be at a nearer distance from the S atom (3.57 kX) than the two others (3.65 kX).

The layers of molecules are superimposed on one another such that the two ammonium groups of the upper molecule mesh with the carbon atom of one thiocyanate group of the underlying molecule and vice versa. The other thiocyanate group abuts against the two NH_3 groups still lower than the positioned molecule (Fig. 8). Precisely this interaction of the NH_3 groups with the C atom, on the one hand removes the NH_3 groups insignificantly one from another, altering that same square around the Ni atoms, and on the other hand alters the thiocyanate group from the normal to the plane of the rectangle of the four NH_3-groups.

*It is certain that the character of the Ni − N bonds in the NCS group is different from the kind in methyl thiocyanate $N \equiv C - S$, CH_3 130°.

The distance C – NH_3 (3.47 kX) corresponds to the Van der Waal bond and consequently the layers are loosely connected among themselves.

This causes and explains the good cleavage observed in the crystal along plane $(\bar{2}01)$.

SUMMARY

1. Crystals of $Ni(NH_3)_4(NCS)_2$ belong to the monoclinic crystal system. The parameters of the lattice are: a = 11.46 ± 0.02, b = 8.18 ± 0.02, c = 5.68 ± 0.02 kX; β = 105°. Their ratio is a:b:c = 1.401:1:0.694. The space group is C2/m; d_n = 1.550 g/cm³; N = 2; d_x = 1.568 g/cm³. The crystals are optically biaxial: n_g = 1.674, n_m = 1.618, n_p = 1.561. The compound is paramagnetic, μ = 3.31 Bohr magnetons. The piezoelectric effect is absent.

2. As in the complex compounds $Ni(NC_5H_5)_4Cl_2$ and $Co(NC_5H_5)_4Cl_2$, in the crystal structure of $Ni(NH_3)_4(NCS)_2$ nickel has a sixfold octahedral coordination. The linear NCS groups are located in the trans-position, connected with the nickel atom through the nitrogen atom and are distributed along the line of the Ni – N bond. The distance Ni – N = 2.07 ± 0.03, Ni – NH_3 = 2.15 ± 0.02 kX. The distances in the thiocyanate group are: N – C = 1.20 ± 0.05, C – S = 1.61 ± 0.04 kX.

3. The molecules $[Ni(NH_3)_4(NCS)_2]$ are close packed in layers parallel to plane $(\bar{2}01)$. The loose connection of layers with one another causes the cleavage observed of the crystals along this plane.

We are deeply grateful to V. I. Belova for the determination of magnetic susceptibility and to V. A. Koptsik for the investigation of the piezoelectric properties of the crystals.

LITERATURE CITED

[1] M. A. Porai-Koshits, "X-ray examination of complex compounds of bivalent cobalt and nickel," Trudy Inst. Krist. 10, 117 (1954).

[2] J. N. Niekerk and F. R. L. Schoening, "The crystal structures of nickel acetate, $Ni(CH_3COO)_2 \cdot 4H_2O$, and cobalt acetate, $Co(CH_3COO)_2 \cdot 4H_2O$," Acta Cryst. 6, 609 (1953).

[3] C. I. Beard and B. P. Dailey, "Microwave spectrum and structure of isothiocyanic acid," J. Chem. Phys. 15, 762 (1947).

[4] C. I. Beard and B. P. Dailey, "The structure and dipole moment of isothiocyanic acid," J. Chem. Phys. 18, 1437 (1950). Erratum, J. Chem. Phys. 19, 975 (1951).

[5] B. L. Crawford and D. E. Mann, "Spectroscopy," Ann. Rev. Phys. Chem. 1, 151 (1950).

[6] Z. V. Zvonkova and G. S. Zhdanov, "X-ray examination of ammonium thiocyanate," Zhur. Fiz. Khim. 23, 1495 (1949).

[7] H. Scouloudi, "The crystal structure of mercury tetrathiocyanate-copper diethylenediamine, $[Hg(SCN)_4][Cu(en)_2]$," Acta Cryst. 6, 651 (1953).

[8] S. M. Ohlberg and P. A. Vaughan, "The crystal structure of selenium dithiocyanate," J. Am. Chem. Soc. 76, 2649 (1954).

[9] R. Abegg, Handbuch der anorganischen Chemie (Leipzig, 1937) 4, 682.

[10] H. Grossman, Über die Verbindungen der Metallrhodanide mit organischen Basen, 37, 559 (1904).

[11] G. S. Zhdanov and Z. V. Zvonkova, "Crystallochemistry of metal thiocyanates," Uspekhi Khim. 22, 3 (1953).

[12] M. A. Porai-Koshits, X-ray xamination of the Structure of Potassium Tetranitropalladite (1948).

[13] A. J. C. Wilson, "Determination of absolute form relative x-ray intensity data," Nature 150, 152 (1942).

[14] M. A. Porai-Koshits, "Reduction of structure amplitude values to absolute scale," Trudy Inst. Krist. 9, 305 (1954).

[15] B. K. Vainshtein, "Qualitative relations in the Fourier series of the electron density of a crystal," J. Exptl.-Theoret. Phys. (USSR) 27, 44 (1954).

[16] C. S. Shaw, "Physicochemical studies in the formation of nickel ammines in solution," Z. Phys. Chem. 204, 194 (1955), Leipzig.

M. V. Lomonosov
Moscow State University

Received December 14, 1956

ELECTRON DIFFRACTION STUDY OF THE STRUCTURE OF THIN FILMS OF MOLTEN TIN

A. I. Bublik

On the basis of an analysis of the curves of radial distribution of the atoms, constructed from the data of electron diffraction patterns, it is shown that at the melting point the short-range order in tin remains substantially the same as in the crystalline form. With increase in temperature, there is a tendency to close packing in molten tin. The problem of the separation of the non-coherent background from the total intensity curve is also discussed.

1. The study of the structure of molten metals and alloys has been carried out up to the present time mainly by means of x-ray analysis. It may, however, be useful to employ for this purpose the electron diffraction method, which has certain advantages over the x-ray method. The production of x-ray diagrams of liquid substances (if monochromatic radiation is used) takes several tens and sometimes hundreds of hours, and it is also necessary to make a continuous exposure and maintain the specimen at a definite temperature, whereas the electron diffraction pattern can be observed on the screen, and therefore an exposure of a few seconds only is required for fixing it on a photographic plate. It is thus easy to follow the transformations occurring in metals and alloys with variation in temperature and to study the kinetics of crystallization, the change in structure in the liquid and solid states, etc. The possibility of obtaining electron diffraction patterns from molten metal films was pointed out in reference [1]. The present paper gives the results of a study of the structure of molten tin at two temperatures.

The electron diffraction patterns were photographed in a high-temperature electron diffraction camera [1]. Photographs were made of free, thin ($2 - 3 \cdot 10^{-6}$ cm) films, prepared by a method developed previously [2].

2. When the films of tin were heated, the change in the diffraction pattern with increase in temperature was clearly visible on the screen. At a temperature close to the melting point, slight diffusion of the diffraction lines commences and the relative intensity of the far lines diminishes. With further increase in temperature, disappearance of the far lines is observed and at the melting point only a few diffuse rings are left in the small angle region. If the molten film is superheated (by several tens of degrees), the appearance of the diffraction pattern changes and one or two diffuse rings remain.

Two photographs of molten tin were obtained – one at t = 235°C and the other at a temperature approximately 70 °C above the melting point. Figure 1 shows the microphotometer curves of these electron diffraction patterns. The first curve, corresponding to the pattern obtained from the specimen heated to the melting point, shows two clearly defined maxima and two fainter ones. Curve 2 has two relatively intense and strongly diffuse maxima. In addition, between them at the point corresponding approximately to the second maximum of curve 1, a slight increase in intensity can be seen.

The position of the diffraction maxima is shown in Table 1. The table also shows the corresponding values obtained in an x-ray diffraction analysis of molten tin, taken from references [3 and 4], and the position of the lines on electron diffraction patterns of polycrystalline specimens of tin. The table shows that the

• Student V. A. Sivochub assisted in the evaluation of the electron diffraction patterns.

position of the intensity maxima on electron diffraction patterns of molten tin coincide with the mean position of part of the lines on the photographs from polycrystalline tin, which on the whole is in agreement with the results of reference [4].

TABLE 1

Temperature, °C	Position of max sin θ/λ				
	1	2	3	4	5
20 (cryst. phase)	0.172 0.176	0.24 0.25	0.3	0.34	
235 (curve 1, Fig. 1)	0.17	0.24	0.3	0.34	
300 (curve 2, Fig. 1)	0.17	0.24	0.31		
250 [3]	0.174	—	—	0.355	0.49
390	0.175	—	—	0.330	0.50
Melting point [4]	0.17	0.24	—	0.34	

The considerable difference between our data on the position of the interference maxima and the data of reference [3] is possibly due to the fact that in reference [3] the investigation was made at different temperatures (see Table 1).

3. Curves of the radial distribution of the atoms were computed from the data of the electron diffraction diagrams. In this calculation, use was made of the formula

$$4\pi R^2\rho(R) = 4\pi R^2\rho_0 + \frac{2R}{\pi}\int_0^\infty sJ_n(s)\sin sRds, \quad (1)$$

used in x-ray studies of the structure of monatomic liquids. Here $\rho(R)$ is a function of atomic density, ρ_0 the mean density of the atoms.

$$J_n(s) = \frac{J(s)}{Nf^2} - 1, \qquad s = \frac{4\pi\sin\vartheta}{\lambda}, \quad (2)$$

f^2 an atomic factor, which in the case of electron scattering is expressed by

$$f^2 = \frac{(Z - f_p^2)}{s^4},$$

where Z is the order number of the element, and f_p is the atomic amplitude of X-ray scattering.

J(s) in Formula (2) represents the intensity of coherent scattering. The values of J_{exp}, which we can determine from the blackening values after microphotometric measurement of the electron diffraction patterns, represents the sum of the intensities of coherent and noncoherent scattering, i.e.

$$J_{exp} = J_{depend.\ coh.} + J_{indep.\ coh.} + J_{non\text{-}coh.} \quad (3)$$

To perform the calculation, the noncoherent background must be deducted from the experimental curve, and this presents some difficulty for the case of electron scattering.

We shall discuss this problem in more detail.

In reference [5], in calculating the electron diffraction patterns of amorphous antimony for determining the experimental electron scattering curve, the so-called method of blackening curves was used. This comprises obtaining several short exposure photographs from one film with constant intensity of the electron beam. All the photographs are then measured photometrically, and the blackening at a series of points for each exposure is found from the resulting curves. The relative intensities at points on the photometric curves for different values of $\sin\vartheta/\lambda$ are then determined from the blackening curves; these intensity values are then used for constructing an intensity curve, which is subjected to further evaluation.

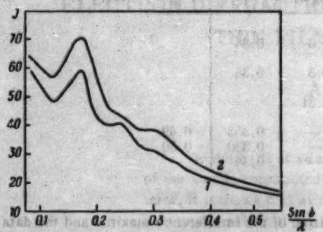

Fig. 1. Photometric curves of electron diffraction diagrams from molten tin: 1) for t = 235°C, 2) for t = 300°C.

The authors ignored the correction for the noncoherent background, and used the curve obtained as a curve of coherent scattering. As will be seen from the reference cited, such a method of finding the I(s) curve gives satisfactory results and may be used successfully, but is very cumbersome. It is not very acceptable, particularly in the study of molten substances, since considerable difficulties are involved in making a series of photographs at different exposures under the same conditions.

We used several methods for finding the curve of coherent scattering. In all these methods, the electron diffraction patterns were photographed with exposures giving a linear relationship between blackening and intensity, this being confirmed specially by experiments on electron diffraction patterns from polycrystalline specimens. Therefore, after the microphotometer measurements, the experimental intensity curves were obtained (on a corresponding scale). We proceeded further as follows.

1) Due to the fact that the presence of only a short-range order is inherent in the liquid state, well-pronounced diffraction maxima are observed on electron diffraction patterns only at small angles. The intensity of the electron rays scattered by the liquid at large angles ϑ, where interference maxima are already poorly distinguished, ought to tend to a mean intensity, corresponding entirely to the disordered arrangement of the particles. Starting from this, we may write

$$\frac{J_1 - J_x}{f_1^2} = \frac{J_2 - J_x}{f_2^2}, \qquad (4)$$

where J_1 and J_2 are the intensities at two adjacent points taken from the experimental curve at large angles, where interference maxima do not appear; J_X is the noncoherent background; $J_{exp} - J_X$ represents the value of the independent coherent scattering; f_1^2 and f_2^2 are atomic factors of electron scattering corresponding to appropriate values of $\frac{\sin\vartheta}{\lambda}$.

Thus, the value of the noncoherent scattering at the selected point $\frac{\sin\vartheta}{\lambda}$ was found from (4). Deducting J_x from the experimental value of the intensity at that point, we obtain the intensity of the independent coherent scattering, $J_{indep.\ coh.}$ at the given point. By means of $J_{indep.\ coh.}$ obtained for one value of $\frac{\sin\vartheta}{\lambda}$, the independent coherent scattering for all the other points was obtained by multiplying $J_{indep.\ coh.}$ by a series of corresponding values of f^2. Further, the so-called dependent coherent scattering, to which the appearance of interference maxima is due, was calculated. For this purpose, a smooth background line was drawn beneath the maxima of the experimental curve. The height of the maximum at each point reckoned in units of

the scale from the line drawn gives the value of the dependent coherent scattering at the corresponding point. By adding the dependent and independent coherent scattering together for each value of s, we obtain the curve of total coherent scattering $J(s)$.

2) An experimental method was also used for separating the noncoherent background. This consisted in obtaining in the same conditions electron diffraction patterns from molten films and from films obtained by rapid cooling from the melting point to room temperature. The latter were found to be single crystal films [1]. The curve of the noncoherent background was also obtained from them.

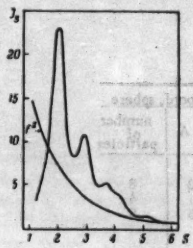

Fig. 2. Intensity curve for molten tin at 235°C.

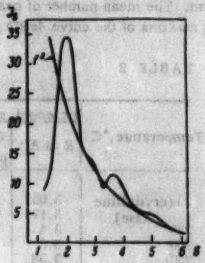

Fig. 3. Intensity curve for molten tin at 300°C.

3) Noncoherent scattering was also found directly from the curve obtained by microphotometer measurement of the electron diffraction patterns from molten tin by means of the relationship

$$\frac{J_{tot}}{J_{non\text{-}coh.}} = \frac{f^2 + S/s^4}{S/s^4},$$

where S is a function of the noncoherent background [6]. By means of this formula, the intensity of noncoherent scattering can be calculated for a point where there are no interference maxima, and then using the calculated relation [6] S/Z as a function of the quantity $v = [s \cdot 0{,}176] \cdot z^{-2/3}$ or the relations used in the x-ray examination of liquids [3], the curve of noncoherent scattering is obtained in the entire range of angles.

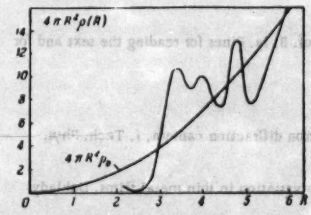

Fig. 4. Function of radial distribution for tin at 235°C

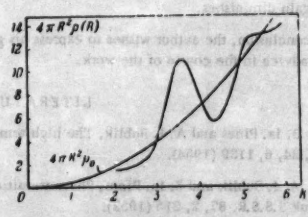

Fig. 5. Function of radial distribution for tin at 300°C

Satisfactory results in the calculation of the noncoherent background were obtained by means of the second and third methods. The first method can also be used, but it sometimes leads to considerable errors.

4) The $J(s)$ curves obtained after deducting noncoherent scattering from the experimental curves are shown in Figs. 2 and 3. These figures also show the form of the curve of atomic scattering f^2.

To obtain $J_n(s)$ [see Formula (2)], $J(s)$ was normalized according to Nf^2. Integration was performed graphically, R being taken from 1 to 7.5 A by steps of 0.25 A.

Figures 4 and 5 show the function of radial distribution, calculated for molten tin. The curves of mean atomic density have been drawn in. The figures clearly show that the structure of molten tin changes considerably with increase in temperature. On the curve of Fig. 4, constructed for molten tin at the melting point, three maxima are clearly to be seen, whereas on the curve of Fig. 5 corresponding to tin at 300°C, there is one diffuse maximum. The mean number of nearest neighbors round a given fixed atom was determined from the areas below the maxima of the curve $4\pi R^2\rho$ (R).

TABLE 2

Temperature, °C	1st coord. sphere		2nd coord. sphere		3rd coord. sphere	
	R in A	number of particles	R in A	number of particles	R in A	number of particles
20 (crystalline phase)	3.05	4	3.78	4	4.42	8
	3.17	2			4.91	4
235	3.4	7	3.95	6	4.75	8
300	3.6	11,5				
250	3.38	10				
390 [3]	3.36	8,9				

Table 2 gives the qualitative data obtained by us for the structure of molten tin. It also gives the number of particles in the nearest coordination spheres for crystalline and molten tin taken from reference [3].

5) The data of Table 2 show that the same order in the arrangement of the particles exists in molten tin as in crystalline tin.

This order remains not only at the closest distances but at more remote distances. The difference is that in tin, even at the melting point, there occurs some redistribution of the particles and a slight increase in the distance between them. At 300°C short-range order only is observed in tin with a quantity of particles corresponding to very close packing.

If our results are compared with data obtained in x-ray studies [3] (see Table 2), it may be concluded that the structure of molten tin varies as follows with increase in temperature: at the melting point, the structure is close to that of (white) tin in the solid state; with increase in temperature, the arrangement of the atoms tends to very close packing (which is reached at $t \approx 300$°C); on further increase in temperature, the distribution density again diminishes.

In conclusion, the author wishes to express his gratitude to Prof. B. Ia. Pines for reading the text and for valuable advice in the course of the work.

LITERATURE CITED

[1] B. Ia. Pines and A. I. Bublik, The high temperature electron diffraction camera, J. Tech. Phys. (U.S.S.R), 24, 6, 1139 (1954).

[2] A. I. Bublik and B. Ia. Pines, Phase transition in thickness variation in thin metal films, Doklady Akad. Nauk S.S.S.R. 87, 2, 215 (1952).

[3] N. S. Gingrich, X-ray diffraction of liquid elements. Uspekhi Khim. 15, 3, 297 (1946).

[4] A. I. Danilova, V. I. Danilov and E. Z. Spektor, "The order character of the atomic structure of molten metals," Problems of Metallography and the Physics of Metals [in Russian] (1952) p. 342.

[5] L. I. Tartarinova and Z. G. Pinsker, "Electron diffraction study of amorphous antimony by Fourier analysis of the intensity curve," Doklady Akad. Nauk S.S.S.R. 87, 2, 265 (1954).

[6] L. Bewilogua, "Über die inkohärente Streuung der Röntgenstrahlen", Phys. Zeitschrift, 32, 740 (1931).

A. M. Gor'kii Kharkov State University

Received June 30, 1956

DETERMINATION OF THE RADIAL-DISTRIBUTION FUNCTION FOR ATOMS IN A LIQUID METALLIC ALLOY FROM ELECTRON-DIFFRACTION DATA

A. I. Bublik and A. G. Buntar'

1. In references [1] and [2] were described the results of an electron-diffraction study of the structure of liquid Sn, Al and Bi at various temperatures. It was shown that at the melting point the arrangement of the atoms in molten tin, aluminum and bismuth is essentially the same as that in the crystalline state of these metals. Moreover the arrangement of atoms appears to be identical not only in the first coordination sphere, but also at greater distances. With rise of temperature of the liquid metals, a change of structure is observed at a few tens of degrees above the melting point: in Al a decrease takes place in the number of particles in the first coordination sphere, while in Sn and Bi the arrangement of the atoms approximates to close packing. On further rise in temperature the density of the arrangement of atoms decreases again and at considerable superheat it approximates to the mean density.

These data were obtained from an analysis of the curves for the radial distribution of the atoms. In calculating the curves use was made of the formula

$$4\pi R^2\rho(R) = 4\pi R^2\rho_0 + \frac{2R}{\pi}\int_0^\infty s\left(\frac{I(s)}{NF^2} - 1\right)\sin sR\,ds, \qquad (1)$$

which is used in the x-ray study of monatomic liquids and amorphous solids. In our case, in place of the x-ray atomic factor F^2 we substituted in the formula the atomic factor for electron scattering

$$f^2 = \left(\frac{Z - F}{s^2}\right)^2, \qquad (2)$$

where Z is the atomic number of the element and

$$s = \frac{4\pi\sin\Phi}{\lambda}.$$

If a molecular material consisting of various kinds of atoms or molecules is being studied, the calculation becomes more complicated. By considering the distribution of electrons instead of the distribution of atoms and by introducing the "mean scattering function" for x-rays by a single electron in the molecule, f_e, determined by the relationship

$$f_e = \sum\frac{F_m}{\Sigma Z_m}, \qquad (3)$$

where F_m is the atomic scattering amplitude for x-rays by an atom of the kind m and Z_m is the number of electrons in an atom of m, the authors of reference [3] obtained the formula

$$\sum k_m 4\pi R^2\rho_m(R) = \sum k_m 4\pi R^2\rho_0 + \frac{2R}{\pi}\int_0^\infty si(s)\sin sR\,ds.$$

Here $i(s) = \frac{I'(s) - \Sigma F_m^2}{f_e^2}$, $k_m = \frac{F_m}{f_e}$ is the effective number of scattering electrons in an atom of m and $I'(s)$ is the experimental value of the intensity. Equation (4) is widely used nowadays in x-ray studies of the structure of liquid molecular compounds, aqueous solutions, etc. [4, 5].

As regards the electron-diffraction study of liquids, so far as we know the evaluation of an electron-diffraction photograph from a liquid alloy has not hitherto been carried out.

In the present paper a relationship is discovered, analogous to Equation (4), for the case of electron scattering, which is applicable to the construction of the radial-distribution curve for atoms in a liquid metallic alloy from electron-diffraction data.

2. Let us consider the scattering of electrons in a liquid alloy of any composition, consisting of atoms of several kinds. If f_p is the atomic amplitude of electron scattering by an atom of p, then the relative intensity of scattering, as in the case of x-rays, can be written

$$I(s) = \sum_p f_p^2 + \sum_{p \neq q} \sum f_p f_q \frac{\sin sr_{pq}}{sr_{pq}}, \tag{5}$$

where $f_p = \frac{Z_p - F_p}{s^2}$.

We shall take into consideration a certain quantity φ, determined from the relationship

$$\varphi = \frac{\sum_p f_p}{\sum_p Z_p}, \tag{6}$$

where Z_p is the atomic number of the atom p. Summation here is carried out with respect to all atoms of the scattering volume. The quantity φ represents a certain mean scattering capacity of the system proton-electron (imaginary scattering particles) in the alloy under consideration.

The ratio

$$k'_p = \frac{f_p}{\varphi} \tag{7}$$

will represent the "effective" number of imaginary scattering centers contained in an atom of p. Averaging this quantity with respect to all angles, we obtain the mean "effective" number of imaginary particles k_p.

In this case the binary sum (5) for the relative intensity of electron scattering by an alloy containing atoms of several kinds can be written as follows:

$$A = \varphi^2 \sum_p k_p \left\{ \sum_a k_a \frac{\sin sr_{pa}}{sr_{pa}} + \sum_b k_b \frac{\sin sr_{pb}}{sr_{pb}} + \cdots + \sum k_n \frac{\sin sr_{pn}}{sr_{pn}} \right\}, \tag{8}$$

Since in a liquid the atoms may be situated at any distances, the summation must be replaced by integration with respect to r. For this purpose we shall introduce the radial-distribution function for atoms $\rho'_m(r)$, determined as usual by the condition: $4\pi r^2 \rho'_m(r) dr$ atoms of the m kind occur at a distance between r and r + dr from the given atom.

Then

$$A = \varphi^2 \sum_p k_p \left\{ 4\pi \int_0^L r^2 \rho'_a(r) k_a \frac{\sin sr}{sr} dr + \right.$$

$$\left. + 4\pi \int_0^L r^2 \rho'_b(r) k_b \frac{\sin sr}{sr} dr + \cdots\cdots + 4\pi \int_0^L r^2 \rho'_n(r) \frac{\sin sr}{sr} dr \right\}. \tag{9}$$

Here $\rho_m^r(r)k_m = \rho_m(r)$ represents the density of imaginary particles of the m kind.

After carrying out the corresponding transformations in Formula (9), we obtain the following expression for the intensity of scattering of electron waves by a liquid alloy:

$$I(s) = I_0(s) + I_g(s) + N\varphi^2 \int_0^\infty 4\pi r^2 k_{al}[\rho_{al}(r) - \rho_{0al}] \frac{\sin sr}{sr} dr, \quad (10)$$

where

$$k_{al} = C_a k_a + C_b k_b + \cdots + C_n k_n,$$

$$\rho_{al}(r) = \rho_a(r) + \rho_b(r) + \cdots + \rho_n(r)$$

$$\rho_{0al} = \rho_{0a} + \rho_{0b} + \cdots + \rho_{0n}$$

$$I_g(s) = \sum_p f_p^2 = C_a N f_a^2 + C_b N f_b^2 + \cdots + C_n N f_n^2,$$

C_m is the atomic concentration of the components in the alloy, N is the total number of atoms in the scattering volume, $I_0 = \int_0^L 4\pi r^2 \rho_{0al} \frac{\sin sr}{sr} dr$ is the so-called "zero" scattering (i.e., the scattering which depends on the size and shape of the specimen), which differs significantly from zero only at small scattering angles. It is possible to make an approximate allowance for it by extrapolating the experimental intensity curve to zero [6]. Equation (10) can be rewritten as

$$i(s) = \frac{I(s) - I_0(s) - I_n(s)}{N\varphi^2} = \int_0^\infty 4\pi r^2 k_{al}[\rho_{al}(r) - \rho_{0al}] \frac{\sin sr}{sr} dr.$$

Applying the theorem of the Fourier integral, we obtain

$$4\pi r^2 k_{al}\rho_{al}(r) = 4\pi r^2 k_{al}\rho_{0al} + \frac{2r}{\pi}\int_0^\infty si(s)\sin(sr)\,ds. \quad (11)$$

3. We have used Formula (11) to calculate the curve for the radial distribution of atoms in a liquid (at 520°C) Al – Sn alloy (60% Al and 40% Sn). The calculation was made based on an electron-diffraction photograph taken from an unsupported liquid film of the alloy, 3×10^{-6} cm thick, obtained by evaporation and condensation of the metals in vacuo. Melting was carried out in the electron-diffraction camera itself [7]. The concentration of the components in the alloy was calculated from weighing data [8].

The electron-diffraction photograph was photometered on a MF-2 microphotometer, and from the blackening values an experimental intensity curve was constructed from which the incoherent scattering was then calculated by means of the ratios:

$$\frac{I_{inc}}{I_{tot}} = \frac{S/s^4}{\Sigma f_p^2 + S/s^4}; \quad \frac{I_{inc}}{I_{coh}} = \frac{S/s^4}{\Sigma f_p^2}; \quad \frac{I_{coh}}{I_{tot}} = \frac{\Sigma f_p^2}{\Sigma f_p^2 + S/s^4}.$$

Here S is the inelastic electron scattering function [9].

For the alloy we used: $S = C_{Al}S_{Al} + C_{Sn}S_{Sn}$, where C_{Al} and C_{Sn} are the atomic concentrations of the

components; $\sum f_p^2 = C_{Al} f_{Al}^2 + C_{Sn} f_{Sn}^2$ (the atomic scattering factor for electrons by the alloy).

The coherent scattering curve obtained in this way was combined with the curve for the atomic factor of the alloy and the following function calculated:

$$i(s) = \frac{I'(s) - \Sigma f_p^2}{N\varphi^2} = \frac{I'(s)/N - (C_{Al} f_{Al}^2 + C_{Sn} f_{Sn}^2)}{\varphi^2}.$$

After integrating, which was carried out with the help of special tables (strips), the radial-distribution curve shown in Fig. 1 was obtained. There is a clearly defined maximum at $R_1 = 2.7$ A and two superimposed maxima in the region 3-4 A. The position of the first maximum agrees well with the value for the smallest distance between the atoms in liquid aluminum [2], while the position of one of the two superimposed maxima ($R_2 = 3.4$ A) corresponds to the most probable distance between atoms in liquid tin [1]. The third peak on the radial-distribution curve occupies an intermediate position between the first two, its value $R = 3.05$ A being equal to the arithmetic mean of R_1 and R_2. Hence it is natural to assume that it corresponds to the distances between the unlike (Al-Sn) atoms in the liquid alloy.

Under the radial-distribution curve are shown the separate areas corresponding to all three maxima and from these the number of nearest neighbors has been calculated. The area under the maximum is determined by means of an expression of the form $S_{ij} = 2C_i k_i k_j n_{ij}$ and from that the number of neighbors is found from the relationships:

1) Al — Al $\quad n_{11} = \dfrac{S_1}{2k_{Al}^2 C_{Al}}$ $\qquad$ 3) Sn — Sn $\quad n_{22} = \dfrac{S_2}{2k_{Sn}^2 C_{Sn}}$

2) Al — Sn $\quad n_{12} = \dfrac{S_2}{2k_{Al} \cdot k_{Sn} C_{Al}}$ $\qquad$ 4) Sn — Al $\quad n_{21} = \dfrac{S_2}{2k_{Al} k_{Sn} C_{Sn}}$

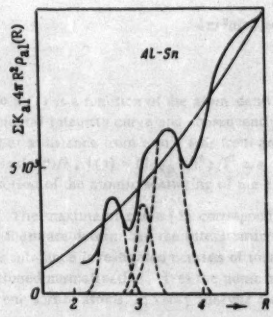

Fig. 1

TABLE

Alloy	No. of maxima	Type of alloy	Distance, A	No. of neighbors
Al — Sn (60% Al)	1	Al — Al	2.70	10.0
	2	Sn — Sn	3.40	6.2
	3 { 3′	Al — Sn	3.05	1.0
	3 { 3″	Sn — Al	3.05	1.5—1.6

In our case k_{Sn} and k_{Al} proved to be 45.0 and 16.35, respectively.

From the calculation it was established that on the average there are (see the table) 10.0 Al atoms and 1.0 Sn atoms per aluminum atom and 6.2 Sn and 1.5 Al atoms per tin atom.

From the data presented above it follows that complete mixing of the atoms is not observed in liquid Al — Sn films at the melting point. The presence on the radial-distribution curve of large maxima at distances corresponding to the most probable distances in pure liquid aluminum and tin indicates that in the liquid alloy studied there are regions where the atoms of each component are surrounded by neighbors of the same kind.

LITERATURE CITED

[1] A. I. Bublik, "Electron-diffraction study of thin liquid tin films," Kristallografiia 2, 2, 249-254 (1957) [present issue, translation page 240].

[2] A. I. Bublik and A. G. Buntar, "Determination of the distribution density of atoms in liquid Al and Bi at various temperatures from electron-diffraction data," Fiz. Metal. i Metalloved. (in the press).

[3] B. E. Warren, H. Krutter, and O. Morningstar," Fourier analysis of x-ray patterns of vitreous SiO_2 and B_2O_3," J. Am. Ceram. Soc. 19, 202 (1936).

[4] V. I. Danilov and A. F. Skryshevskii, "On the application of the integral analysis of intensity curves to the study of liquid structures," Voprosy Fiz. Metal. i Metallovedenie, 3, 63 (1952).

[5] A. F. Skryshevskii, A. V. Romanova, and V. I. Danilov, "X-ray study of aqueous NaOH and KOH solutions," Voprosy Fiz. Metal. i Metalloved. 3, 73 (1952).

[6] V. I. Filipovich, "On the theory of x-ray scattering in gases, liquids, amorphous solids and polycrystals I." J. Tech. Phys. (USSR) 25, 1604 (1955).

[7] B. Ia. Pines and A. I. Bublik, "High-temperature electron-diffraction camera," J. Tech. Phys. (USSR) 24, 6, 1139 (1954).

[8] S. A. Vekshinskii, A New Method for the Metallographic Investigation of Alloys [In Russian] (1944).

[9] Z. G. Pinsker, Electron Diffraction [In Russian] (1949) p. 289.

A. M. Gor'kii State University
Kharkov

Received October 3, 1956

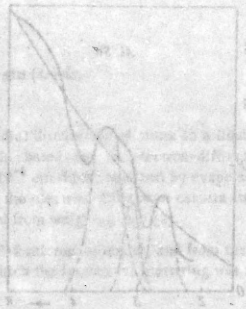

ELECTRON DIFFRACTION STUDY OF AMORPHOUS ANTIMONY SULFIDE

L. I. Tatarinova

The method of integral analysis has been applied to the study of the semiconductor compound Sb_2S_3. The curve of experimental intensity has been normalized by comparison of the areas $I(s)\cdot s^2$ and $\sum_m \sum_m f_m^2(s)\cdot s^2$. The function of scattering of the lighter atom, i.e., the sulfur atom, has been selected as unit function; the relative weights K_i of the atoms in the investigated compound have been determined. The following interatomic distances have been found from the radial distribution curve: $r_1 = 2.33$ A, $r_2 = 3.42$ A, $r_3 \sim 4.0$ A. It has been established that there are 5.7 sulfur atoms around an antimony atom and 3.8 antimony atoms around a sulfur atom, which provides a basis for the supposition that the atoms in the amorphous phase of Sb_2S_3 tend to an arrangement in the form of a closed-packed structure.

1. In the x-ray and electron diffraction study of amorphous substances, use is made of the method of the integral analysis of the experimental intensity curve obtained from x-ray or electron diffraction patterns. As a result of the analysis, the curve of radial distribution of the atoms is obtained according to the equation

$$4\pi r^2 u(r) = 4\pi r^2 u_0 + \frac{2r}{\pi}\int_0^\infty si(s)\sin srds, \qquad (1)$$

where u (r) is a function of the atom density, determined from the condition that for normalization of the experimental intensity curve and consequently of i (s), $4\pi r^2 u(r)$ is the mean number of atoms in a spherical layer at a distance from r to r + dr from any selected atom; u_0 is the mean number of atoms in unit volume, $s = (4\pi \sin \vartheta)/\lambda$, $i(s) = (I_{exp} - f^2)/f^2$ are quantities determined from the experimental intensity curve; f is a function of the atomic scattering of the electrons.

The maxima of curve (1) correspond to the existence of a short-range order in the amorphous substance; from them are determined the interatomic distances and the number of nearest neighbors round any given atom. If the substance investigated consists of identical atoms, the area below the peaks of curve (1), after the above-mentioned normalization, gives the number of neighbors directly. If, however, the substance contains more than one sort of atoms, in x-ray analysis a certain mean function of the distance to one electron is introduced:

$$f_e = \sum_m f_m / \sum_m Z_m,$$

by means of which the scattering function f_m of each atom is determined as

$$f_m = K_m \cdot f_e;$$

K_m being the effective number of electrons in the atom, a magnitude which is constant for the given atom. Expression (1) assumes the form

$$4\pi r^2 \sum_m K_m u_m(r) = 4\pi r^2 u_0 \sum_m K_m + \frac{2r}{\pi} \int_0^\infty si(s) \sin sr\, ds, \tag{2}$$

where

$$i(s) = \frac{I_{exp} - \sum_m f_m^2}{f_e^2}. \tag{3}$$

In x-ray analysis I_{exp} after normalization is expressed in electron units. In the case of complex compounds, the areas below the maxima have to be interpreted as twice the product of the numbers of electrons of those atoms which are connected to each other by the given distance r.

In electron diffraction analysis, integral analysis has been used so far only for the study of substances consisting of the same atoms [1, 2]. In this case, the experimental intensity curve is normalized for one atom according to the curve of the atomic factor f^2. The maxima of curve (1) are interpreted, as in x-ray analysis, as the number of neighbors surrounding any selected atom.

B. K. Vainshtein [3], discussing the theory of the radial distribution method, shows that it is possible to employ integral analysis for the electron diffraction study of amorphous substances containing different kinds of atoms; he examines the significance of the subtraction of $\sum_m f_m^2$ in Formula (3) as well as the division by the unit curve f_u^2. The former eliminates the peak at the origin, analogous to that in Patterson's function in the examination of crystalline substances. Division by the unit curve f_u^2 is analogous to the elimination of the trough in the I (s) curve.

In x-ray analysis, the unit selected is the scattering of the x-rays by an electron, in accordance with which the units are termed electronic units. Such a choice, however, is not obligatory, especially since the values of K_i are not integral values in electronic units. The relative values of K_i of the scattering powers of the atoms are alone important. As unit function, therefore, it is possible to select the atomic scattering function of any atom forming part of the substance investigated, for example, the lightest (f_1^2). B. K. Vainshtein [4] shows that the calculation of the K_i values should take into account the values of f_i^2 in the entire volume of the reciprocal space, which leads to the formula

$$\frac{\int f_i^2(s) \cdot s^2 ds}{\int f_j^2(s)\, s^2 ds} = \frac{\sum_s f_i^2(s) \cdot s^2}{\sum_s f_j^2(s) \cdot s^2} = K_i^2, \tag{4}$$

integration being replaced by summation. In performing the calculation, the values of the atomic factors are taken within the experimentally determined limits (sin ϑ)/λ or s.

A more general form of the dependence of K_i upon the atomic number may be found. In the above-mentioned reference [4] it is shown that in x-ray and electron diffraction analysis, the integrals in (4) are proportional to Z^α, where Z is the atomic number:

$$\alpha_{x\text{-ray}} = 2.66, \quad \alpha_{el} = 1.50. \tag{5}$$

By determining K_i with respect to the lightest atom "1," we find from (4) and (5) that

$$K_{x\text{-ray}} = (Z_i/Z_1)^{1.3}; \quad K_{el} = (Z_i/Z_1)^{0.75}. \tag{6}$$

The unit curve f_u^2 is naturally determined as the sum f_m^2 of the curves of all the atoms divided by the sum of K_m^2:

$$f_u^2 = \sum_m f_m^2 / \sum_m K_m^2.$$

Expression (3) for the calculation of i(s) finally assumes the form

$$i(s) = \frac{I_n - \sum_m f_m^2}{f_u^2} = \sum_m K_m^2 \left(\frac{I_n}{\sum_m f_m^2} - 1 \right).$$

Here I_n are the normalized values of the experimental intensity.

In x-ray work, the method adopted for normalizing the experimental intensity curve according to the atomic factor curve is to superimpose both curves for large values of $(\sin \Phi)/\lambda$ or s. The disadvantage of such a method of normalizing is the large error in determining the values of both curves in this region of s. The above-mentioned reference [4] proposes the method of normalizing by equating the areas below the curves $\sum_m f_m^2(s) \cdot s^2$ and $I_e(s) \cdot s^2$. This method of normalizing does not suffer from the above-mentioned disadvantage. It is merely necessary to endeavor to cover, as far as possible, large values of s.

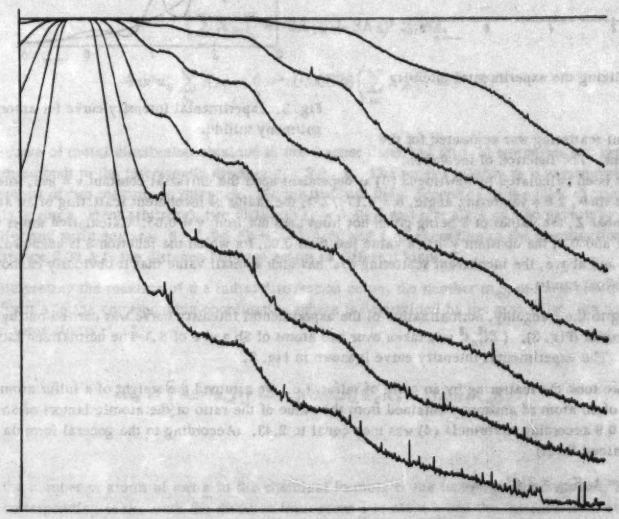

Fig. 1. Microphotometric curves from electron diffraction patterns of Sb_2S_3.

3. The electron diffraction study of amorphous substances is confined to the investigation of molecules in vapors or gases, and is principally carried out either by a method of trial and error or by the radial distribution method of Pauling and Brockway [5].

Direct methods of investigation are limited to a study of simple substances (one sort of atoms) or are developed on the basis of the use of a rotating sector. A method will now be described for evaluating an electron diffraction pattern obtained in an electron diffraction camera under normal conditions.

The compound Sb_2S_3 was selected for the investigation. The atomic numbers are: $Z_{Sb} = 51$, $Z_S = 16$. Amorphous films of Sb_2S_3 were produced on a celluloid support by sublimation in a vacuum.

Six short-exposure electron diffraction patterns of the films were obtained. The electron diffraction patterns were measured by means of an MF-4 microphotometer (Fig. 1). The blackening curves were then constructed and from them the experimental intensity curve was constructed in the usual way.

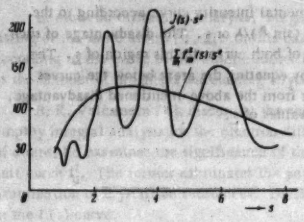

Fig. 2. Normalizing the experimental intensity curve.

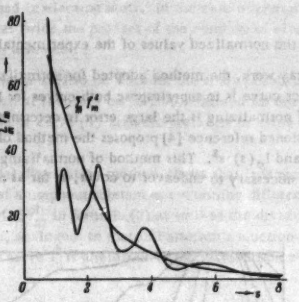

Fig. 3. Experimental intensity curve for amorphous antimony sulfide.

Incoherent scattering was neglected for the following reasons. The function of incoherent scattering S has been calculated by Bewilogua [6] as dependent upon the universal constant $v = ksb$, where $k = 2\pi/\lambda$, $s = 2\sin\vartheta$, 2ϑ = scattering angle, $b = 0.176/Z^{2/3}$, the radius of incoherent scattering of an atom with the atomic number Z, the values of S being given not from zero but from $v = 0.05$. Calculation shows that for $(\sin\vartheta)/\lambda = 0.1$ and 0.2, the constant v has a value less than 0.05, for which the function S is unknown. For $(\sin\vartheta)/\lambda = 0.3$ and above, the incoherent scattering S/s^4 has such a small value that it obviously cannot appreciably affect the final results.

According to the foregoing, normalization of the experimental intensity curve was carried out by comparing the two areas (Fig. 2). ($\Sigma f_m^2 s^2$ was taken over two atoms of Sb and 3 of S.) The normalized factor was equal to 13.68. The experimental intensity curve is shown in Fig. 3.

As unit, we took the scattering by an atom of sulfur, i.e., we assumed the weight of a sulfur atom to be 1. The weight of an atom of antimony obtained from the value of the ratio of the atomic factors of Sb and S for $(\sin\vartheta)/\lambda = 0.9$ according to formula (4) was then equal to 2.43. (According to the general formula (6) we would have obtained 2.38.)

Thus, $K_S = 1$, $K_{Sb} = 2.43$.

$$\sum_m K_m^2 = 3\cdot 1^2 + 2\cdot 2.43^2 = 14.8.$$

$$f_u^2 = \frac{\sum_m f_m^2}{\sum_m K_m^2} = \frac{\sum_m f_m^2}{14.8},$$

i.e.,

$$i(s) = 14.8\left(\frac{I_n}{\sum_m f_m^2} - 1\right).$$

Having determined the value of i(s), we found the curve of si(s) (Fig. 4).

The calculation of the integral in Formula (2) was performed by an algebraic method [2] by summation of a large number of terms through equal intervals of the region s utilized.

The first term on the right-hand side of Equation (2) was calculated with the use of the value for the density of crystalline antimonite d = 4.64 g/cc:

$$n_0 = \frac{d}{M \cdot m_H} = 0.00828 \sum_m K_m \frac{1}{A^3}.$$

Since we are seeking the number of atoms of the assumed weight in unit volume, the factor is here $\sum_m K_m$. Consequently, in the first term of Equation (2), containing n_0, this factor is squared: $\left(\sum_m K_m\right)^2$. M is the molecular weight of Sb_2S_3, $m_H = 1.65 \cdot 10^{-24}$ g, the weight of an atom of hydrogen.

$$\left(\sum_m K_m\right)^2 = (2K_{Sb} + 3K_S)^2 \cong 62,$$

$$4\pi r^2 n_0 \sum_m K_m = 4\pi r^2 \cdot 0.00828 \left(\sum_m K_m\right)^2 = 6.45\, r^2.$$

The curve of radial distribution obtained in the manner described (Fig. 5) comprises two isolated maxima. The first corresponds to the interatomic distance r_1 = 2.33 A. The second maximum is asymmetrical indicating the presence of two maxima in this peak. Having resolved them according to the rules of geometrical analysis (which is to some extent arbitrary), two distances r_2 = 3.42 A and $r_3 \sim$ 4.0 A can be detected. The atomic radii of sulfur and antimony are: S – 1.04; Sb – 1.34, 1.56 and 1.61 according to the coordination. It is clear that the distance 2,33 A is the distance between atoms of different kinds.

In interpreting the maxima of the radial distribution curve, the number m_{ab} of neighbors of sort b round an atom of sort a in the corresponding coordination sphere is determined by the area below the peak $4\pi r^2 n_{ab} \cdot (r - r_{ab})$ in some limits r', r'':

$$m_{ab} = \int_{r'}^{r''} 4\pi r^2 n_{ab}(r - r_{ab})\, dr / 2n_a K_a K_b = S/2n_a K_a K_b. \qquad (7)$$

Here n_a is the number of atoms of sort a in the chemical formula of the investigated compound; S is the area below the corresponding peak. Both the distance from atom a to atom b and the distance from atom b to atom a are reflected in each peak; 2 therefore appears in the denominator.

Since, by reason of stoichiometry,

$$m_{ab} n_a = m_{ba} n_b, \qquad (8)$$

it is easy to find m_{ba} also from (7).

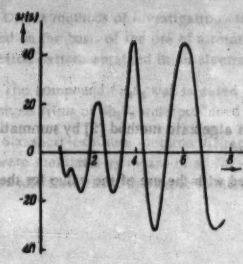

Fig. 4. Curve of si(s).

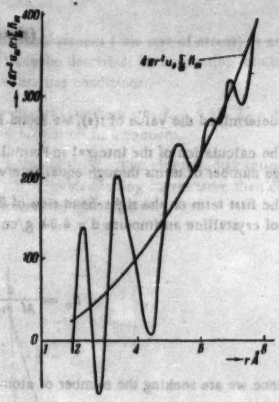

Fig. 5. Curve of radial distribution of amorphous Sb_2S_3.

The area below the first peak of the radial distribution curve $S_1 = 55.3$. To determine the number of sulfur atoms round an antimony atom, we have

$$n_{Sb} = 2. \quad n_S = 3,$$

$$K_{Sb} = 2.43; \quad K_S = 1.$$

According to (7), we have

$$m_{SbS} = 55.3/2 \cdot 2 \cdot 2.43 \cdot 1 = 5.7,$$

i.e., there are about 6 sulfur atoms round one antimony atom. In exactly the same way, we find from (7) or (8)

$$m_{SbS} = 55.3/2 \cdot 3 \cdot 2.43 \cdot 1 = 3.8 = \frac{5.7}{3/2}.$$

Consequently, each sulfur atom is surrounded by about 4 antimony atoms.

We have dealt specifically with the question as to the accuracy of the results obtained. In some x-ray studies, it was found that, depending upon the method of normalizing the experimental intensity curve for different values of $(\sin\vartheta)/\lambda$, the position of the first maximum on the radial distribution curves does not vary by more than $1 - 1/2$ % and the area below it by 10%. In the present investigation, using the normalization method described, this source of error is eliminated. The intensities were measured with an accuracy of not less than 5%.

In crystalline antimonite [7], each of the two Sb atoms is surrounded by three S atoms, forming in one case an equilateral triangle and in the other an approximately equilateral triangle. The closest distances Sb – S are: 2.33, 2.50, 2.52, 2.67 A. If we also add the distances to the more remote atoms: 2.84, 3.15, 3.16, 3.38, 3.60 A, we obtain a coordination number 7. The structure of the crystalline phase is made up of columns of octahedra connected in tetrad chains with columns of polyhedra having the coordination number 7 [8].

Thus, the coordination in amorphous antimony sulfide is different from that in the crystalline sulfide. It should be pointed out that a number of compounds of the type A_2B_3 (for example Sb_2S_3) are constructed on a close packing basis and have coordination numbers 6 and 4. It is also known that for some metals, such as

for example Hg, Sn, Zn, close packing is characteristic in the liquid state. This suggests that, similarly, the atoms of amorphous Sb_2S_3 tend to a close packing.

In the ideal closest packing of sulfur atoms, the antimony atoms being accommodated in 2/3 of the octahedral cavities, each Sb atom would be surrounded by 6 sulfur atoms. The structure of the amorphous phase is, however, loose. In agreement with this, in the first coordination group, the Sb atom is surrounded not by 6 S atoms, but by less, namely 5.7. In the case of closest packing, the Sb atom would be at the center of an octahedron at a distance of 2.33 A from the S atoms; in such a case, the side of the octahedron ought to be equal to $2.33\sqrt{2} = 3.30$ A. The second distance obtained from the radial distribution curve, 3.42 A, is close to this value and confirms the accuracy of the model in the form of a loose close packing; the increase in this distance compared with the distance in close packing may be understood if it is borne in mind that 5.7 neighbors around a given atom are, on the average, situated further apart than 6 neighbors, i.e., in simple language, the closeness of packing diminishes with decrease in the coordination number.

All possible combinations of distances between the atoms of the substance investigated may be represented in the second peak, namely: 1) Sb – Sb, 2) S – S, 3) Sb – S. Each of these distances contributes to the size of the area below the peak:

$$1)\ 2n_1 \cdot 2.43^2 \cdot 2 = 23.6n_1,$$

$$2)\ 2n_2 \cdot 1^2 \cdot 3 = 6.0n_2,$$

$$3)\ 2n_3 \cdot 2.43 \cdot 1 = 4.86n_3.$$

The area below the second peak of the radial distribution curve is approximately equal to 100; the total area below the second and third maxima is equal to 159.2. It is possible to select different combinations of the distances written above which satisfy experiment (numerically). For example, four distances Sb – Sb and one S – S, three Sb – Sb and three S – S; two Sb – Sb, eight S – S and one Sb – S, etc. A number of these combinations may be at once eliminated as being incompatible with the proposed grouping of the atoms in the amorphous phase.

In the case of close packing, like atoms only can be located in the 2nd coordination sphere. Consideration of cubic and hexagonal close packing shows that cubic packing is less appropriate in the case of Sb_2S_3.

In hexagonal very close packing, at a distance of 3.30A, there would be twelve sulfur atoms around one sulfur atom and six antimony atoms around one antimony atom. In agreement with the formula Sb_2S_3, it will be necessary to take $2/3 \cdot 6 = 4$ of the latter atoms. For the area below the second maximum, calculation gives:

$$2 \cdot 2.43^2 \cdot 4 \cdot 2 + 2 \cdot 1^2 \cdot 12 \cdot 3 = 166.5.$$

It is obvious that below the second and third peaks quite a collection of interatomic distances is represented, of which those of 3.42 and 4.0 A are most strongly in evidence. In close packing, with a distance between the spheres of 2.33 A, the atoms are at a distance of $2.33\sqrt{3} = 4.03$ A from each other in the second coordination sphere. Carrying the analogy further with structures of the type A_2X_3, we find that the number of Sb – Sb distances is 4 and the number of S – S distances is 12. The theoretical area below the 2nd and 3rd maxima of the radial distribution curve is:

$$S_{2,3} = 2 \cdot 2.43^2 \cdot 4 \cdot 2 + 2 \cdot 1^2 \cdot 12 \cdot 3 = 166.5.$$

Experiment gives 159.2. This confirms once more the correctness of the assumption regarding the loose packing of the atoms in amorphous Sb_2S_3.

In conclusion, I should like to express my gratitude to B. K. Vainshtein for constant assistance in the work and interest shown in it.

LITERATURE CITED

[1] L. I. Tatarinova, "Electron diffraction study of amorphous antimony," Trudy Inst. krist. Akad. Nauk SSSR, 11, 104-114 (1955).

[2] L. I. Tatarinova, "Electron diffraction study of amorphous GaSe," Kristallografiia 1, 1, 534-536 (1956).

[3] B. K. Vainshtein, "Theory of the radial distribution method," Kristallografiia 2, 1 (1957) [See Soviet Physics – Crystallography].

[4] B. K. Vainshtein, "Accuracy of the potential Fourier series in electron diffraction analysis," Kristallografiia 1, 5, 495-501 (1956).

[5] L. Pauling and O. Brockway, J. Chem. Phys. 2, 867 (1934).

[6] L. Bewilogua, "Über die inkohärenten Streuung der Röntgenstrahlen," Physik Zeitschift 32, 740 (1931). Physik Z. 32, 740 (1931).

[7] Strukturbericht, Vol. III, p. 49.

[8] H. V. Belov, Structure of Ionic Crystals and Metallic Phases (1947) p. 134.

Institute of Crystallography
Academy of Sciences, USSR

Received December 15, 1956

REFRACTOMETRIC DETERMINATION OF THE STRUCTURE OF COMPLEX COBALT COMPOUNDS

S. S. Batsanov

The geometric configurations and interatomic distances in complex compounds of trivalent cobalt are determined by the refractometric method. The values of coordinate refractions are used for quantitative characterization of the trans-interaction of the atoms.

We have used the refractometric method in a number of previous works [1-6] for the determination of the atomic structure of complex platinum and cobalt compounds. The present work is devoted to a generalization of the results of an optical examination of cobalt compounds.

For the determination of the geometric configuration of the complex, it is sufficient to compare the experimentally measured refraction (refractive indices) with the theoretically calculated values for the different isomeric forms. The interatomic distances in the inner sphere of the complex compounds are calculated from the coordinate refractions. Thus, the measurement and calculation of the molecular refractions is the chief problem in optical determination of the structure of complex compounds.

TABLE 1

Refractions of Cobalt Nitroammines

Compound	M	d_4^{25}	$\bar{n}_{co}$	R_{co}
$[Co(NH_3)_6]Cl_3$	267.50	1.712	1.651	57.06
$[Co(NH_3)_6](NO_3)_3$	347.50	1.807	1.569	63.00
$[Co(NH_3)_4(NO_2)_2]Cl$- cis	254.54	1.903	1.665*	49.67
$[Co(NH_3)_4(NO_2)_2]NO_3$- cis	281.09	1.940	1.640	52.22
$[Co(NH_3)_4(NO_2)_2]Cl$- trans	254.54	1.875	1.663	50.29
$[Co(NH_3)_4(NO_2)_2]NO_3$-trans	281.09	1.948	1.654	52.89
$Co(NH_3)_3(NO_2)_3$	248.07	2.024	1.701	47.42
$K[Co(NH_3)_2(NO_2)_4]$	316.13	2.123	1.660	54.97
$NH_4[Co(NH_3)_2(NO_2)_4]$	295.07	1.970	1.677	56.41
$K_3[Co(NO_2)_6]$	452.28	2.431	1.656	68.35
$(NH_4)_3[Co(NO_2)_6]$	389.11	1.965	1.677	74.57

*Refined values of refractive indices in yellow light equal $n_g = 1.740$, $n_m = 1.719$, $n_p = 1.690$.

In Table 1 are given the results of extrapolations of refractive indices measured by the author earlier [7] (at different wave lengths) and the densities of nitroammonium compounds of trivalent cobalt. The extrapolation of refractive indices was carried out strictly[1] according to the Wulf method [8], and averaging according to the formula

$$\bar{n} = \sqrt[3]{n_g \cdot n_m \cdot n_p}.$$

Moreover, we have synthesized and examined a series of chloroammonium compounds of trivalent cobalt. In Table 2 and 3 are given the experimental data on these substances. The densities and refractive indices (in yellow light) being measured for the first time are marked by an asterisk. Extrapolation to $\lambda = \infty$ was effected here also by the Wulf method [8].

TABLE 2

Dispersion of Refractive Indices of Cobalt Chlorammines

Compound	n	λ, mμ						
		486	520	555	589	620	656	∞
$[Co(NH_3)_5Cl]Cl_2$	n_g	1.736	1.726	1.718	1.711	1.706	1.701	1.660
	n_m	1.724	1.714	1.706	1.699	1.694	1.689	1.648
	n_p	1.712	1.701	1.693	1.686	1.681	1.676	1.636
$[Co(NH_3)_5Cl](NO_3)_2$	n_g	1.679	1.670	1.662	1.655*	1.651	1.647	1.613
	n_m	1.555	1.549	1.544	1.540*	1.537	1.534	1.513
$[Co(NH_3)_4Cl_2]Cl \cdot H_2O$ trans	n_g	1.856	1.844	1.833	1.825*	1.818	1.812	1.753
	n_m	1.755	1.743	1.734	1.726*	1.721	1.716	1.674
	n_p	1.691	1.681	1.674	1.667*	1.663	1.659	1.625
$[Co(NH_3)_4Cl_2]NO_3 \cdot H_2O$ trans	n_g	1.785	1.774	1.765	1.757*	1.751	1.747	1.701
	n_m	1.751	1.739	1.730	1.722*	1.717	1.712	1.670
	n_p	1.571	1.565	1.560	1.556*	1.553	1.550	1.528

The molecular refractions being known, it is possible to calculate the coordinate refractions [9] of the complex compounds of trivalent cobalt. For this, it is necessary to subtract the ionic refractions of Cl^- or NO_3^- [6] from the molecular refraction and to distribute the remainder according to the geometric coordinates of the complex. In the case of a heterogeneous complex, for example $[Co(NH_3)_5Cl]^{+2}$, for calculation of the refraction of the coordinate $Cl - Co - NH_3$ it is sufficient to subtract twice the refraction of the coordinate $NH_3 - Co - NH_3$ from the refraction of the complex ion.

In nitro- and nitrate-ammonium compounds the possibility of the formation of hydrogen bonds $N - H \cdots O$ must also be considered. It is known that hydrogen bonds with oxygen always form under suitable geometric conditions, i.e., at distances of the order 2.7-3.0 A with preservation of the usual valence angles [10]. Considering the tetrahedral direction of the hydrogen bonds, formed by oxygen, and the tetrahedral structure of ammonia it can be assumed that each oxygen atom of the NO_3 group forms only one such bond with the adjoining ammonia. Since each compound tends to yield the maximum number of hydrogen bonds [11], the remaining hydrogen atoms of the ammonia molecules will form bonds with the oxygen atoms of the outer-sphere ions (each NO_3^- ion can form a maximum of 9 hydrogen bonds). The refraction of the hydrogen bond $N - H \cdots O$ with the NO_3^- group equals 0.12 cm^3 and with the NO_3^- ion – 0.04$_5$ cm^3 [12]. In Table 4 are given the coordinate refractions calculated with correction for the maximum number of hydrogen bonds; the refraction of the water of crystallization was equal to 3.42 cm^3 [12].

[1] In a previous work [3], devoted to the examination of cobalt compounds, the simplified graphic extrapolation method is used.

TABLE 3

Refractions of Cobalt Chlorammines

Compound	M	d_4^{20}	$\bar{n}_{\infty}$	R_{∞}
$Co(NH_3)_5Cl$	250.47	1.799	1.647	50.62
$[Co(NH_3)_5Cl](NO_3)_2$	303.57	1.731*	1.545	55.45
$[Co(NH_3)_4Cl_2]Cl \cdot H_2O$- trans	251.45	1.873*	1.683	50.91
$[Co(NH_3)_4Cl_2]NO_3 \cdot H_2O$- trans	278.00	1.880*	1.631	52.68

TABLE 4

Determination of Geometric Configuration

Coordinate	Initial compound	R_{∞}	$\overset{\infty}{R}$ coord.	$\bar{\overset{\infty}{R}}$ coord.
$NO_3-Co-NO_3$	$K_3Co(NO_3)_6$	68.35	20.53	20.53
$NO_3-Co-NH_3$	$[Co(NH_3)_4(NO_3)_2]Cl$-cis	49.67	15.11	15.20
	$[Co(NH_3)_4(NO_3)_2]NO_3$-cis	52.22	15.29	
$NH_3-Co-NH_3$	$[Co(NH_3)_6]Cl_3$	57.06	10.73	10.67
	$[Co(NH_3)_6](NO_3)_3$	63.00	10.60	
$NH_3-Co-Cl$	$[Co(NH_3)_5Cl]Cl_2$	50.62	12.70	12.93
	$[Co(NH_3)_5Cl](NO_3)_2$	55.45	13.15	
$Cl-Co-Cl$	$[Co(NH_3)_4Cl_2]Cl \cdot H_2O$- trans	50.91	17.86	17.77
	$[Co(NH_3)_4Cl_2]NO_3 \cdot H_2O$- trans	52.68	17.69	

The values that we obtained for the coordinate refractions can be used for the determination of the geometric configuration of complex cobalt compounds. In Table 5 is given the comparison of experimental and theoretically calculated (for the different isomeric forms) molecular refractions. The coordinate refractions were calculated (Table 4) from the experimental data on isomers, and in the case of these isomers their structure was determined with the aid of refractions calculated, of course, from other compounds.

In Table 5 it is apparent that in all cases the molecular refractions calculated on the basis of the correct assumption concerning the structure of the given compound lie considerably closer to the experimental values than do those calculated on the basis of an assumption known to be incorrect. Thus, the geometric configuration of complex compounds of trivalent cobalt can quite safely be determined by the refractions. The least reliable determination of the structure is in the case of $[Co(NH_3)_4(NO_2)_2]Cl$-trans. As we have noted earlier [3], the cause here is the extremely strong optical anisotropy ($\Delta n = n_g - n_p = 0{,}25$), which makes it impossible to apply the same concept of molecular refraction that worked for isotropic or weakly double-refracting substances. The limited applicability of the Lorentz-Lorenz formula in the case of strong double-refraction is therefore also a limitation of the refractometric method for determining the structure of complex compounds.

Refractometric data on complex compounds can be used not only for determining the geometric configuration but for finding the interatomic distances in the inner sphere of these compounds.

Since the molecular refraction is a measure of the molecule's own size [13], there ought to be a linear relation between the size of the spherical molecule and $\sqrt[3]{R}$. In previous work [2, 3, 6] it was shown that the length of the bond depends on the refraction of this bond in the following manner:

$$l = 1 \cdot 123 \sqrt[3]{R_{bond}}$$

TABLE 5

Coordinate Refractions of Trivalent Cobalt Compounds

Coordinate	R_{∞} exptl.	R_{∞} calc.	ΔR_{∞}
$[Co(NH_3)_4(NO_2)_2]$-cis	49.67	cis 50.02	0.35
		trans 50.64	0.97
$[Co(NH_3)_4(NO_2)_2]Cl$- trans	50.29	cis 49.84	0.45
		trans 50.64	0.35
$[Co(NH_3)_4(NO_2)_2]NO_3$-cis	52.22	cis 51.86	0.36
		trans 52.84	0.62
$[Co(NH_3)_4(NO_2)_2]NO_3$-trans	52.89	cis 52.04	0.35
		trans 52.84	0.05
$Co(NH_3)_3(NO_2)_3$- trans	47.42	cis 46.32	1.10
		trans 47.12	0.30
$K[Co(NH_3)_2(NO_2)_4]$	54.97	cis 53.90	1.07
		trans 54.70	0.27
$[NH_4[Co(NH_3)_2(NO_2)_4]$	56.41	cis 55.50	0.91
		trans 56.30	0.11

TABLE 6

Values of Interatomic Distances

Bond	Compound	Refraction of bond	Interatomic distance (optical)	Interatomic distance (x-ray value)
$Co-N_{H_3}$	$[Co(NH_3)_6]Cl_3$	5.37	1.96	1.9[3]
	$[Co(NH_3)_6](NO_3)_3$	5.30	1.96	—
	$K[Co(NH_3)_2(NO_2)_4]$	5.47	1.98	2.00[14]
Co—Cl	$[Co(NH_3)_4Cl_2]Cl \cdot H_2O$- trans	8.93	2.33	2.33[15]
	$[Co(NH_3)_4Cl_2]NO_3 \cdot H_2O$-trans	8.84	2.32	—
$Co-N_{O_2}$	$K_3Co(NO_2)_6$	10.27	2.00	
	$K[Co(NH_3)_2(NO_2)_4]$	10.27	2.00	1.96[14]

The interatomic distances were calculated with the aid of this formula; some of them are given (together with x-ray data) in Table 6. In the case of addenda of complex structure, for example the NO_2- groups, the interatomic distances from the center atom to the gravitational center of the addendum are obtained by the formula. In crystallochemistry, however, by interatomic distance Me – NO_2 is understood the length of bond Me – N. Therefore the value 0.435 A [3] must be subtracted from the value l obtained by the formula, in order to go from the distance Me – NO_2 to Me – N.

From Table 6 it is apparent that the interatomic distances determined by refractometric and x-ray methods coincide within the limits of experimental error. This gives confidence in the correctness of the values for the remaining bond lengths, determined for the first time by the optical method.

The coordinate refractions can be used not only for structure determinations, but also for theoretical purposes.

TABLE 7

Comparison of Coordinate Refractions

Coordinate	R_{X-Co-Y}	$\frac{1}{2}(R_{X-Co-Y}+R_{Y-Co-Y})$	ΔR
$NO_2-Co-NH_3$	15.20	15.60	−0.40
$Cl-Co-NH_3$	12.93	14.22	−1.29

It was shown earlier [16, 6] that information on the capacity of atoms for trans-interaction can be obtained by a comparison of the refractions of dissimilar and corresponding similar coordinates [17]. The interaction of atoms in the inner sphere of complex compounds is revealed in the instability of the bonds of the addendum occurring in the trans-position of the active substituent. This instability of the bonds obviously must be accompanied by an increase in bond refraction.

Accordingly, a comparison of the refraction of a coordinate, for example $NO_2-Co-NH_3$, with half the amount of the refractions of coordinates $NO_2-Co-NO_2$, $NH_3-Co-NH_3$, allows information to be obtained about the difference between the increased refraction of NH_3 which is under the influence of NO_2, and the increased refraction of the NO_2- group because of the trans-interaction of another nitro group. An analogous comparison for the chloro-ammonium coordinates allows comparing the capacity of NO_2 and Cl for developing instability of the molecules of ammonia positioned opposite them.

From Table 7 it is evident that the NO_2- group increases the refraction of ammonia to a greater degree (in comparison with a similar coordinate) than does the chlorine atom. Accordingly, the trans-interaction of the nitro group is greater than that of chlorine, in complete agreement with the chemical data [18].

LITERATURE CITED

[1] G. B. Bokii and S. S. Batsanov, "A new method for determining the structure of complex compounds. I," Vestnik Moskov. Univ. 2, 147-163 (1952).

[2] G. B. Bokii and S. S. Batsanov, "A new method for determining the structure of complex compounds. II," Vestnik Moskov. Univ. 9, 89-94 (1952).

[3] G. B. Bokii and S. S. Batsanov, "A new method for determining the structure of complex compounds. III," Vestnik Moskov. Univ. 10, 87-96 (1954).

[4] G. B. Bokii and M. N. Liashenko and S. S. Batsanov, "A new method for determining the structure of complex compounds, IV," Vestnik Moskov. Univ. 12, 75-78 (1954).

[5] G. B. Bokii and S. S. Batsanov, "A crystallooptical method for determining the structure of complex compounds," Izv. AN OXN 2, 193-196 (1955).

[6] S. S. Batsanov and G. B. Bokii, "The crystallooptical determination of the structure of complex platinum compounds," Vestnik Moskov. Univ. 1 (1957).

[7] S. S. Batsanov, "Crystals of complex compounds of platinum group metals," Trudy Inst. Krist. 12, 93-97 (1956).

[8] P. Wulf, "Ein neues Verfahren zur Darstellung des Dispersionsverlaufes im Sichtbaren und Ultravioletten," Z. Phys. Chem. 21, 368-382 (1933).

[9] M. M. Iakshin, "The atomic polarization and bond refraction of complex platinum compounds," Izv. Sektora Plat. 21, 146-160 (1948).

[10] J. Donohue, "The hydrogen bond in organic crystals," J. Phys. Chem. 56, 502-510 (1952).

[11] J. Robertson, Organic Crystals and Molecules (New York, 1953) p. 228.

[12] S. S. Batsanov and A. S. Sonin, "Refraction of the hydrogen bond in inorganic compounds. II," Kristalografiia 1, 321-327 (1956).

[13] S. S. Batasnov, "The development and application of refractometry in chemistry," Uspekhi Khim. 24, 688-729 (1955).

[14] Y. Komiyama, "The crystal structure of $KCo(NH_3)_2(NO_2)_4$," Bull. Chem. Soc. Japan 29, 300-304 (1956).

[15] Y. Tanito, Y. Shaito and H. Kuroya, "The crystal structure of $[Co(NH_3)_4Cl_2]Cl \cdot H_2O$," Bull. Chem. Soc. Japan 25, 328-331 (1952).

[16] G. B. Bokii and S. S. Batsanov, "The question of the quantitative character of trans-interaction," Doklady Akad. Nauk 94, 1205-1206 (1954).

[17] I. I. Cherniaev, "The theory of complex compounds," Izv. Sektora Plat. 5, 118-156 (1927).

[18] A. V. Ablov, "The development of trans-interaction in complex compounds of trivalent cobalt," VII All-Union Conference on the Chemistry of Complex Compounds [in Russian] p. 7-11 (1956).

M. V. Lomonosov
Moscow State University

Received November 15, 1956

STUDY OF SLIP LINES IN SILVER CHLORIDE CRYSTALS

V. E. Kochnov and M. P. Shaskol'skaia

It is established that slip lines originate and develop in silver chloride in the same way as in metals. It is found that the traces of slip lines on the crystal surface are steps of a height of $\sim 3 \cdot 10^3$ A, and that wavy slip lines are the result of the fusion of straight slip traces.

Silver chloride crystals belong to the so-called "transparent metals." These ionic crystals with rock-salt type of structure, transparent and optically isotropic, also possess the mechanical properties of metals; as was shown by Stepanov [1], the stress-strain curve of silver chloride is perfectly analogous to that of copper on a scale of 1/10. Silver chloride crystals can, without difficulty, be subjected to pressing, rolling, forging, drop forging and any other of the operations [2] employed in the industrial working of metals. The transparency of silver chloride crystals and their birefrigence in the stressed condition makes them suitable for use in the photoelastic study of deformation. The annealing and recrystallization properties of silver chloride are likewise similar to these properties in metals. A study of the processes of elastic and plastic deformation in silver chloride crystals ought therefore to provide information concerning the mechanism of similar processes in metals.

We have investigated the origin of the slip lines produced when polycrystalline silver chloride sheets, monocrystalline in thickness, were subjected to tension.

Single crystals of silver chloride in the form of cylinders 10-12 cm long and up to 3 cm in diameter were grown from the melt by the method of slowly passing the crucible through a tube furnace of given temperature gradient. The specimens were then subjected to pressing followed by rolling. The sheets, several tenths of a millimeter thick, finally obtained were annealed at 400-440°C for 10 to 24 hours; variation of the duration and temperature of annealing enabled the grain size to be varied. The structure of the specimens after annealing was revealed by etching with a saturated solution of hyposulfite. The specimens we used had a grain size varying from a few tenths of a square millimeter to 500 mm^2. The sheets were subjected to tension by the application of a smooth, gradual load and were studied in the process of extension. Examination was carried out by polarized light with a magnification of 256, as well as by transmitted and reflected light with a magnification of 480.

Nye [3] investigated the plastic deformation of silver chloride sheets. He made a careful study of the origin of the birefrigence under tension, and came to the conclusion that the mechanism of slip in these crystals is analogous to "pencil slip." Like Nye, we found that the deformation of silver chloride is accompanied almost at once by the appearance of birefrigent bands, visible in polarized light, similar to those observed by Obreimov and Shubnikov [4] and Brilliantov and Obreimov [5] in rock salt crystals. By studying these bands, it is possible to discover the stress distribution in the crystal during elastic and plastic deformation. This has partly been done by Nye in the work already referred to. If the load is increased, in addition to the birefringent bands in AgCl, thin straight or wavy lines appear, visible without polarized light by both transmitted and reflected light (Fig. 1). Nye makes a brief reference to these lines and considers that they are formed on the

• A. Blistanov, P. Pashkov, D. Pashchenko and Ia. Soifer, students of the Moscow Steel Institute, assisted in this work.

surface. By successively altering the focus of the microscope, we found that the lines pass through the entire crystal, evidently originating not on the surface bui in the body of the grain. These thin lines are perfectly analogous to the slip lines observed on the polished surface of deformed metals. The lines do not disappear when the load is removed.

It is interesting to note that the orientation of these lines – in future we shall call them slip lines – is not in any way related to the orientation of the birefrigence bands. So far we have found no explanation of this fact and we hope later to make a special study of it.

With gradual increase in the load (or the deformation), the slip lines lengthen, become branched and increase in number (Fig. 2). Preliminary calculations show that the increase in the number of lines and their total length as a function of the load occurs discontinuously, similar to that observed for pure metals, for example for aluminum [6]. At the same time, the newly formed slip lines proceed in the same direction as those previously formed. When the load is increased still further, in addition to the continued development of the first system of slip lines, a second system of lines is produced, intersecting the first system and developing in exactly the same way (Fig. 2, b).

The orientation of the two systems of slip lines is different in different grains and is not in any way connected with the direction of the applied force. We have not yet completed the determination of the orientation of these lines. Preliminary data indicate that the lines are oriented along the [110] direction.

It is interesting to note that the grain boundary does not always form an obstacle for the development of a slip line. Sometimes a system of lines is arrested on reaching a boundary, but more often the slip lines cross the grain boundaries without altering either their form or their orientation. It may be that this peculiar phenomenon is due to the fact that our specimens represent a texture,* and consequently the orientation of the individual grains may be very nearly alike; this, however, naturally requires further special investigation.

If a slip line which is gradually increasing in length (under increasing load) encounters on its path another slip line, it may be seen that a zig-zag is formed at the point of encounter (Fig. 3). By visual observation, it can at once be seen how the advancing slip line travels, so to speak, along the encountered slip line and then continues in the former direction. Sometimes, such zig-zags occur where slip lines meet a grain boundary (Fig. 4).

Fig. 1. Birefrigence lines (thick) and slip lines (thin) in silver chloride polycrystals. Photographed in polarized light. × 240.

Subsequent investigation was made with the object of ascertaining whether the lines seen by us were micro-cracks or actually traces of slip. If the surface of the specimen is examined under the same magnification (× 480) but with oblique illumination, it becomes clear that the thin lines are the traces of steps issuing from the surface. Nye [3] came to the same conclusion when using a shadow technique for examining the surface of a deformed specimen and estimated the height of the steps to be 4000 A; unfortunately, Nye merely refers to this in one passage without explanation.

To demonstrate the fact that what we were observing were actually steps, we employed the method of measuring the microhardness, using a Khrushchev microhardness gauge. The impression of the diamond pyramid directly in the visible trace of a slip line clearly shows the trace to be a step (Fig. 5). An estimation of the distortion of the impression indicates that the height of the step is approximately $3 \cdot 10^3$ A.

Thus, the thin lines appearing on silver chloride crystals during plastic deformation are slip traces, typical of the mechanism of the plastic deformation of metals. Slipping of the crystal layers results in the appearance

* "Texture" (tekstura) – "A homogeneous body with non-lattice structure, composed of many particles of any physical nature definitely oriented in space according to the laws of symmetry." A. V. Shubnikov, Piezoelectric Textures [in Russian] (1946) – Publisher's note.

of steps, the traces of which are visible by transmitted and reflected light in the form of thin lines. Evidently, the zig-zag formed at the point of intersection of two lines is due to the fact that one step "climbs" on to another.

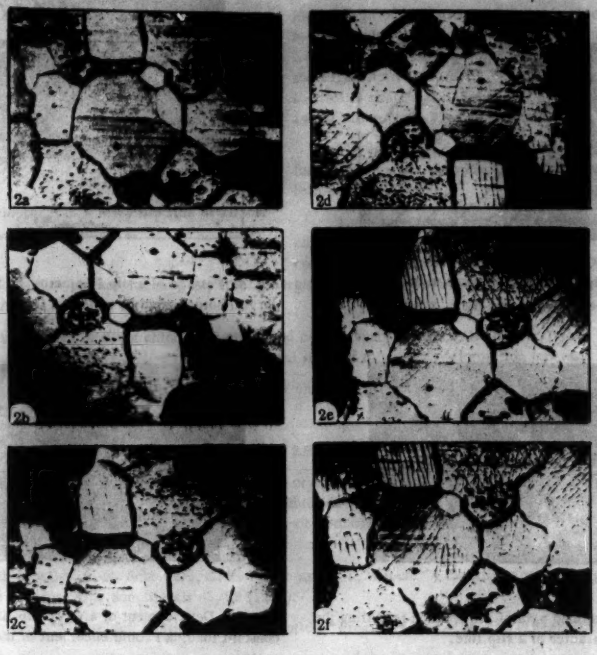

Fig. 2. Appearance and gradual development of slip lines with increasing load. Load respectively equal to: a) 0.33 kg/mm^2, b) 0.65 kg/mm^2, c) 0.67 kg/mm^2, d) 0.70 kg/mm^2, e) 0.77 kg/mm^2, f) 0.87 kg/mm^2. Photographed by reflected light. × 480.

Considerable interest is aroused by the question as to why both straight and wavy slip lines can occur in the same grain, which, as is well known, also occurs in metals [7]. The answer was obtained by observing the initial stage in the formation of slip lines. It was discovered that a slip line appears either at once in the form of a thin straight line or in the form of a system of separate straight striae, parallel to each other. These striae are visible only in the very initial stage of the process of formation of the line, after which they merge with each other, forming a single wavy line. This process is extremely difficult to observe and photograph. Figure 6 shows a series of photographs of a specimen on which we were able to follow the gradual development of a wavy line. It will be seen that when the specimen was subjected to load, a system of parallel striae appeared. With a small increase in load, these striae increased slightly in length and thickness, but did not merge into one another when observed for a period of two hours. The specimen was left under load and the final photograph (Fig. 6, d) shows the same specimen after 6 days; the striae have united or fused to form a single wavy line and the traces of the striae can no longer be distinguished on the photograph; they are scarcely noticeable in visual examination.

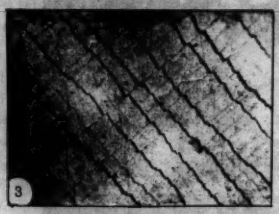

Fig. 3. Zig—zags at the intersections of slip lines. Photographed by reflected light. × 480.

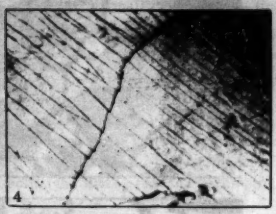

Fig. 4. Passage of a slip line across an intergrain boundary. Photographed by reflected light. × 480.

Fig. 5. Diamond pyramid impression revealing the stepped character of a slip line.

Fig. 6a. Development of a wavy slip line at almost constant load. a) commencement of the process.

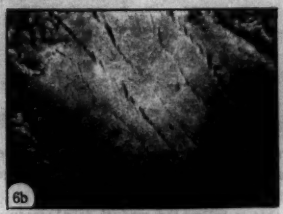

Fig. 6b. Development of a wavy slip line at almost constant load. b) after 10 minutes.

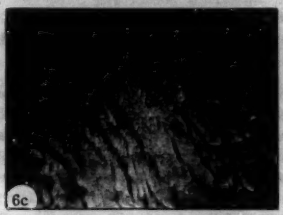

Fig. 6c. Development of a wavy slip line at almost constant load. c) after 30 minutes.

Usually, the stage of the formation and fusion of the striae proceeds so rapidly that it is not always possible to notice it. This is evidently the reason why the phenomenon was not observed previously.

Fig. 6d. Development of a wavy slip line at almost constant load. d) after 6 days.

Careful examination of wavy slip lines on silver chloride crystals under high magnification frequently reveals traces of the striae, evidently existing in the initial stage of formation of such lines. We have come to the conclusion that the wavy slip lines in silver chloride crystals and consequently, evidently, also in pure metals, are formed always as the result of the fusion of a series of straight slip lines. The mechanism of the actual fusion process is not yet clear to us.

The investigation of the processes of plastic deformation in silver chloride crystals thus leads to the following conclusions:

1. In the process of plastic deformation of silver chloride crystals, slip traces are formed which have no connection with the birefrigence lines of Obreimov – Brilliantov – Shubnikov but are traces of slip steps emerging on the crystal surface. The height of these steps attains $3 \cdot 10^3$ A.

2. Wavy slip lines in silver chloride crystals (and consequently probably also in metals) are formed by the fusion of straight slip traces, appearing in the initial stage of the plastic deformation process.

3. The processes of plastic deformation in silver chloride crystals take place in quite an analogous manner to the same processes in metals.

LITERATURE CITED

[1] A. V. Stepanov, "Plastic properties of single crystals of silver and thallium halides," Phys. Z. Sowjetunion 6, 312 (1934); "The plastic properties of silver chloride and sodium chloride," Phys. Z. Sowjetunion 8, 25 (1935); "New optical method of investigating stresses by polarized light," J. Tech. Phys. (USSR) 19, 205 (1949).

[2] R. D. Moeller, F. W. Schonfeld, C. R. Tipton and J. T. Waber, "A metallurgical investigation of silver chloride," Trans. Am. Soc. Metals 43, 28 (1951).

[3] J. F. Nye, "Plastic deformation of silver chloride," Proc. Roy. Soc. 198, 190 (1949); 200, 47 (1949).

[4] I. V. Obreimov and L. V. Shubnikov, "Investigation of the plastic deformation of rock salt by the optical methods," Zhurn. Russk. fiz.-khim. obshchestva, Physics part, 58, 817-828 (1926).

[5] N. A. Brilliantow and J. W. Obreimow, "Über die plastiche Verformung von Steinsalz," Phys. Z. Sowjetunion, 6, 587, 1934.

[6] N. K. Chen and R. B. Pond, "Dynamic formation of slip bands in aluminum," J. Metals (October, 1952) p. 1085.

[7] R. Maddin and N. K. Chen. Geometrical aspect of the plastic deformation of metal single crystals. Prog. in Metal Phys. 5, 53 (1954).

Moscow Steel Institute

Received September 22, 1956

BRIEF COMMUNICATIONS

CRYSTALLINE STRUCTURE OF CIS-[Pt(NH$_3$)$_2$(SCN)$_2$]

Ia. Ia. Bleidelis

Cis-dithiocyanodiammineplatinum—[Pt(NH$_3$)$_2$(SCN)$_2$]—was synthesized by Grinberg's method [1]. On recrystallization from a mixture of ethyl alcohol and acetone (in a ratio of 1:3) the substance was deposited as thin, yellow, needle-like crystals. Goniometric investigation showed only a straight band of faces; the cross-section of the crystal has a rectangular form which is almost square. Optically the crystals of cis-[Pt(NH$_3$)$_2$(SCN)$_2$] are biaxial; in white light $n_g = 1.828$, $n_m = 1.780$, $n_p = 1.730$. The angle of the optical axes is $2\theta = 90°$. The extinctions are straight.*

The symmetry of the oscillation x-radiograms shows that the crystals belong to the mmm diffraction class. The lattice parameters were determined from oscillation x-radiograms (accuracy ± 0.05 kX):

$$a = 13{,}74\,kX,\ b = 8{,}06\,kX,\ c = 13{,}71\,kX.$$

The specific gravity of the crystals is $\sigma_p = 3.05$ g/cm^3. Each unit cell has 8 molecules. The x-ray density is $\sigma_x = 3.02$ g/cm^3.

The primitive form of the lattice was established by oscillation x-radiograms taken along a diagonal and by resolution of the first layer line, h1l. The absence of reflections of the 0kl type with $k = 2n-1$, h0l with $l = 2n-1$ and hk0 with $h + k = 2n-1$ unequivocally defined a Pbcn space group.

The coordinates of the atoms were determined by projections of the interatomic vector and electron density functions. Experimental data were obtained with a camera for photographing the reciprocal lattice using molybdenum radiation. 106 independent reflections were observed on the h0l photograph, 60 on the 0kl photograph and 35 on the hk0 photograph. The intensity of the reflections was evaluated visually from the blackness of the spots; in calculating the values of F^2, Lorentz factors and polarization were taken into account.

A clearly expressed pseudoperiod, equal to b/2, appeared on the x-radiogram for oscillation around the Y axis. It follows from a projection of the interatomic vector function that this pseudoperiod was caused by the location of the Pt atoms one above the other in glide planes. The 16 sulfur atoms, belonging to each unit cell, form two rectilinear systems of points. The projections of the F^2-series contain maxima, which are interpreted as Pt − Pt, Pt − S_I, Pt − S_{II} (the maxima $S_I - S_I$, $S_I - S_{II}$, $S_{II} - S_{II}$ are also partially expressed). The heights of the Pt−Pt and Pt−S maxima are on the average 5:1.

The coordinates of the Pt, S_I and S_{II} atoms were used for calculating the signs of the structural amplitudes. Thus, we discovered that the S_I and S_{II} atoms do not change the signs of the structural amplitudes, determined by the position of the Pt atoms.

*M. N. Liashenko obtained the crystallooptical data.

Besides, Pt, S_I and S_{II} atoms, the NH_{3I} and NH_{3II} groups and the C and N atoms appeared on the electron density projections. All the atoms occupy common positions. The structure is characterized by 27 parameters which are shown in Fig. 1 (the coordinates are given in fractions of periods). Recalculation of the structural amplitudes, taking into account the coordinates of all the atoms, did not result in a change in the signs.

The structure of cis-$[Pt(NH_3)_2(SCN)_2]$ is molecular. The coordination number of the platinum atom is equal to four. The addenda are placed coplanarly and form several deformed squares. Structural investigation confirmed the cis-structure of the molecule. The thiocyano groups are linear and joined to the platinum atom by the sulfur atoms to form an angle of the order of 70° with the plane of the complex.

The planes of the complex are at an angle of approximately 30° to the XZ coordination plane. The complexes are placed one above the other forming "columns," stretched out along the Y axis. In each such "column" the complexes rotate in their own planes in turns. Figure 1 shows the projection of the unit cell on the XZ plane.

TABLE 1

	Pt	S_I	S_{II}	NH_{3I}	NH_{3II}	C_I	N_I	C_{II}	N_{II}
x	0.250	0.398	0.331	0.126	0.169	0.383	0.373	0.405	0.461
y	0.116	0.167	−0.012	0.050	0.208	0.285	0.400	0.114	0.224
z	0.084	0.157	−0.044	0.021	0.196	0.242	0.302	−0.083	−0.125

A comparison of the experimental and theoretical values of the structural amplitudes indicates that the structural pattern determined is correct. The convergence coefficient $R_{XZ} = 0.20$, $R_{YZ} = 0.26$.

In this work we did not try to determine the coordinates of the atoms exactly, as we were mainly interested in the overall pattern of the structure.

Certainly, the projection method using in one case 106 and in the other 60 independent reflections (projection on XZ and YZ planes) could not give a highly accurate determination of the coordinates. Existing experience in investigating structures with heavy atoms and analysis of the cross-section maxima of the electron density projection makes it possible to evaluate approximately the probable error in the coordinates: for platinum ± 0.02 kX, for sulfur ± 0.05 kX, for NH_3 ± 0.15 kX and for carbon and nitrogen ± 0. kX.

However, even within the limits of this accuracy, the character of the bond in the complex may be determined by the metal–addendum interatomic distances. The values we obtained for the distances

$$Pt - S_I = 2.29\,kX, \quad Pt - NH_{3I} = 2.0\,kX,$$
$$Pt - S_{II} = 2.31\,kX, \quad Pt - NH_{3II} = 2.0\,kX,$$

are normal for complex compounds and indicate, firstly, the covalent character of the bonds (as applied to complex compounds) and, secondly, the equivalence of both Pt − S and Pt − NH_3 bonds (within the limits of experimental accuracy).

The distances between the addenda in the complex

$$S_I - S_{II} = 3.23.\,kX, \qquad NH_{3I} - NH_{3II} = 2.75\,kX$$
$$S_I - NH_{3II} = 3.20\,kX, \qquad NH_{3I} - S_{II} = 3.00\,kX$$

indicate a certain deformation of the square coordination of the complex. The angles between the bonds of the central atom and its addenda are equal to

$$S_{II} - Pt - S_I = 89°, \quad NH_{3I} - Pt - NH_{3II} = 87°,$$
$$S_{II} - Pt - NH_{3I} = 88°, \quad NH_{3II} - Pt - S_I = 95°.$$

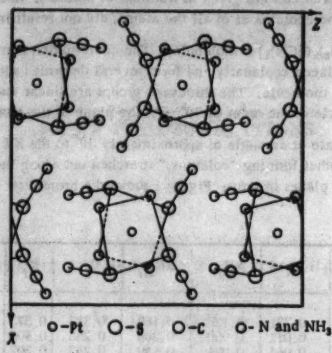

Fig. 1. Projection of the unit cell of cis-$[Pt(NH_3)_2(SCN)_2]$ on the XZ plane.

As the difference in the two S—NH_3 distances (3.00 kX and 3.20 kX) lies beyond the limits of error, the deformation of the complex is caused, apparently, not only by the difference in the size of the sulfur atoms and the NH_3 groups, but also by the conditions of molecular packing in the crystal.

The following values were obtained for the interatomic distances in the thiocyano groups:

$$S_I - C_I = 1.55\,kX, \quad S_{II} - C_{II} = 1.56\,kX,$$
$$C_I - N_I = 1.24\,kX. \quad C_{II} - N_{II} = 1.30\,kX.$$

The probable error in calculation here is very great; however, the similarity of two independent results indicates that the actual error is considerably less. The values obtained agree with those usually assigned to S = C = N bonds.

The closest distances between the atoms in different molecules are equal to:

$$Pt - Pt = 4.03\,kX, \quad S_I - S_I = 3.76\,kX,$$
$$S_{II} - N_I = 3.90\,kX, \quad S_I - NH_{3_I} = 3.45\,kX,$$
$$S_{II} - NH_{3_I} = 3.70\,kX, \quad S_{II} - S_{II} = 4.45\,kX,$$
$$S_I - N_{II} = 4.18\,kX.$$

The volume of the cis-$[Pt(NH_3)_2(SCN)_2]$ molecule itself equals 129.1 kX^3. The packing coefficient k = 0.68.

SUMMARY

1. The atomic structure of cis-$[Pt(NH_3)_2(SCN)_2]$ crystals was determined.

2. It was shown that the structure of cis-$[Pt(NH_3)_2(SCN)_2]$ is molecular and the cis-structure was confirmed.

3. We determined the crystallooptical and crystallochemical constants of cis-$[Pt(NH_3)_2(SCN)_2]$ crystals.

The author expresses his gratitude to his scientific instructor, Professor G. B. Bokii; the author is also grateful to the Physics and Mathematics Candidate, M. A. Porai-Koshits, for consultation and help in the work.

LITERATURE CITED

[1] A. A. Grinberg, Izv. Inst. Plat. 5, 130 (1927).

Institute of Chemistry
Academy of Sciences Latvian SSR

Received January 18, 1957

THE CRYSTALLINE STRUCTURE OF THE TRANS-DIAMMINEDITHIOCYANIDE OF DIVALENT PLATINUM

Ia. Ia. Bleidelis and G. B. Bokii

Trans-$[Pt(NH_3)_2(SCN)_2]$ was synthesized by A. A. Grinberg's method [1]. The crystals were prepared by recrystallization from acetone. In order to confirm the composition, a platinum analysis was performed by thermal decomposition of the substance and weighing the metallic platinum.

Under a microscope the trans-$[Pt(NH_3)_2(SCN)_2]$ crystals have the form of thin, slightly elongated plates of a golden yellow color. The crystals have an oblique extinction of 8-10°.* The refractive indices, determined in white light, have the following values:

$$n_g = 1.990,\ n_m = 1.737,\ n_p = 1.625.$$

The parameters of the unit cell were determined by oscillation x-radiograms, taken with copper radiation, and were found to be the following:

$$a = 7.31 \pm 0.05\ kX,$$
$$b = 8.27 \pm 0.05\ kX,$$
$$c = 13.27 \pm 0.05\ kX,$$
$$\beta \simeq 90°.$$

Ratio $a : b : c = 0.884 : 1 : 1.605$.

The oscillation x-radiograms along diagonals and the $h1l$ kforograms** showed that the unit cell is primitive. Kforograms, plotted on all three coordination planes, established that the trans-$[Pt(NH_3)_2(SCN)_2]$ crystals belong to the rhombo-prismatic form of monoclinic syngonic symmetry, and if the monoclinic angle is taken as $\beta \simeq 90°$, then the space group $P2_1/n$ is unequivocally determined (instead of $P2_1/c$ in the case of an oblique-angled coordinate system).

The specific gravity of the substance, determined pyknometrically is $\sigma_p = 2.90$ g/cm³. The x-ray density of the substance is $\sigma_x = 2.88$ g/cm³. The unit cell contains 4 molecules of $[Pt(NH_3)_2(SCN)_2]$. The trans-$[Pt(NH_3)_2(SCN)_2]$ crystals belong to the C_{2h} = 2/m.diffraction class.

The coordinates of the atoms were determined by projections of interatomic vector functions and projections of electron density on the XZ and YZ coordination planes. Kforograms were taken with molybdenum radiation. 103 independent reflections were on the $h0l$ kforogram and 76 on the $0kl$ kforogram. The intensities of the reflections were evaluated visually by the blackening of the spots. The relative reflection intensities were divided by Lorentz and polarization factors.

The coordinates of the platinum and sulfur atoms were determined by projections of the interatomic vector functions. All the atoms occupy common positions, and the 8 sulfur atoms belonging to the unit cell occupy two fourfold positions. Thus, the trans-$[Pt(NH_3)_2(SCN)_2]$ structure has two thiocyano groups $S_1C_1N_1$ and

* M. N. Liashenko obtained the crystallooptical constants.

** Kforogram: Transliteration of Russian term meaning 'reciprocal lattice photograph.'

$S_{II}C_{II}N_{II}$ which are different crystallochemically. The platinum atoms occupy a common fourfold position near the double screw axes.

TABLE 1

	Pt	S_I	S_{II}	NH_{3I}	NH_{3II}	C_I	N_I	C_{II}	N_{II}
x	−0.073	−0.208	0.193	−0.130	0.131	−0.354	−0.475	0.344	0.467
y	0.184	0.080	0.333	0.135	0.230	0.154	0.256	0.215	0.115
z	0.217	0.128	0.309	0.380	0.081	0.104	0.083	0.354	0.392

The signs of the structural amplitudes and then the projection of the electron density were calculated from the coordinates of the Pt, S_I and S_{II} atoms, determined by projections of the interatomic vector function.

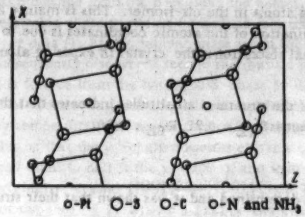

Fig. 1. The projection of the trans-$[Pt(NH_3)_2(SCN)_2]$ structure on the XZ plane.

Maxima, corresponding to NH_{3I} and NH_{3II} groups and to the C and N atoms of thiocyano groups, appeared on these projections. All 27 atomic parameters were determined from the electron density projections.

The relative atomic coordinates are given in Table 1.

Recalculation of the signs of structural amplitudes was carried out using these coordinates but all the structural amplitudes retained their signs.

The interatomic distances in the complex, calculated from the atomic coordinates, were found to be the following:

$$Pt - S_I = 2.26\,kX, \quad Pt - NH_{3I} = 2.13\,kX$$
$$Pt - S_{II} = 2.27\,kX, \quad Pt - NH_{3II} = 2.10\,kX.$$

The distances between addenda in the complex are:

$$NH_{3II} - S_{II} = 3.18\,kX, \quad NH_{3I} - S_{II} = 2.94\,kX,$$
$$NH_{3I} - S_I = 3.01\,kX, \quad NH_{3I} - S_I = 3.25\,kX.$$

The angles between the central atom and addenda are:

$$\sphericalangle S_{II} - Pt - NH_{3II} = 93°. \quad \sphericalangle S_I - Pt - NH_{3I} = 95°,5,$$
$$\sphericalangle S_I - Pt - NH_{3II} = 87°. \quad \sphericalangle S_{II} - Pt - NH_{3I} = 84°,5.$$

Distances in the $S-C-N^-$ groups are:

$$S_I - C_I = 1.60\,kX, \quad S_{II} - C_{II} = 1.59\,kX,$$
$$C_I - N_I = 1.25\,kX, \quad C_{II} - N_{II} = 1.30\,kX.$$

The nearest distances between atoms in different complexes are:

$$NH_{3II} - N_{II} = 3.06\,kX, \quad N_{II} - S_I = 3.86\,kX, \quad NH_{3I} - S_I = 3.46\,kX,$$
$$NH_{3II} - N_I = 2.70\,kX, \quad S_{II} - S_I = 4.15\,kX.$$

The volume of the trans-$[Pt(NH_3)_2(SCN)_2]$ molecule itself equals 129.3 kX^3. The packing coefficient is 0.649.

Similarly to the structure of cis-$[Pt(NH_3)_2(SCN)_2]$, the structure of trans-$[Pt(NH_3)_2(SCN)_2]$ is molecular. The addenda are placed around the platinum coplanarly and the coordination number of platinum equals 4. The SCN^- groups are linear and form angles $S_IC_IN_I = 78°$, $S_{II}C_{II}N_{II} = 72°$ with the plane of the complex.

Figure 1 shows the projection of the unit cell on the XZ plane.

The accuracy of determination of the atomic coordinates in the structure of trans-$[Pt(NH_3)_2(SCN)_2]$ was evaluated from the heights of the maxima of the electron density projection and in the case of the Pt and S atomic coordinates, it was found to be not less than that in the cis-isomer structure. As far as the accuracy of determination of the coordinates of the NH_3 groups and the C and N atoms is concerned, it is lower than the accuracy of determination of the coordinates of the corresponding atoms in the cis-isomer. This is mainly due to the y coordinates of these atoms. The low accuracy of determination of the atomic coordinates is due to the crystal's habit, in particular, to the strong effect of the unequal absorption of the crystal in exposing along the X axis.

A comparison of the experimental and theoretical values of the structural amplitudes indicates that the proposed structural pattern is correct as the convergence coefficient is $R_{XZ} = 0.21$, $R_{YZ} = 0.30$.

SUMMARY

The atomic structure of trans-$[Pt(NH_3)_2(SCN)_2]$ crystals was determined and it was shown that their structure is molecular.

We proved the trans-structure of the compound, confirmed the planar coordination of the addenda around the platinum and the linearity of the SCN^- groups. It was established that the latter groups are bound to the platinum atoms by a sulfur atom.

The distances Pt – S = 2.27 kX, Pt – NH_3 = 2.12 kX were established. The distances Pt-S are the same within the limits of error, in both isomers; the Pt-NH_3 distance is greater in the trans-isomer than in the cis-isomer.

The distances in the SCN^- group was determined.

In conclusion, the authors would like to express their gratitude to Physics and Mathematics Candidate, M. A. Porai-Koshits for consultion and advice, which helped in the given work.

LITERATURE CITED

[1] A. A. Grinberg, Izv. Inst. Plat. 5, 130 (1927).

Institute of Chemistry
Academy of Sciences Latvian SSR

Received January 11, 1957

CRYSTAL STRUCTURE OF THE METASTABLE PHASE FORMED DURING THE TEMPERING OF Cu – Sn ALLOYS CONTAINING 24 27% Sn

Iu. A. Bagariatskii

As long ago as 1932, Isaichev and Kurdiumov [1] found that in low-temperature tempering of Cu – Sn alloys quenched from the β-region, the eutectic decomposition $\beta \rightarrow \alpha + \gamma$ does not take place directly, but a metastable phase γ' is first formed, so that the decomposition process is $\beta \rightarrow \beta + \gamma' \rightarrow \alpha + \gamma$.* According to x-ray data [1, 2], the temper phase is not identical with the low temperature martensitic phase β' (nor with the subsequently discovered second martensitic phase β'' [3], possessing a rhombic lattice [4]) but in contrast to it, is formed from the hardened β-phase by diffusion, as is confirmed by direct experiments [5]. As the result of constructing and analyzing the polar diagrams for all the observed reflections of the γ'-phase, formed during tempering in the single crystal β-phase, I. V. Isaichev and G. V. Kurdiumov came to the alternative conclusion that the γ'-phase possesses either a cubic lattice similar to the lattice of the γ-phase (which also induced them to call it the γ'-phase), and with the same law of orientation of the precipitates with respect to the original γ' crystal ($[001]_{\gamma} \parallel [001]_{\beta}$ [1]), or a hexagonal lattice with the axis ratio c/a = 0.354, direction of the axes $a \parallel [11\bar{2}]_{\beta}$, $c \parallel [111]_{\beta}$ and constants a = 7.28, c = 2.58 kX. In the second case, the elementary cell has 9 atoms. The paper indicated the similarity possible for the γ'-phase of hexagonal lattice to the lattice of the ζ-phase of AgZn, which, according to the data of reference [6], has almost the same ratio of axes (0.367), the same number of atoms per elementary cell and the same orientation of the axes as the high-temperature β-phase of AgZn. At that time, the disposition of the atoms was not known, either in the Cu – Sn γ'-phase or in the AgZn ζ-phase, so that it was impossible to draw any definite conclusions in favor of either the first or second suppositions.

Recently, two papers have appeared on the study of the crystal structure of the ζ-phase [7, 8]. In [7], using polycrystalline material, the method of successive approximations was employed to ascertain the difference in the arrangement of the atoms in the ζ-phase relatively to the β-phase of AgZn, and in [8], the conclusions of reference [7] were checked and confirmed as the result of an investigation of a single crystal of β-Ag – Zn alloy, reduced to the ζ form. The positions of the atoms in the elementary cell of the ζ-phase, as determined in reference [7], are shown in the first column of Table 1; the first three positions (a and d for the space group $C^{4}_{3i} = C\bar{3}$ according to the International Tables) being occupied by zinc atoms, and the remaining 6 (g) being occupied 75% by silver atoms and 25% by zinc atoms; the second column of the table gives the approximate coordinates of the atoms, small displacements in the xy plane being ignored. The third column of Table 1 shows the coordinates of the atoms in the β-phase if it is described in the hexagonal lattice with 9 atoms per cell and not in the body-centered cubic lattice. The ratios between the cubic and hexagonal axes are here just the same as those found by Weerts [6] for $\beta \parallel \zeta$ in the Ag – Zn system. Four modes of selection of the above-mentioned hexagonal axes in the β crystal are possible, in correspondence with the number of triad axes in the cube.

It follows from Table 1 that in the $\beta \rightarrow \zeta$ transition, the atoms are in principle displaced along these directions, producing four possible orientations of the β-phase with respect to the original β-crystal. (The correlation of the two lattices is well shown by the illustrations in reference [7].) With such a rearrangement, the constants along the axes are also easily varied.

* In reference [2], the temperature range of the formation of the γ'-phase was found to be 150-350°C in the compact material and 100-200°C in powders.

It seems to us that the peculiarities of the $\beta \rightarrow \zeta$ transformation observed in Ag – Zn provide a cogent argument in support of the second hypothesis regarding the crystal structure of the temper phase in Cu – Sn alloys.

TABLE 1

Positions of the Nine Atoms in a Hexagonal Elementary Cell

No. of atom	ζ-phase of AgZn [7, 8] exact coordinates	ζ-phase of AgZn [7, 8] approximate coordinates	Cubic β-phase (A1 type)	ω-phase [9, 10] (approximate coordinates)
1	0 0 0	0 0 0	0 0 0	0 0 0
2	1/3 2/3 1/4	1/3 2/3 1/4	1/2 1/2 0	1/2 1/2 0
3	2/3 1/3 3/4	2/3 1/3 3/4	1/2 0 1/2	1/2 0 1/2
4	0.350 0.032 1/4	1/3 0 1/4	0 1/2 1/2	0 1/2 1/2
5	0.650 0.968 3/4	2/3 0 3/4	0 1/2 1/2	0 1/2 1/2
6	0.968 0.316 1/4	0 1/3 1/4	1/2 1/2 1/2	1/2 1/2 1/2
7	0.032 0.684 3/4	0 2/3 3/4	1/2 1/2 1/2	1/2 1/2 1/2
8	0.684 0.652 1/4	2/3 2/3 1/4		
9	0.316 0.348 3/4	1/3 1/3 3/4		
	c/a=0.392	0.392	c/a=0.353	$c/a=\frac{0,612}{\sqrt{3}}$=0.353

To check this supposition, we have calculated the relative intensities of the lines of the Cu – Sn phase having a structure similar to the ζ-phase of AgZn, but without ordered arrangement of the different sorts of atoms in the possible positions. As a first approximation, the positions of the atoms shown in the second column of Table 1 were used, i.e., ignoring displacements in the xy plane. In view of the estimatory character of the calculation, the angular factors of intensity were left out of consideration, only the structural (S^2) and recurrence [p] factors were taken into account. The position of reflections from the hexagonal phase was also calculated with respect to the original cubic phase on the basis of the relationship found for the orientations of the two phases. The results obtained are given in Table 2, where they are compared with the data of Isaichev and Kurdiumov [1]. Despite the crudeness of the approximation made, agreement is quite good. (The most important difference is the absence in the x-ray diagram of lines and reflections of type $13 \cdot 1$; in angle θ and texture, however, they are similar to the very strong reflections $22 \cdot 1$, which in addition partly coincide with the reflections 200 from the original β-phase, so that they may be masked by them.)

The calculations performed support the view that the temper phase in Cu – Sn alloys is isomorphous with the Ag – Zn ζ-phase (it should no doubt be called the Cu – Sn ζ-phase and not the γ'-phase, especially since there is a martensitic phase in the Cu – Al system isomorphous with the Cu – Sn β''-phase), but that exact calculations of the position of the atoms ought to be performed on the basis of additional experimental material.

The law of the $\beta \rightarrow \zeta$ lattice rearrangement is reminiscent of the rearrangement law in $\beta \rightarrow \omega$ transformation in titanium alloys [9, 10]. In that case also, the displacement of the atoms is mainly only in the $[111]_\beta$ direction, but the resulting hexagonal lattice has a cell with a base one-third of that of the ζ-phase. In describing it in the same axes as the ζ-phase, the approximate values of the coordinates of the atoms in the ω-phase will correspond to the data of Table 1. Like the temper phase in Cu – Sn alloys, the ω-phase in titanium alloys is formed (on tempering) with a change in concentration of the original hardened β solid solution and its electrical resistance differs appreciably from that of the β-phase. Both phases (ζ and ω) are pseudocubic and since the ratio of the axes c/a for the Cu – Sn ζ-phase is equal to $1/\sqrt{8}$ and for ω, $\sqrt{3}/\sqrt{8}$, the lines on the x-ray diagrams are situated at angles θ for which $\sin^2\theta$ = constant $\cdot$ N, where $N = H^2 + HK + K^2 + 6L^2$ in the first case and $N = H^2 + HK + K^2 + 2L^2$ in the second.

It should be noted that the data obtained in reference [1] by the very laborious method of constructing the polar diagrams can be obtained merely by photographing the rotation of a well-orientated crystal, as was done by us in connection with the ω-phase [9]. The basis of this method will be explained in one of the subsequent papers.

TABLE 2

Comparison of the Calculated Values of pS^2 with the Experimental data of I. V. Isaichev and G. V. Kurdiumov [$\kappa_1, \kappa_2, \kappa_3$ – coordinates of the angles of the reciprocal lattice of the hexagonal phase in the reciprocal lattice of the β-phase for regular rearrangement of the lattices. Conversion formulas: $\kappa_1 = 1/3\,(2L-H)$, $\kappa_2 = 1/3\,(2L-K)$, $\kappa_3 = 1/3\,(2L+H+K)$].

Phase isomorphous with the ζ-phase of AgZn for the atom positions given in the second column of Table 1*											Cu-Sn temper phase [1]			
N	$HK \cdot L$ hexag.	for $L>0$** S^2	p	pS^2	$\kappa_1'\kappa_2\kappa_3\times 3$	for $L<0$** S^2	p	pS^2	$\kappa_1\kappa_2\kappa_3\times 3$	ΣpS^2	intensity of lines for K_α Fe-irradiation	hkl hexag.	hkl-cubic (texture relative to single crystal β-phase)	Remarks
1	10 0	0	—	—	—	—	—	—	—	0				
3	11 0	0	—	—	—	—	—	—	—	0				
4	20 0	0	—	—	—	—	—	—	—	0				
6	00 1	1	1	1	222	1	1	1	222	2		—	—	
7	21 0	0	—	—	—	—	—	—	—	48	weak	101	321	
	10 1	0.5	6	3	123	7.5	6	45	321					
9	30 0	81	6	486	303	—	—	—	—	822	very strong	111	110 and 441	Coincides with line 110 of the β-phase
	11 1	17.6	6	106	114	38.4	6	230	330					
10	20 1	7.5	6	45	024	0.5	6	3	420	48	medium	201	210	
12	22 0	0	—	—	—	—	—	—	—	0				
13	31 0	0	—	—	—	—	—	—	—	96	medium	121	510 and 431	
	21 1	0.5	12	6	015	7.5	12	90	431					
15	30 1	1	6	6	125	1	6	6	521	12	—	—	—	
16	40 0	0	—	—	—	—	—	—	—	0				
18	22 1	38.4	6	230	006	17.6	6	106	442	336	very strong	221	100 and 211	Coincides with 200 β
	32 0	0	—	—	—	—	—	—	—	96	—	—	—	
19	31 1	7.5	12	90	116	0.5	12	6	532					
21	41 0	0	—	—	—	—	—	—	—	0				
22	40 1	0.5	6	3	226	7.5	6	45	622	48	—	—	—	
24	00 2	49	1	49	444	49	1	49	444	98	strong	002	111	
	50 0	0	—	—	505	—	—	—	—		strong	500	110	
25	32 1	0.5	12	6	107	7.5	12	90	543	144		221	710	
	10 2	4	6	24	345	4	6	24	543			102	543	
27	33 0	81	6	486	336	—	—	—	—	1206	very strong	411	721 and 211	Coincides with 211 β
	41 1	17.6	12	216	217	38.4	12	460	633					
	11 2	4	6	24	336	4	6	24	552					
28	42 0	0	—	—	—	—	—	—	—	48	very weak	202	321	
	20 2	4	6	24	246	4	6	24	642					
31	51 0	0	—	—	—	—	—	—	—	144	medium	122	732 and 651	
	50 1	7.5	6	45	327	0.5	6	3	723					
	21 2	4	12	48	237	4	12	48	654					
33	33 1	1	6	6	118	1	6	6	554	600	very strong	302	741	
	30 2	49	6	294	147	49	6	294	741					

* For the space group $C_{3i}^1 = C\bar{3}$ in the general case four values of S^2 are possible for given indices HKL, but in the special case for even values of L, all four values coincide, and for L = 1 they are reduced to two values, corresponding to HKL and $H\bar{K}\bar{L}$.

** For the sake of clarity and economy of space, the minus signs which ought to be above some values of $\kappa_1, \kappa_2, \kappa_3$ have been omitted.

LITERATURE CITED

[1] I. V. Isaichev and G. V. Kurdiumov, "Transformations in eutectic Cu – Sn alloys," Article 1. "Phase formed on the decomposition of β -phase in the tempering process and their orientation," Metallurg 1, 25, 1932*; Physik. Z. Sowjetunion 5, 1, 6 (1932).

[2] V. Bugakov, I. V. Isaichev and G. V. Kurdiumov, The same series, Article 2. "On the change in properties of quenched alloys on tempering," Metallurg 1, 35 (1932); Physik. Z. Sowjetunion 5, 1, 22 (1932).

[3] I. V. Isaichev and I. Salli, Article 5. "β -Phase transformation at low temperatures," J. Tech. Phys. (USSR) 10, 9, 752 (1940).

[4] I. V. Isaichev, Article 6. "Structure and orientation of the β "-phase," J. Tech. Phys. (USSR) 17, 7, 828 (1947).

[5] I. V. Isaichev, Article 4. "Decomposition of the β -phase on tempering," J. Tech. Phys. (USSR) 9, 20, 1867 (1939).

[6] J. Weerts, "Über Umwandlungsvorgänge im β -Messing und in Silber-Zinklegierungen," Zs. Metallkunde, 24, 265 (1932).

[7] J. G. Edmunds and M. M. Qurashi, "The structure of the ζ -phase in the silver-zinc system," Acta Cryst. 4, 5, 417 (1951).

[8] G. Bermann and R. W. Jaross, "On the crystal structure of the ζ -phase in the silver-zinc system and the mechanism of the β – ζ transformation," Acta Cryst. 8, 4, 232 (1955).

[9] Iu. A. Bagariatskii, G. I. Nosova and T. V. Tagunova, "On the crystal structure and nature of the ω-phase in alloys of titanium with chromium," Doklady Akad. Nauk SSSR 105, 6, 1225 (1955).

[10] J. M. Silcock, M. H. Davies and H. K. Hardy, "Structure of the precipitation in titanium 16 per cent vanadium alloy," Nature 175, 4460, 731 (1955); Inst. Metals (London) Monograph and Rep. Ser. 18, 93 (1956).

Institute of the Physics of Metals and Metallography
Central Scientific Institute for Ferrous Metals

Received October 13, 1956

* In this article, the captions to the figures and their numbers have been transposed; their correct arrangement may be obtained from the article in German.– Translator's note.

ELECTRON DIFFRACTION STUDY OF InSb FILMS

S. A. Semiletov and M. Rozsíbal*

Compounds of the elements of groups III and V of the periodic system ($A^{III}B^{V}$) possess high charge-carrier mobility and other valuable properties, which make their application in semiconductor technology very promising. According to the literature, all these substances possess a zinc blende type of structure, and differ from many compounds of another analogous group $A^{II}B^{VI}$ (CdS, ZnS and others) in that they have no hexagonal modifications.

The present article deals with an electron diffraction study of the structure of InSb films obtained by sputtering in a vacuum. The specimens were prepared for investigation either by sublimation of the starting components or sublimation of the previously prepared alloy,** corresponding in composition to the formula InSb. The supports employed for condensation were celluloid films and rock-salt crystals.

When the starting components were sublimed from different evaporators, the specimens formed on the supports were of variable composition, representing the entire phase diagram of the In – Sb system. The electron diffraction diagrams of such specimens showed lines of crystalline Sb (or rings of amorphous Sb), the compound InSb and In. When the electron diffraction patterns were measured, we failed to detect any marked change in the lattice constants of any of the above-mentioned phases which would have been evidence of the formation of solid solutions. This latter circumstance is in agreement with the phase diagram of the In – Sb system.

In addition to sublimation of the starting components, as indicated already above, we carried out sublimation of the alloy InSb. As a rule several sublimations were effected from one weighing of alloy amounting to several milligrams. From the electron diffraction study of specimens prepared in this way, it was found that during the first sublimations, a film of Sb was formed on the support, then InSb and finally InSb + In.

Thus, for example, in one of the series of experiments, about twenty sublimations were carried out with one piece of InSb alloy, the InSb lines appearing only on the electron diffraction pattern obtained from the specimen prepared in the twentieth sublimation, while only antimony lines were observed on the electron diffraction patterns from all the preceding specimens. This fact was observed earlier by one of us and was related to the different vapor tensions of the components – in this case with the much higher vapor tension of Sb compared with the vapor tension of In.

Figure 1 shows one of the electron diffraction patterns we obtained from InSb films. The majority of the lines of this pattern can be indexed on the basis of a cubic lattice with the constant a = 6.46 A, corresponding to the data in the literature.

Table 1 gives the results of the measurement and indexing of this electron diffraction pattern. It will be seen from this table that in addition to lines corresponding to the cubic face-centered lattice of InSb, the diffraction pattern has a few extra lines of comparatively weak intensity. The values of the interplanar spacings corresponding to these lines do not fit either the In lattice or the Sb lattice.

The ratio of the diameter of the 220 InSb ring to the diameter of the first extra ring was found to be $\sqrt{3}$ i.e., it corresponds to the indices $11\bar{2}0$ and $10\bar{1}0$ of the hexagonal lattice. An analogous picture was observed

* Scientific worker of the Institute of Technical Physics of the Czechoslovak Academy of Sciences.

** The alloy was obtained from the Leningrad Physico-Technical Institute from N. A. Goriunova.

TABLE 1

Results of Measurement and Indexing of InSb Electron Diffraction Patterns. $2L\lambda = 75.3$

No. of ring	2r	d_{exp}	I*	$d_{t.cub}$	hkl	$d_{t.hex}$	hkil
1	19.2	3.93	MS	—	—	3.93	$10\bar{1}0$
2	20.2	3.72	S	3.73	111	—	—
3	21.4	3.52	MS	—	—	3.50	$10\bar{1}1$
4	27.8	2.71	MS	—	—	2.71	$10\bar{1}2$
5	33.0	2.28	S	2.28	220	—	—
6	35.7	2.11	M	—	—	2.1_0	$10\bar{1}3$
7	38.8	1.94	VS	1.95	311	—	—
8	40.0	1.88	F	1.86	222	—	—
9	46.5	1.62	VF	1.61	400	—	—
10	48.7	1.54	VF	—	—	1.55	$20\bar{2}3$
11	51.0	1.47	M	1.48	331	—	—
12	54.0	1.39	VF	—	—	1.39	$21\bar{3}2$
13	57.2	1.31	M	1.32	422	—	—
14	60.5	1.25	MF	1.24	511	—	—
15	66.2	1.13	F	1.14	440	—	—

* Intensities; s-strongest; vs- very strong; ms-moderately strong; m-moderate; mf-moderately faint; vf-very faint; f-faintest.

previously by one of us in the study of films of CdTe [1]. It was established in [1] that the presence of extra rings on electron diffraction patterns of CdTe was associated with the formation in the films of a previously unknown hexagonal modification of this compound with a structure of wurzite type.

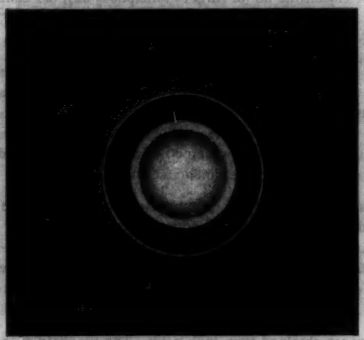

Fig. 1. Electron diffraction pattern of a film of InSb.

Since the compound InSb belongs to the same class of substances as CdTe (equidistance of the elements composing it from the C, Si, Ge, Sn group), it was natural to assume that in this case the presence of extra lines in the electron diffraction patterns of InSb was connected with the existence of a hexagonal modification of this compound in the films.

To check this assumption, we calculated the values of the interplanar distances on the basis of a hexagonal lattice with the constants:

$$a_H = a_C\sqrt{2} = \frac{6.46}{\sqrt{2}} = 4.56,$$

$$c_H = 2a_C\sqrt{3} = \frac{12.92}{\sqrt{3}} = 7.46\,kX.$$

As is well known, such a ratio of the constants occurs in the case of the sphalerite and wurzite type of structure, based respectively on a three-layered cubic and a two-layered hexagonal packing of the anions, while the cations occupy half the tetrahedral vacancies.

The theoretical values of d, calculated on the basis of a hexagonal lattice, and the corresponding indices are given in Table 1. Comparison of these values with the values of d_{exp} obtained by measuring the diameters of the extra rings on the InSb electron diffraction pattern shows that they agree completely.

Thus in InSb films obtained by sputtering in a vacuum, in addition to the formation of crystals of cubic modification with a zinc blende type of structure, crystals of hexagonal modification with a wurzite type of

structure are also formed. The existence of the hexagonal phase was observed in all the films we investigated irrespective of the method of preparation (sublimation of the alloy itself or of the starting components), the temperature of the support during sputtering and the temperature of subsequent annealing.

LITERATURE CITED

[1] S. A. Semiletov, "Electron diffraction study of the Cd – Te alloy system." Trudy Inst. Krist. Akad. Nauk SSSR 11, 121 (1955).

Institute of Crystallography
Academy of Sciences, USSR

Received February 7, 1957

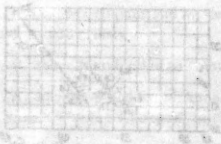

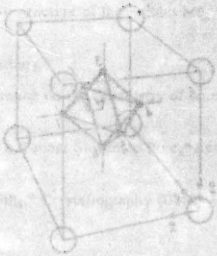

CRYSTAL CHEMISTRY OF THE METAL HEXABORIDES

G. S. Zhdanov, N. N. Zhuravlev, A. A. Stepanova and M. M. Umanskii

An interesting group among the metal hexaborides are the compounds with the general formula MB_6 with cubic structure (Fig. 1). The boron atoms form a three-dimensional structure with the metal atoms occupying the empty spaces in it. The structure is of the CsCl type in which metal atoms of the B_6 octahedrons are the structural units.

The elements which form hexaborides belong to the left side of the periodic table, i.e., to groups II, III, and IV. In the literature [1] there is a hypothesis of the existence of hexaborides of Group I, but so far it has not been confirmed experimentally.

Among the elements of Group II, Be, Mg, Ca, Sr and Ba form hexaborides, and those of Be and Mg do not have the cubic structure of the CaB_6 type [2, 3].

Of the elements of Group III, Y, La, Ce, Pr, Nd, Gd, Er and Yb form hexaborides, and it may be supposed that the same is true of the rest of the lanthanides and Sc.

Among the elements of Group IV, Si and Th form hexaborides. A number of metal hexaborides have valuable physical properties. The question of the stability of MB_6 was discussed in [4]. It was shown that, depending on the valence of the metal, hexaborides may be either insulators or conductors. This effect of valence is confirmed by crystallochemical data.

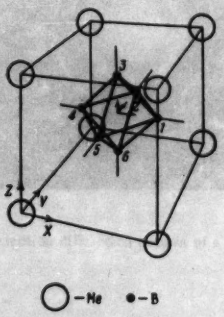

Fig. 1

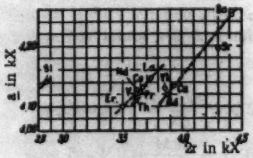

Fig. 2

Figure 2 shows the parameters of the unit cell of hexaborides as functions of the atomic radius of the metal for the 12-fold coordination. The numerical values are taken from Bokii's text [5]. The parameters of the unit cells are given according to [1, 6, 7].

On the graph, the points corresponding to the hexaborides of the bivalent alkaline earths and trivalent rare earths fall upon differnt curves. Experimental data on the structure of the tetravalent hexaborides are very scant. The structure of silicon hexaboride was recently determined by one of the authors [8]. It is possible that the points corresponding to silicon and thorium, which are placed in different subgroups in the periodic table, fall upon different curves. The data given in

Figure 2 show that there are several subgroups in the cubic hexaboride group. Membership in this or that subgroup is determined by the valence of the metal atom. Ytterbium hexaboride falls on the curve for the bivalent metals since it is bivalent. Cerium is either tri- or tetravalent. Structural data on cerium hexaboride show it to be trivalent in this compound. Structural data on some of the hexaborides need refinement. This should be done for strontium and ytterbium hexaborides.

The coefficients of thermal expansion were deteremined by us by the x-ray method for the hexaborides of Ca and Si (Fig. 3), adding to the previously made determinations for hexaborides of Ba, Li and Ce [6].

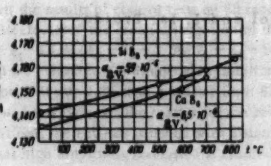

Fig. 3

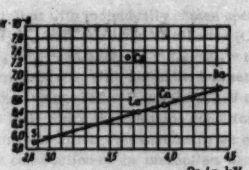

Fig. 4

Figure 4 gives average values of the coefficients of thermal expansion of these hexaborides as functions of the atomic radii of the metals. The coefficient increases with decrease in valence and increase in atomic radius of the metal. The reason for the high values of the coefficients of thermal expansion of the hexaborides of La and Ce is not clear.

LITERATURE CITED

[1] G. V. Samsonov and L. Ia. Markovskii, "The chemistry of boron," Uspekhi. Khim. 25, 190 (1956).

[2] L. Ia. Markovskii, Iu. D. Kondrashev and G. V. Kanutovskaia, "Composition and properties of beryllium borides," J. Chem. Soc.(USSR) 25, 1045 (1955).

[3] L. Ia. Markovskii, Iu. D. Kondrashev and G. V. Kanutovskaia, "Composition and chemical properties of magnesium," J. Chem. Soc. (USSR) 25, 433 (1955).

[4] H. C. Longuet-Higgins and M. de V. Roberts, "The electronic structure of the borides MB_6," Proc. Roy. Soc. 224, A, 336 (1954).

[5] G. V. Bokii, Introduction to Crystal Chemistry (1954) [In Russian].

[6] A. A. Stepanova and M. M. Umanskii, Proceedings of Conference on the Chemistry of Boron and its Compounds, Karpov Physico-Chemical Institute (1955).

[7] P. Blume and F. Bertaut, "Contribution a l'Etude des Borures a Teneur Elevee en Bore," Acta Cryst. 7, 81 (1954).

[8] N. N. Zhuravlev, "X-ray determination of the structure of SiB_6," Crystallography (USSR) 1, 6, 666-668 (1956).

Moscow State University

Received October 8, 1956

PHOTOELECTRIC MULTIPLIER FOR SCINTILLATION GAMMA SPECTROMETERS

L. G. Leiteizen, B. M. Glukhovskoi and I. Ia. Breido

The resolving power of scintillation spectrometers depends mainly on the luminescent properties of the crystals and on the amplitude resolution of the photoelectric multiplier. The pre-1955 industrially produced multiplier of type FEU-19 with an end-face semitransparent cathode of ~9cm² area had, as a rule, a low amplitude resolution; for γ -spectrometry only single specimens were suitable. The modernization of the construction of the multiplier with the introduction of a number of technological innovations, carried out in 1955-56, led to a radical improvement in all the parameters of the multiplier, particularly its amplitude resolution. Many of the FEU-19 multipliers manufactured in 1956 had amplitude resolutions R≤ 12%.* About 60% of them had integral cathode sensitivities $\Sigma_{cw} \geq 30\mu$ a/lu, and 'blue' sensitivities [1] $\Sigma_{cb} \geq 6\mu$ a/lu. More than ⅘ of the latter multipliers have R<10% and are manufactured under the designation FEU-29. Their distribution with respect to resolution is given in Fig. 1.

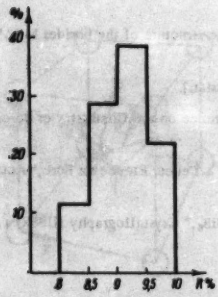

Fig. 1. Distribution of 200 FEU-29 instruments (in %) with respect to amplitude resolution R.

The multipliers with R ≈ 9% were compared with some foreign and home multipliers under the same conditions, and no advantages of one over any other were detected. These observations and also the considerations expressed below were reasons for introducing a systematic selection of the multipliers giving high amplitude resolution.

As we know, one of the important factors affecting amplitude resolution is the collection coefficient for photoelectrons on the first emitter. This coefficient depends on the focussing properties of the electron optical system. Figure 2 shows the electron trajectories for the cathode-diaphragm– first emitter system of the modernized multipliers. We can see that the construction of the electrodes and their position ensures the collection of photoelectrons from practically the whole surface of the photocathode. This is confirmed both by direct measurements of the collection coefficient and by the above-noted marked improvement in the amplitude resolution of the modernized multipliers.

* The resolution was measured with a good NaI(Tl) crystal 30 mm in diameter under γ -irradiation from Cs^{137}.

A second no-less-important factor is the sensitivity (particularly the 'blue' sensitivity) of the photocathode. The scatter of this parameter in mass-produced FEU instruments is due to a sum of small technological deviations which have not yet been brought under control; therefore the selection of particular multipliers for high cathode sensitivity is quite legitimate, particularly since the remaining multipliers are perfectly suitable for scintillation radiometers.

The advantage of employing an individual choice of inter-electrode voltages in multipliers has already been pointed out [1]. In Fig. 3 we give statistical graphs for 200 FEU-29 instruments for the stages C – D, D – E_1, E_1 – E_2, and E_2 – E_3. It can be seen that the stages are distributed in a cluster, with a slight scatter. For a verification of their criticality we conducted a special experiment.

From the results of control tests on 30 randomly taken multipliers with individually chosen operating conditions we calculated the mean distribution of the interstage voltages. With this fixed distribution (C – D – 1.5%; D – E_1 – 14.7%; E_1 – E_2 – 1.5%; E_1 – E_3 – 12.3%; E_3 – E_4 ... E_{10} – E_{11} – 5% each; E_{11} – E_{12} – E_{13} – total – 10% each) we measured the amplitude resolution of the same 30 multipliers. With the individual setup, the mean value of R was 9.2% with a scatter from 8.3 to 10%. With the average setup, R was 9.6%, and two multipliers showed R > 10%, but the scatter for the rest was from 8.5 to 10%. Since the operating conditions do not appear critical, the FEU-29 is issued with a standard set of operating conditions. Measurements we conducted showed that high amplitude resolution is ensured by the particular construction of the multipliers when various materials are used for the emitters and photocathodes. This preserves the distribution of interstage voltages, shown above.

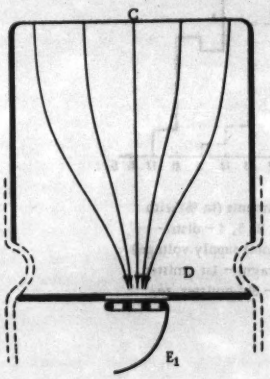

Fig. 2. Diagram of electron optical system and trajectories of photoelectrons in modernized multipliers FEU-19 and FEU-29. C – cathode; D – diaphragm; E_1 – emitter.

A third factor is the linearity, i.e., the proportionality between the pulse amplitude on the multiplier output and the energy of radiation incident on the crystal. Tests showed that the FEU-29 operates linearly up to an amplitude of output pulse of about 7 v with R_L = 50 kohm, $C_{assembly} \leq 10 \mu\mu f$.

Below we give the mean values of the basic parameters of FEU-29:

Ingegral cathode sensitivity, Σ_{cw}	40μ a/lu
'Blue' cathode sensitivity, Σ_{cb}	8μ a/lu
Amplification (in rated spectrometric operating conditions with U_{av} = 1000 v)	$2 \cdot 10^5$
Noise amplitude (expressed as energy, for NaI(Tl) crystal)	≤ 5 kev.
Resolution for $Cs^{137} \rightarrow$ NaI(Tl)	8.2-9.4%

At the present time the amplitude resolution of the multiplier is determined in pair with an NaI(Tl) crystal irradiated by Cs^{137} or Co^{60} preparation. In effect, in this way the energy resolution of a crystal-multiplier pair is measured. An account has already been given [2] of the marked difference between the resolutions determined by a crystal and by a pulse source of light, giving a photocathode illuminance equal to that of the crystal. We conducted comparative measurements of the amplitude resolution of 10 FEU-29 instruments; 1) by a selected crystal of NaI(Tl) irradiated by Cs^{137} and 2) by a pulse gas-discharge lamp through a blue (λ_{max} = 4000 A) filter. The results of measurement are given on Table 1.

The results of Table 1 show that the energy resolution of the spectrometer could be substantially improved at the expense of the crystal.

For the purpose of selecting good crystals we carried out measurements of resolution and pulse amplitude with the 'IN' series of crystals of the Khar'kov Chemical Reagent Factory on a good FEU-29 multiplier. As a control we conducted measurements with several crystals put at our disposal by the Institute of Crystallography; with them we obtained resolutions between 8.2 and 9%. As regards the factory crystals, only 3 out of 24 tested gave values of R ≈ 9%, the remainder being much poorer; 2 gave R ≈ 10%, 3 gave 12.5 to 14%, the remainder – 10.5 to 14%. With all these crystals we obtained a pulse amplitude U_p 10-30% less than with the crystals of the Institute of Crystallography. On comparing the factory data for the 'light yield' with the values of U_p and R obtained in our measurements, we did not manage to find any relation between these parameters. It is essential, we conclude, that the values of R and U_p for the crystals should be measured directly in the factory. A selection of the necessary assembly of 'standard' multipliers and crystals does not present much difficulty at present.

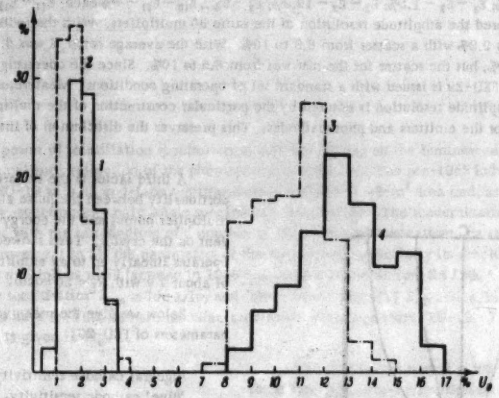

Fig. 3. Distribution of 200 FEU-29 instruments (in %) with respect to interstage voltages; Curves 1, 2, 3, 4 – distribution with respect to voltages (as % of total supply voltage) for the stages cathode-diaphragm, diaphragm – 1st emitter, 1st emmiter – 2nd emitter, 2nd emitter – 3rd emitter, respectively.

TABLE 1

No. of FEU (arbitrary)	1	2	3	4	5	6	7	8	9	10
R from crystal	8.2	9.5	8.6	9.0	9.2	8.8	9.6	9.0	9.5	8.2
R from pulse illuminator	4.8	5.0	4.5	6.0	6.0	5.5	6.2	5.5	5.5	4.3

In conclusion the authors express their great appreciation to L. M. Beliaev and his colleagues for supplying the crystals and participating in discussion of the experiments.

LITERATURE CITED

[1] I. Ia. Breido, B. M. Glukhovskoi and L. G. Leitelzen, "Industrial types of photoelectric multipliers," Radiotekh. i Elektron. 10 (1956).

[2] T. Godlav and V. Uedi, "Homogeneity of the photocathode and resolution of a scintillation spectrometer," Problemy Sovremennoi Fiziki 12, 49-54 (1955).

Received January 21, 1957

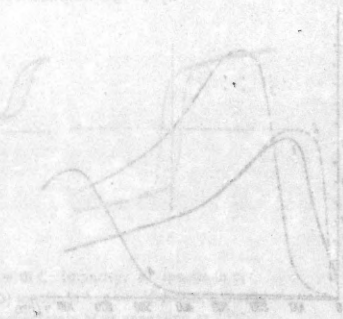

THE NATURE OF POLARIZATION IN CRYSTALS OF IMPURE ROCHELLE SALT

V. P. Konstantinova and V. A. Iurin

It is known that the introduction of various impurities into ferroelectric crystals can change the electrical properties to a considerable extent. Thus, for example, the work of Kurchatov and Eremeev [1, 2] shows that the addition of only 1% of sodium ammonium tartrate to a solution of pure Rochelle salt cuts in half the ferroelectric temperature range of the crystals growing from this solution. The addition of 3% of the same salt completely deprives Rochelle salt of its ferroelectric properties. With a decrease in the percentage of Rochelle salt in solution to 79%, the ferroelectric properties of the crystals have a new character, narrower in the region of low temperatures. There are also other studies devoted to the effect of impurities on the electrical properties of Rochelle salt crystals [3-5]. Then there is the interesting case of the effect of impurities which form in a crystal of Rochelle salt as the result of radioactive exposure, when an anomalous electrical polarization develops in the crystal [6].

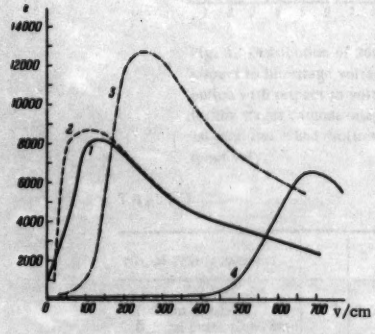

Fig. 1. Dielectric constant – field intensity curves for crystals of Rochelle salt with various impurities. 1) pure Rochelle salt; 2) with B impurity; 3) with Al impurity; 4) with Cu impurity. Measurements were made with a ballistic galvanometer at 11°C.

The present paper will touch only on questions connected with the irregular distribution of impurities in the growth pyramids of the separate faces, and with the anomalous polarization of specimens cut out of the growth pyramid of face c (001) of Rochelle salt crystals grown from a solution with the addition of 2% of $CuCO_3$.

A study of the polarization in a constant electrical field of Rochelle salt crystals grown with different impurities showed (Fig. 1) that, among the other impurities, the addition of $CuCO_3$ occupies a special place. While crystals grown from solutions with additions of Al and H_3BO_3 powder possess nearly the same nonlinear polarization as does pure Rochelle salt, crystals grown from a solution with the addition of $CuCO_3$ behave quite differently. The dielectric constant in the direction of axis a of a crystal with $CuCO_3$ impurity is not large and is practically constant down to a constant field intensity of 400-450 v/cm. This necessitated a more thorough study of these crystals.

Crystals of sky-blue color grow from a solution of Rochelle salt containing 2% of $CuCO_3$, with the color intensity variable in different parts of the crystal. The color intensity, extremely high in the growth pyramid c (001), diminishes in the growth pyramid of the other faces in the following order: (001), (210),

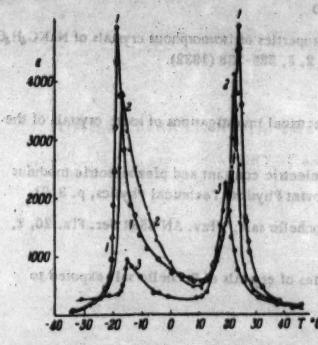

Fig. 2. Dielectric constant – temperature curves for Rochelle salt with Cu impurity. Curves 1, 2, 3 are for specimens cut out of growth pyramids of faces b (010), p (120) and c (001), respectively. Measurements were made on the NIE-1 bridge at a frequency of 50 cps.

(110), (100) and (010). The electrical properties of the crystal also change parallel to the change in color. Thus, a study of the temperature dependence of the dielectric constant in the direction of axis a of specimens cut out of growth pyramids of faces (010), (120) and (001) shows that the Curie points in these specimens are different (see Fig. 2). From the curves presented in Fig. 2 it is apparent that specimens cut out of the growth pyramids of face c (001), which absorb the copper ions, have the lowest value of dielectric constant and the narrowest temperature interval of the ferroelectric range.

The investigation of polarization in strong alternating fields by hysteresis loops shows (see Fig. 3, a) that in specimens cut out of the growth pyramids of face b (010), normal hysteresis loops are observed. However, in specimens cut out of the growth pyramids of face c (001) anomalous loops are observed, analogous to the hysteresis loops of nonferroelectrics down to fairly high values of field intensity (450-500 v/cm) the crystal behaves practically like a linear dielectric, and only in the fields at the ends of the linear section of the curve are there nonlinear branches (Fig. 3, b). The latter circumstance is in keeping with the data presented for these same specimens in Fig. 1.

Interesting phenomena are observed for specimens with double loops during heat treatment. Annealing of the specimens for 5-6 hours at 40°C and subsequent slow cooling (1-2 hours) to 18-19°C bring a specimen to a condition characterized by a normal hysteresis loop (Fig. 3, c). After "relaxation" of the specimen at room temperature for two days, the condition producing polarization with the original double loop is completely reestablished (Fig. 3, d).

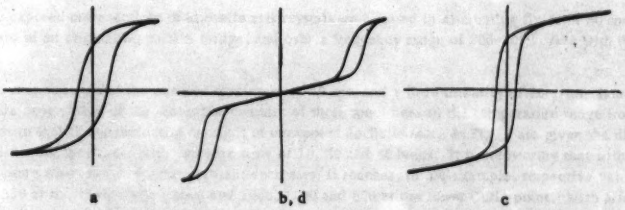

Fig. 3. Hysteresis loops for Rochelle salt with Cu impurity. a) specimen cut out of growth pyramid of face b (010); b) specimen cut out of growth pyramid of face c (001); c) the same specimen immediately after annealing at 40°C; d) the same specimen 50 hours after annealing. Temperature 19.5°C, frequency 50 cps.

The anomalous polarization in crystals of Rochelle salt is apparently caused by strains originating in the crystal lattice as a result of the introduction of an impurity. For an explanation of phenomena occurring during and after annealing, a more detailed investigation of the physical properties of these crystals is required, in particular their domain structure, as well as elucidation of the character of the entry of the copper ions into the crystal lattice.

The authors express appreciation to Academician A. V. Shubnikov for close interest in the work and to I. S. Zheludev for discussion of the results.

LITERATURE CITED

[1] M. A. Eremeev and B. V. Kurchatov, "The electrical properties of isomorphous crystals of $NaKC_4H_4O_6 \cdot 4H_2O$ and $NaNH_4C_4H_4O_6 \cdot 4H_2O$," J. Expti.-Theoret. Phys. (USSR) 2, 5, 329-338 (1932).

[2] B. V. Kurchatov, Ferroelectrics [in Russian] (1933).

[3] J. N. Thorp and H. E. Buckly, "Morphological and dielectrical investigations of some crystals of the Rochelle salt type," Acta Cryst. 2, 5, 333-337 (1949).

[4] T. Kh. Chormonov, "The effect of impurities on the dielectric constant and piezoelectric modulus of Rochelle salt," J. Tech. Phys. (USSR) 26, 2, 323-326 (1956) [Soviet Physics—Technical Physics, p. 319].

[5] I. Ia. Eisner, "Some physical properties of crystals of Rochelle salt," Izv. AN SSSR Ser. Fiz. 20, 2, 215-218 (1956).

[6] I. S. Zheludev and V. A. Iurin, "Some physical properties of crystals of Rochelle salt exposed to radioactive rays," Izv. AN SSSR, Ser. Fiz. 20, 2, 211-214 (1956).

Institute of Crystallography
Academy of Sciences USSR

Received February 7, 1957

SOME ALTERATIONS IN THE DIELECTRIC PROPERTIES OF ROCHELLE SALT CRYSTALS EXPOSED TO X-RAYS

I. Ia. Eisner

In the work of Vigness [1] there is a brief note to the effect that Rochelle salt turns yellow under the action of x-rays. Studies by Zheludev, Iurin and others [2, 3] are devoted to the investigation of some properties of Rochelle salt exposed to radioactive irradiation.

The study of the effect of crystal-lattice dislocations connected with color centers on the dielectric constant of monocrystals of Rochelle salt is of definite interest. In view of this, the author has exposed cross sections of Rochelle salt crystals to x-rays (with the aid of the BSV x-ray tube with iron anticathode, 30 kv voltage in the tube and 10 ma current). The specimens were placed in the appropriate chambers at a distance of 5 cm from the protective casing of the x-ray tube. The exposure of the samples was made either by simultaneous use of four apertures of the tube with different exposure time for the individual specimens, or just one specimen was exposed with a gradually increasing exposure time, each time after preliminary measurements. It should be noted that in the first case all four specimens were cut out of the same lamina of the cross section of the Rochelle salt crystal.

The exposed cross sections of Rochelle salt crystals were tested in alternating fields of 50 cps frequency with the aid of an alternating current bridge, and over a frequency range of 200-500 kc/sec with the aid of a Q-meter.

The examinations of the exposed specimens at 50 cps and a field intensity of 20 v/cm showed that the temperature dependence of the dielectric constant of these specimens in the temperature range from −20 to 40°C corresponds to that of the dielectric constant of unexposed Rochelle salt. In Fig. 1 are given the dielectric characteristics for specimens with exposure time of 10, 20 and 40 hours. It is noteworthy that with an increase in the exposure time, the dielectric constant decreases; it reaches, in the example, respective values of 1660, 1460 and 880 at the upper Curie point, and 1250, 1100 and 500 at the lower Curie point. With a further increase in exposure time for the specimens the temperature dependence of the dielectric constant levels off; the constant remains abnormally high, but the difference between its values in the range of spontaneous polarization and at the Curie points is sharply reduced. In the paraelectric range, the dielectric constant of specimens exposed for not more than 50 hours as well as the dielectric constant of unexposed specimens follows the Curie-Weiss law. To resolve the question of the displacement of phase transition points in Rochelle salt crystals as a result of their exposure to x-rays requires additional examinations of specimens which undergo especially long exposure.

The exposed specimens were also examined in strong electrical fields of the order 1000 v/cm. A dependence of dielectric constant on the electrical field intensity is observed for all of the specimens, while a sharper dependence of dielectric constant on intensity is observed for less exposed specimens. The dielectric constant increases with an increase in intensity and reaches a maximum at a certain field intensity. Thus, for example, for a specimen with 40 hours exposure $\epsilon = 2850$ at a field intensity of 350 v/cm and at 17.5°C;

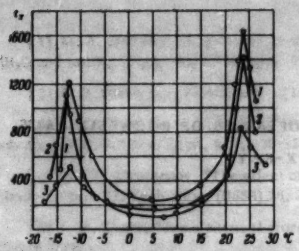

Fig. 1. Temperature dependence of the dielectric constant of cross sections of exposed Rochelle salt. 1) exposure time 10 hours; 2) exposure time 20 hours; 3) exposure time 40 hours.

with a further increase in intensity the dielectric constant decreases. With an increase in specimen exposure time, the field intensity at which the dielectric constant of the exposed specimen reaches a maximum is displaced to greater values.

The examinations of specimens in high-frequency fields were made at intensities of 20-25 v/cm. The results of studies in the frequency range 500-5000 kc/sec show that the dielectric constant of specimens with different exposure time fluctuates around the value 120 (at a temperature of 17°C). It is therefore concluded that at these frequencies the dielectric constant of specimens tested in the range of exposure time used is almost identical with the dielectric constant of unexposed Rochelle salt, for which it was established that in frequency range 500-5000 kc/sec at 17°C, $\epsilon = 120$.

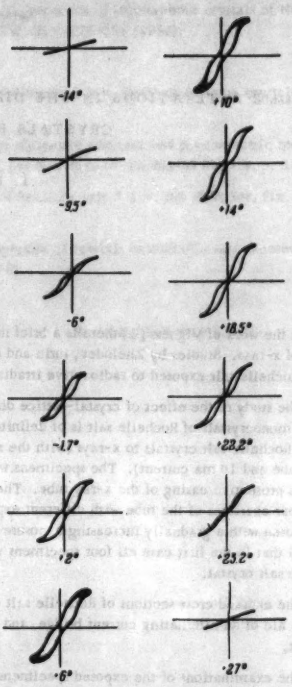

Fig. 2. Oscillograms of hysteresis loops of cross sections of exposed Rochelle salt at different temperatures. Exposure time 15 hours, f = 50 cps, E_{max} = 450 v/cm, $P_{max} = 10.4 \cdot 10^{-8}$ coulombs $\cdot$ cm^{-2}.

It must be assumed that the inert atoms originating in the crystals as a result of exposure – the color centers (in negligible quantity) which accompany these phenomena and deform the crystal lattice – influence only the slowly acting polarization mechanisms connected with dipole polarization. As a result of this, considerable alterations in the dielectric constant of exposed specimens of Rochelle salt are observed (in comparison with the dielectric constant of unexposed specimens) in low-frequency fields (for example, 50 cps). In alternating fields with a frequency of the order $10^5 - 10^6$ cps, at which the dielectric constant of Rochelle salt is determined by a different quick-acting polarization mechanism, the color centers originating in specimens not exposed especially long to x-rays do not change the dielectric constant of these specimens appreciably.

A study of the dielectric hysteresis in cross sections of Rochelle salt crystals with different exposure time was made. The examinations show that the dielectric hysteresis loops of exposed specimens are distorted in comparison with the normal loops of unexposed Rochelle salt; for specimens with 15-hour exposure, the loops are narrowed in the middle; for specimens with 50-hour exposure, double loops are observed which suggest

hysteresis loops of nonferroelectrics; a further increase in exposure time of a specimen leads to a linear dependence of the instantaneous polarization value on the field intensity.

In Fig. 2 is given a series of oscillograms obtained in the temperature range −16-26°C for specimen with 15 hours exposure (the operation of the BSV tube is the same as in the foregoing examples). The coercive force, which reaches a maximum value of 60 v/cm, and the residual polarization, which reaches a value of 54 CGSE at t = 8°C, were determined on the basis of these oscillograms. The temperature dependence of P_{max} shows a decrease in polarization of approximately 30% in comparison with the polarization of an unexposed specimen in an electrical field of intensity E_{max} = 450 v/cm.

The changes described in Rochelle salt as a result of exposure to x-rays can be viewed as the emergence of some impurities in these crystals. From this point of view, the electrical properties of Rochelle salt crystals exposed to x-rays are in all probability closely connected with the properties of crystals of Rochelle salt grown in the presence of an impurity in the solution [4].

LITERATURE CITED

[1] I. Vigness, "Dilatations in Rochelle salt," Phys. Rev. 48, 198-202 (1935).

[2] I. S. Zheludev, M. A. Proskurnin, V. A. Iurin and A. S. Boberkin, "Some peculiarities in the polarization of Rochelle salt under radioactive exposure," Doklady Akad. Nauk SSSR 103, 207-208 (1955).

[3] I. S. Zheludev and V. A. Iurin, "Some physical properties of Rochelle salt crystals under radioactive exposure," Izv. AN SSSR, Ser. Fiz. 20, 211-214 (1956).

[4] I. Ia. Eisner, "Some physical properties of crystals of Rochelle salt," Izv. AN SSSR, Ser. Fiz. 20, 215-218 (1956).

L'vov Pedagogical Institute

Received February 1, 1957

EXCITATION OF ULTRASONIC VIBRATIONS IN QUARTZ

K. N. Baranskii

A large number of problems of molecular structure of a substance can be solved by investigation of its elastic properties in a wide range of frequencies. At present ultrasonic methods of investigation are widely used up to frequencies of $2 \cdot 10^8$ c/sec. Only a few works are known in which absorption of sound in crystals [1], speed of sound in mercury up to the frequency of $1 \cdot 10^9$ c/sec [2], and diffraction of light by ultrasonic waves in quartz [3] and in liquids [4] up to frequencies of $3 \cdot 10^8$ c/sec have been discussed.

The possibility of investigation of elastic properties of transparent bodies at ultrasonic frequencies ($10^9 - 10^{10}$ c/sec) by the fine structure of light diffracted by heat waves, predicted in the works of Brillouin and Mandelshtam, was first realized by Gross [5] for quartz. For solid bodies this method is complicated by the exceptionally low intensity of diffracted light and therefore optical studies of this type are few.

In the present work an attempt was made to work out a rational radiotechnical method of excitation of supersonic vibrations in quartz in the frequency range of $1 \cdot 10^8$ c/sec to $10^9 - 10^{10}$ c/sec. For detection and investigation of high frequency sound the diffraction of light by ultrasonic waves was chosen because it reveals the processes which take place within the vibrating body and permits measurement of its elastic properties. In utilizing hypersonic vibrations this technique naturally merges into the methods of study of molecular diffraction of light making the latter easier by producing diffracted light of much greater intensity.

The high sensitivity of the light diffraction method as compared with other methods of detecting ultrasonic waves of very high frequencies must be noted. The fact is that, as shown by Motulevich [6], the ratio of the intensity of diffracted light of the first order I_1 to the intensity of incident light I_0 is proportional to the kinetic energy of elastic vibrations $\rho\omega^2 A^2/2$. Therefore, in order to keep the ratio I_1/I_0 constant (for example, at the level allowing visual observation of diffracted light), it is permissible to decrease the displacement amplitude in the ultrasonic wave while increasing the frequency.

Quartz was chosen as the subject for study because it loses little electromagnetic energy at very high frequencies and possesses excellent optical properties. Optically clear quartz was used to prepare polished plates with parallel flat faces.* The edges of the plates, 12, 50 and 20 mm in length, were oriented parallel to the crystallographic axes of quartz, X, Y and Z, respectively. Plates of this size allowed passage of a sufficiently broad beam of light and provided a relatively large volume for propagation of ultrasonic waves.

For observing the diffraction of light in ultrasonic waves, a plate of quartz was placed on the stage of a 30° goniometer GS-30 especially adapted to hold the plate firmly and to permit application of electric current to its edges. Mercury lamps of high and low vacuum were used as the sources of light.

The diffraction of light was studied on longitudinal waves passing through quartz parallel to the X axis. For this purpose, current was directed along the X axis while light was transmitted parallel to the Y or Z axis. Oscillators on coaxial resonators with metal-ceramic lamps GI-11B (LD-11) were used, allowing smooth variation of frequency from $1 \cdot 10^8$ c/sec to $2 \cdot 10^9$ c/sec. The oscillators delivered up to 6 volts. Their frequency was measured by resonance wavemeters of the first order of precision.

*Selection and preparation of plates were done by A. B. Gilvarg, Associate of the Institute of Crystallography of the Academy of Science, and by M. N. Kaposhina, Associate of the Department of Physics, University of Moscow, to whom the author expresses gratitude.

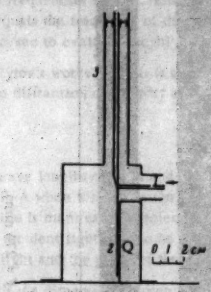

Fig. 1. Mounting of quartz for frequencies from $1 \cdot 10^8$ to $1 \cdot 10^9$ c/sec.
1) coaxial cable from the oscillator; 2) a strip of bronze foil; 3) part of the coaxial cable shorted by a movable piston; Q) quartz plate.

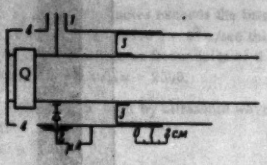

Fig. 2. Coaxial resonator with quartz.
1) coaxial cable from the oscillator; 2) resonator tuning indicator; 3) tuning rod; 4) windows for light; Q) quartz plate.

For frequencies up to $1 \cdot 10^9$ c/sec quartz plates were mounted in the usual way between two strips of copper or bronze foil pressed tightly against the faces normal to the X axis of quartz. High frequency current was delivered from the oscillators to the plate holder by a coaxial cable with resistance of 50 ohms. To insure maximum intensity of the field between the foil strips they were attached to a piece of coaxial cable which could be short-circuited at the opposite ends by a movable plunger (Fig. 1); in this way a system of standing electromagnetic waves was produced in the cable. By varying the length of the cable the densest part of the electric field could be shifted toward the foil strips.

For frequencies of the order of $1 \cdot 10^9$ c/sec it was found possible to connect the foil strips on the ends opposite from the generator and switch off the shorted portion of the cable. The fact is that the length of the electromagnetic wave in quartz ($\epsilon = 4{,}7$) at the frequency of $1 \cdot 10^9$ c/sec is only 14 cm and for a plate 5 cm long the densest part of the electric field falls near its center. In this case the ultrasonic field of sufficient intensity occupies only a small portion of the volume of the plate. Therefore, for the higher frequencies it is advisable to insert quartz into the cavity of a quarter-wave coaxial resonator in which it is possible to obtain a uniform electric field of a much larger magnitude. The use of a coaxial resonator for lower frequencies is not convenient because of its large size and relatively high precision which requires more careful tuning than the condenser with the shorted coaxial cable. In the coaxial resonator (Fig. 2) the quartz plate, Q, was held between the end of the inner tube and the cover of the outer tube whose sides were provided with windows for passage of light.

This technique permitted excitation in the quartz plates of sound vibrations of frequencies up to $1{,}64 \cdot 10^9$ c/sec and observation of diffraction lines of adequate intensity. The stability of the oscillators made it possible to observe diffraction during several hours without noticeable heating of the quartz plate.

The basic frequency of the longitudinal vibrations in the quartz plates was $2{,}4 \cdot 10^8$ c/sec and thus with frequency of $2 \cdot 10^9$ approximately the 6800th harmonic was excited. The length of the longitudinal sound wave at this frequency is $3{,}5 \cdot 10^{-4}$ cm, i.e., it approaches the length of light waves in the infrared region. The ultrasonic lattice had 280 periods per mm, and the angle of diffraction for 5780 A was 9°28'.

The presence of standing ultrasonic waves throughout the plate excited by an electric field was checked by the decrease in intensity of diffracted light as the diaphragmed beam of light was allowed to pass through the thickness of the plate and by the resolution of yellow lines 5769 A and 5790 A in the spectrum of a low pressure mercury lamp.

It was found that from $\nu = 3 \cdot 10^8$ c/sec the quartz plates are equally well excited at both even and odd harmonics. It is interesting to note that with increase of frequency the need for precise tuning of the oscillator

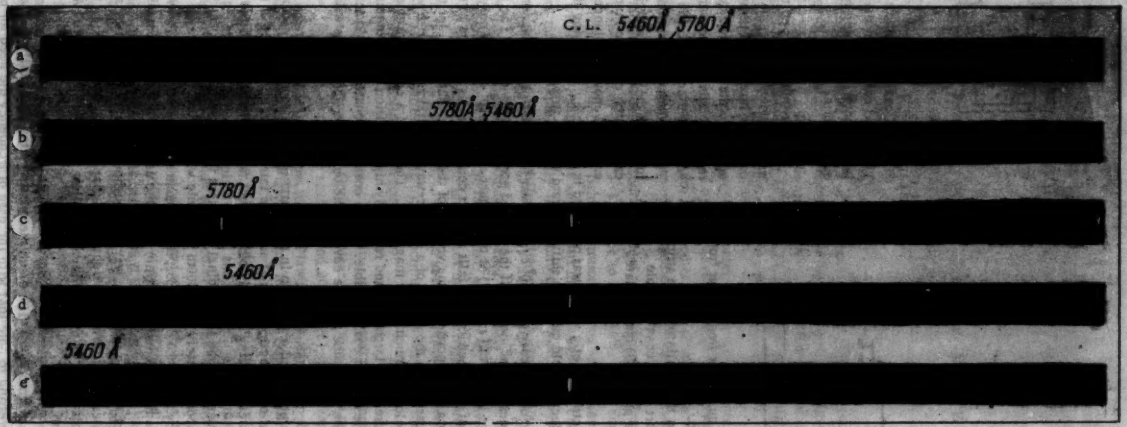

Fig. 3. Spectra of light diffracted by ultrasonic waves in quartz (camera F = 270 mm).
a,b) $\nu = 3.33 \cdot 10^8$ c/sec; c,d) $1.16 \cdot 10^9$ c/sec; e) $1.64 \cdot 10^9$ c/sec.

to the next harmonic of the quartz plate diminished, and starting from frequencies of the order of $6 \cdot 10^8$ c/sec for any frequency, the intensity of light diffracted by the quartz plate is above zero. Evidently this is due to the fact that the width of the resonance curve of the quartz plate at these frequencies exceeds the interval between the frequencies of the overtones excited in quartz. Since for frequencies above $3 \cdot 10^8$ c/sec this interval $\Delta\nu$ equals the frequency of the quartz plate $\nu_0 = 2.4 \cdot 10^6$ c/sec, it is possible at frequencies of the order of $6 \cdot 10^8$ c/sec to evaluate roughly the quality of quartz by the formula $Q = \nu/\Delta\nu = 2500$.

In Rytov's works [7, 8] it is shown that the phenomenon of diffraction of light by ultrasonic waves differs little from diffraction of light by a one-dimensional grating until

$$\frac{\lambda}{\Lambda^2} l \qquad (1)$$

(λ, Λ – wave lengths of light and sound, l – length of path of light) becomes much smaller than unity. With decrease in Λ when the expression (1) becomes greater than unity the three-dimensional character of the ultrasonic lattice is manifested in selective (Bragg) reflection of light. The intensity of light diffracted at an angle φ to the incident light will be be maximum if the plate of quartz is so placed that the angle θ between the incident light and the plane of the sound wave front satisfies the condition $\theta = \lambda/2\Lambda = \varphi/2$.

With the dimensions chosen for the quartz plates $\lambda = 5460$ A and diffraction of light on longitudinal waves, the selective reflection of light began to be apparent even at frequency of $1 \cdot 10^8$ c/sec in asymmetry of intensities in the spectra of +1 and -1 orders when the plate was turned slightly about the direction of incident light. At frequency $3 \cdot 10^8$ c/sec it was possible by changing the sign of the angle to observe either the spectrum of +1 or the spectrum of the -1 order (Fig. 3, a and b). The relation $\theta = \varphi/2$ was strictly fulfilled in the intermediate frequencies.

S. M. Rytov showed that with a fixed value of θ the intensity of diffracted light is not zero in the interval

$$\varphi_1 = 2\theta - \frac{n\Lambda}{l} \quad \text{to} \quad \varphi_2 = 2\theta + \frac{n\Lambda}{l}$$

(n = refractive index). Indeed, by changing the angle in the diffraction spectrum, it is possible to observe only individual spectral regions whose width decreases with shortening of Λ. At $\nu = 1 \cdot 10^8$ c/sec the degree of monochromatization increases to such an extent that the yellow and green lines of mercury are observed at different values of the angle θ (Fig. 3, c and d). Thus the hypersonic lattice in quartz produces monochromatic light just as the crystal lattice produces monochromatic x-rays.

Measurements of the angular positions of diffraction lines of the mercury spectrum with simultaneous measurement of the oscillator frequency have shown that within the investigated range the velocity of propagation of longitudinal waves remains constant within the limits of accuracy of our measurements (±1%) and equals 5750 m/sec. This permits utilization of diffraction of light by ultrasonic waves for wave length measurements within a broad range of frequencies. From the condition of refraction $\Lambda \sin \varphi = \lambda$, it follows that the angular position of the spectral line of light of wave length λ and with constant speed of sound v uniquely determines the frequency of electric oscillations ν, since $\nu = v/\Lambda$.

The author expresses his gratitude to I. A. Iakovlev for suggesting this subject and for his interest in the research and to G. P. Motulevich for valuable discussions.

LITERATURE CITED

[1] S. I. Sokolov, "Absorption of ultrasonic vibrations by crystals," Doklady Akad. Nauk (SSSR) 64, 503-505 (1949).

[2] G. R. Ringo, J. W. Fitzgerald and B. G. Hurdle, "Propagation of u. h. f. sound in mercury," Phys. Rev. 72, 87 (1947).

[3] S. Ia. Sokolov, "Modern problems of application of ultrasonics," Uspekhi Fiz. Nauk 40, 3-30 (1950).

[4] Ramachandra Rao, Satyanarayana Murty, "Diffraction of light by ultrasonic waves at 300 M c/s," Nature 178, 160 (1956).

[5] E. F. Gross, "Über Anderung der Wellenlänge bei Lichtzerstreuung in Kristallen," Z. Physik 63, 685 (1930).

[6] G. P. Motulevich, "Molecular diffraction of light in crystals," (Dissertation) Trudy Fiz. Inst., Akad. Nauk SSSR 5 [In Russian].

[7] S. M. Rytov, "Diffraction of light by high frequency sound," J. Exptl. Theoret. Phys (USSR) 5, 843-856 (1935).

[8] S. M. Rytov, "Diffraction of light by ultrasonic waves," Izvest. Akad. Nauk SSR Ser. Fiz. 2, 223 (1937).

Lomonosov State University of Moscow

Received November 30, 1956

INHOMOGENEITY OF STRESS DISTRIBUTION IN THE GRAIN OF A POLYCRYSTAL IN THE INITIAL STAGE OF PLASTIC DEFORMATION

V. E. Kochnov

In the investigation of elastic and plastic deformation in polycrystalline materials the question of the homogeneity of stress distribution in separate grains is of special interest. Our experiments, conducted on polycrystals of silver chloride, may assist in clarifying this problem.

We observed the initial stage in the formation of the birefringent bands, described by Obreimov and Shubnikov [1] for plastically deformed rock salt crystals and which have since been frequently observed on other cubic crystals, including silver chloride [2, 3].

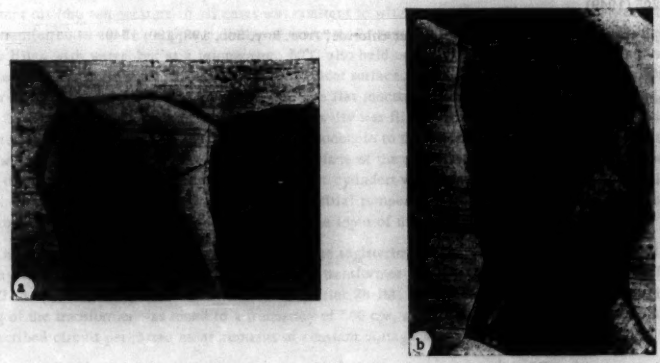

Fig. 1. Appearance and development of birefrigent bands in the initial stage of plastic deformation of polycrystalline AgCl. a) bands appear at junctions of grains; b) with increased load number of bands increases. Polarized light, crossed nicols. 256x.

Plane specimens of polycrystalline silver chloride 60x 6x 0,5 mm (monocrystalline in thickness) were subjected to tension on the stage of a polarizing microscope. A well-annealed specimen in the absence of a load

does not show birefringence. With the application of a small load of the order 35-45 g/mm^2 there occurs a lightening of the grain boundaries or the boundaries of groups of grains. On increasing the load to 70-80 g/mm^2 there is observed an extremely inhomogeneous distribution of the stressed grains in the specimen. Some groups of grains appear light, others remain dark. When the load is removed, the specimen returns to its original condition and does not possess residual birefringence. When the load is increased to 95-100 g/mm^2 birefringent bands appear in the individual grains. The moment these bands form the whole grain appears to 'flash' for an instant. First two to three bands appear in some part of the grain. When the load is removed these bands do not disappear. This obviously signifies that changes have taken place in the grain structure, i.e., the initial stage of plastic deformation is passed; yet observation in transmitted nonpolarized light or examination of the surface of the specimen in reflected light do not reveal any changes in the grain.

Initially the bands are widely spaced, and then new bands appear between the old. All the developing birefringent bands are localized in one grain and are parallel to one another. In every other grain the directions of the bands are different. In order to discover what sites in the grain gave rise to the birefringent bands, we chose specimens with grains of different size. Under tension deformation the birefringent bands arise mainly at the grain boundaries (Fig. 1, a), and new bands form parallel to the old (Fig. 1, b).* From this we may surmise that the sites giving rise to the first birefringent bands are places of overstrain. The random directions of these bands in different grains even of grain-oriented specimens can be explained by the fact that overstrains occur at different sites in the individual grains and the greatest forces act in different directions. Thus, in grains of polycrystalline silver chloride there is observed an inhomogeneity of the stressed condition. The stresses are concentrated at the grain boundaries. The direction of the greatest acting forces determines the direction of the arising birefringent bands.

LITERATURE CITED

[1] I. V. Obreimov and A. V. Shubnikov, "Investigations of plastic deformations in rock salt by the optical method," J. Russ. Phys.-Chem. Soc. Phys. Sec. 58, 817 (1926).

[2] A. V. Stepanov "A new optical method of studying stresses in polarized light," J. Tech. Phys. (USSR) 19, 205 (1949).

[3] J. F. Nay, "Plastic deformation of silver chloride," Proc. Roy. Soc. 198, 190, 1949.

Moscow Steel Institute

Received November 22, 1956

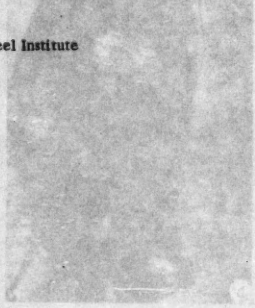

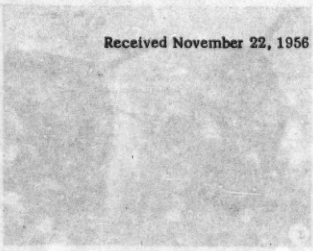

* The fine horizontal bands seen on the photograph are traces of surface treatment.

DETERMINATION OF TEMPERATURE-CONDUCTIVITY COEFFICIENTS IN CRYSTALS OF ETHYLENE DIAMINE TARTRATE

I. M. Sil'vestrova

In this communication a description is given of the measurement of the temperature-conductivity coefficients of a monoclinic crystal of ethylenediamine tartrate (EDT) for different crystallographic directions. For these measurements we used one of the nonstationary methods, namely, the method of causing a temperature movement in the specimen by putting it in contact with a standard [1].

Specimens of the test material were first placed on a copper cylinder 40 mm in diameter and 60 mm long and held for some time at a temperature of 25°C. To ensure the best thermal contact between cylinder and specimen we used glycerine. The cylinder was placed in a thermostat filled either with distilled water or with transformer oil (the temperature in all cases was constant to within ±0.05°C). The specimens were then very swiftly transferred to another copper cylinder of diameter 30 mm and height 50 mm, placed in another thermostat also filled with water, but at a temperature 50°C also held constant to within ±0.05°C. Glycerine was again used to ensure contact of the specimen with the cylinder surface. On the opposite upper surface of the specimen a copper-constantan thermocouple was placed. The flat junction of the thermocouple was inserted in a small cavity, 0.1-0.2 mm deep, made in the crystal; the cavity was filled with a drop of strongly saturated EDT solution which swiftly crystallized, thus gluing the thermocouple to the specimen surface. By means of the thermocouple we measured the temperature of the upper surface of the specimen as a function of time. The other ends of the thermocouple were soldered to two copper cylinders which were placed in a glass vessel lowered into a thermostat at temperature 25°C, equal to the initial temperature of the specimens. Two copper wires going from these cylinders supplied the voltage on the input of the registering device.

The constant voltage applied on the input of the registering device (Fig. 1) was first converted by a polarized relay to a pulsating voltage, and then across the transformer it was applied through the cathode follower on a 6Zh1B tube to the input of the instrument amplifier 28-IM. By means of a parallel condenser the secondary winding of the transformer was tuned to a frequency of 500 cps, at which the transformation was conducted. The described circuit permitted measurements of constant voltage from 10μv to 0.2 mv.

The results of measurements were treated in the following way. As we know [2], the temperature of the upper surface of the specimen, its thickness, temperature conductivity of the substance and time are connected by the formula:

$$T(h,\tau) = T_1 - \frac{4(T_1 - T_0)}{\pi} \sum_{n=1}^{\infty} \frac{1}{2n-1} (-1)^{n+1} e^{-(2n-1)\cdot\frac{2n^2}{4}\cdot F_0}$$

Here h = thickness of specimen, T_1 = temperature of heated thermostat, T_0 = initial temperature, F_0 = Fourier's criterion, equal to $a\tau/h^2$ (a = temperature-conductivity coefficient, τ = time).

From the experimentally obtained values of $T(h, \tau)$ we calculated the value θ, equal to $\frac{T_1 \cdot T(h, \tau)}{T_1 - T_0}$

and called the relative excess temperature. Using the values of θ given in the literature [3] as a function of $F_0/4$ we constructed the graph $F_0/4 = f(\tau)$. From the slope of the obtained straight line we determined a/h^2, and then the value of the temperature-conductivity coefficient a.

Since the temperature conductivity $a = \lambda/c\rho$ where λ (thermal conductivity) is a tensor value, then the temperature conductivity is also a second-rank tensor. The form of this tensor for a monoclinic system, if an axis of the second order is taken for the Y axis, is [4]:

$$\begin{vmatrix} a_{11} & 0 & a_{13} \\ 0 & a_{22} & 0 \\ a_{13} & 0 & a_{33} \end{vmatrix}$$

For measurements of a_{11}, a_{22}, a_{33} and a_{13} of EDT crystals we cut specimens perpendicularly to the three axes X, Y, Z, respectively, and normal to the face (001) [4]. (The angle of monoclinicity of ethylenediamine tartrate is equal to 15.5°). For the measurements we used specimens of different length and different cross-sectional area, cut from a single crystal, as well as specimens cut from different crystals. The lengths of the investigated specimens lay between 5.5 mm and 18 mm, the cross-sectional areas 10 × 20 to 17 × 12 mm². Typical results are shown in Figs. 2 and 3.

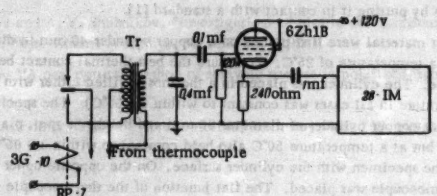

Fig. 1. Thermocouple circuit.

As a result we obtained the following mean values of the temperature-conductivity coefficients of ethylenediamine tartrate:

$$a_{11} = 3.2 \cdot 10^{-3} \text{cm}^2/\text{sec} \qquad a_{33} = 1.8 \cdot 10^{-3} \text{cm}^2/\text{sec}$$
$$a_{22} = 2.7 \cdot 10^{-3} \text{cm}^2/\text{sec} \qquad a_{13} = 0.93 \cdot 10^{-3} \text{cm}^2/\text{sec}$$

a_{13} is calculated from the formula

$$a_{13} = \frac{a'_{33} - (a_{33} \cos^2\varphi + a_{11} \sin^2\varphi)}{\sin 2\varphi},$$

where a'_{33} = value of coefficient of temperature conductivity along the direction perpendicular to the face (001) and $\varphi = 15.5°$.

The scatter of the temperature-conductivity coefficient for plates cut from one crystal was of the order 5%, which is within the limits of accuracy of our measurements. The scatter of the values of the temperature-conductivity coefficients for different crystals was 10% which is outside the accuracy of the measurements.

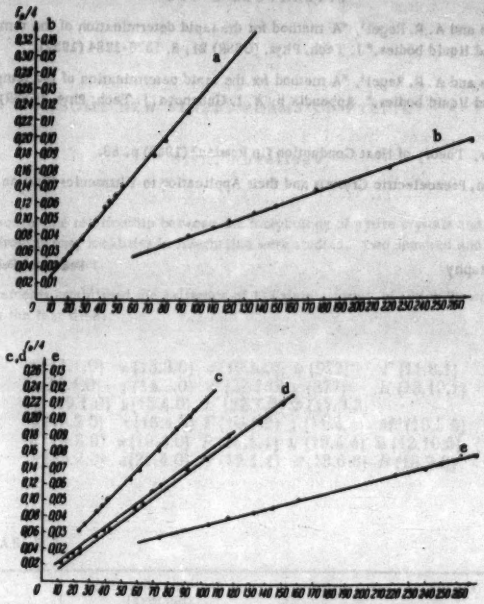

Fig. 2. Fourier's criterion as a function of time for EDT plates. a) X-cut plate, 5.57 mm thick; b) X-cut plate 11.08 mm thick; c) Y-cut plate, 5.58 mm thick; d) Y-cut plate, 6.69 mm thick; e) Y-cut plate, 14.79 mm thick.

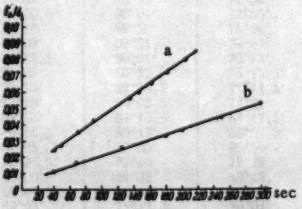

Fig. 3. Fourier's criterion as a function of time for EDT plates. a) Z-cut plates, 11.3 mm thick; b) 20 mm thick plate cut parallel to face (001).

I consider it a pleasant duty to express my thanks to Academician A. V. Shubnikov and V. L. Indenbom for several valuable suggestions.

LITERATURE CITED

[1] V. P. Zhuze and A. R. Regel', "A method for the rapid determination of the temperature-conductivity coefficient of solid and liquid bodies," J. Tech. Phys. (USSR) 21, 8, 1376-1384 (1952).

[2] V. P. Zhuze and A. R. Regel', "A method for the rapid determination of the temperature-conductivity coefficient of solid and liquid bodies," Appendix by A. I. Gubanova, J. Tech. Phys. (USSR) 21, 8, 1382-1384 (1952).

[3] A. V. Lykov, Theory of Heat Conduction [in Russian] (1952) p. 88.

[4] W. P. Mason, Piezoelectric Crystals and their Application to Ultrasonics [Russian translation] (IL, 1952).

Institute of Crystallography
AN SSSR

Received February 1, 1957

SOME NEW SIMPLE FORMS OF PYRITE

G. K. Abdullaev

In order to discover the relationship between the morphology of pyrite crystals and the conditions of their formation, crystals from twenty localities in Azerbaijan were studied. Two hundred and twenty-five crystals were measured on the goniometer.

These measurements established the existence of 113 simple forms, of which 29 were observed on the crystals of pyrite for the first time.

r {11.1.0}	v {13.3.0}	*c* {19.5.0}	*φ* {922}	*Γ* {11.6.1}	
z{18.1.0}	j {14.3.0}	B' {22.5.0}	*α* {877}	*K* {13.10.1}	
g {19.1.0}	k{13.4.0}	*H* {22.7.0}	*Φ* {17.3.3}		
l {13.2 0}	t {15.4.0}	*T* {10.1.1}	*l* {11.4.4}	*M'* {10.5.6}	
u {19.2.0}	w{19.4.0}	*P* {15.1.1}	*L* {19.4.4}	*Ψ* {12.10.5}	
y {25.2.0}	d{21.4.0}	*Q* {19.1.1}	b"{13.6.6}	*B* {18.9.8}	

TABLE 1

Form	Measured coordinates (average)		Computed coordinates	
	φ	ρ	φ	ρ
11.1.0	84°52′	89°57,5′	84°48,5′	90°00′
18.1.0	86°48,5′	90°02′	86°49′	90°00′
19.1.0	87°02′	89°56′	86°59′	90°00′
13.2.0	81°11′	90°03′	81°15′	90°00′
19.2.0	83°52,5′	90°06,5′	83°59,5′	90°00′
25.2.0	85°26′	90°00′	85°25,5′	90°00′
13.3.0	77°01,5′	90°01′	77°00′	90°00′
14.3.0	77°49′	90°03′	77°54′	90°00′
13.4.0	72°56,5′	90°04′	72°58′	90°00′
15.4.0	75°10′	89°58′	75°08′	90°00′
19.4.0	78°09′	89°51,5′	78°07′	90°00′
21.4.0	79°13,5′	90°01′	79°13′	90°00′
19.5.0	75°25′	89°52,5′	75°15,5′	90°00′
22.5.0	77°13′	89°58,5′	77°11,5′	90°00′
22.7.0	72°18′	90°02,5′	72°21′	90°00′
10.1.1	84°13′	84°13,5′	84°17,5′	84°19′
15.1.1	86°18,5′	86°17′	86°07,5′	86°08′
19.1.1	87°05,5′	87°05′	86°59′	86°59,5′
922	77°25,5′	77°40′	77°28′	77°45,5′
877	49°00′	56°33′	48°48,5′	56°38′
17.3.3	80°01,5′	80°06′	79°59,5′	80°08,5′
11.4.4	69°53′	71°13,5′	70°01′	71°07,5′
19.4.4	78°18,5′	78°13,5′	78°07′	78°21,5′
13.6.6	65°20′	67°08′	65°13′	67°16′
11.6.1	61°36,5′	85°18′	61°29,5′	85°26′
13.10.1	52°22,5′	86°34′	52°26,5′	86°30′
10.5.6	63°36′	61°37′	63°26′	61°46′
12.10.5	50°19,5′	72°23′	50°11,5′	72°15′
18.9.8	63°18′	68°25′	63°26′	68°19′

Form r was found on pyrite crystals from Giul'iatag, Vankiu (NKAO), and Gekgiundur (Ordubad District) localities; form v was found on crystals from Urumys (Ordubad District), Karalar (Kedabek District), and Vankiu; form k, on crystals from Paragachai (Ordubad District) and Cholpan (Kedabek District); and form t, on crystals from Cholpan and Karalar localities. Forms α, Γ, M" and B were observed on crystals from Urumys; forms Φ, T, P, Q, w, Φ, and l, on crystals from Paragachai; forms z, j, c, d, B', and Ψ on crystals from Karalar; forms i, y, and b", on crystals from Vankiun; forms g, u, and H, on crystals from Giul'iatag; form k on crystals from Chiragidzar (Khanlar District); and form l on crystals from Kovurmadarin (Ordubad District) localities.

All of these forms were observed on only 2-3 measured crystals. They are, therefore, rare (and some doubtful) forms. Their faces are usually poorly developed and give weak and dull reflections on the goniometer making satisfactory measurements difficult. At the same time, it should be noted that the faces of some (r, z, v, Φ, etc.) are highly perfect and give single, medium-bright and bright reflections, permitting exact measurements.

A table giving the results of measurements and calculations on the new simple forms of pyrite is appended.

M. Azizbekov Azerbaijan Industrial Institute

Received October 19, 1956

SOME EXPERIMENTAL DATA ON THE NATURE OF THE FORMATION OF ETCHED FIGURES IN AN ULTRASONIC FIELD

Kh. S. Bagdasarov and V. Ia. Khaimov-Mal'kov

It was shown in a communication [1] that when monocrystals in a solution were irradiated by ultrasound of frequency 40 kc, a large number of etched figures appeared on their faces. These figures may be produced by ultrasonic irradiation at any stage of dissolution of the monocrystal.

It has been postulated that the formation of the etched figures is due to local defects of some kind – microscopic cracks, etc., when are always present on the faces of a monocrystal. It is known from experiment that ridges, hollows and other defects visible on a crystal surface are often studded with these figures. In the dissolution of monocrystals the etched figures appear, as a rule, at the beginning of dissolution, and then, as the monocrystals dissolve, they disappear.

Since ultrasound causes the appearance of etched figures at any stage of dissolution of the monocrystal, it might be suggested that the ultrasonic irradiation produces on the monocrystal faces a large number of microscopic cracks which are the sites of formation of the etched figures.

TABLE 1

No.	Strength of dry salt g/mm²	Strength of salt in still water, g/mm²	Strength of salt in flowing water, g/mm²	Strength of salt in water actedon by ultrasound g/cm²	
				frequency 717 kc	frequency 22 kc
1	398	2430	4960	3170	450
2	298	2130	5900	2980	200
3	510	2160	3850	4650	476
4	380	2500	3410	5370	150
5	430	2660	6180	—	—

For confirming our hypothesis we used the Ioffe effect. We know that the low experimental values for the breaking strength of rock salt crystals in air are due to the presence of 'dangerous' miscroscopic cracks on the surface. It was shown in [2, 3] that the breaking strength of rock salt crystals in water, as compared with their strength in the dry state, was markedly higher.

We repeated the breaking experiments in water and air at room temperature on NaCl specimens, cut along the direction (100) and, in addition, we carried out tests on the breaking of rock salt specimens in water under the action of ultrasonic radiation of frequency 717 and 22 kc. The results of the measurements are given in Table 1 (the ultrasound intensity was equal to ~ 0.2 w/cm²).

In Table 2 we compare the mean values of our measurements with the results of other authors.

Changing the temperature of the water up to 80°C did not produce any appreciable changes in the strength.

From the given data we can see that the action of ultrasound of frequency 22 kc reduces the strength in water to the value of the strength in air. We can assume that this reduction of strength is due to the formation of 'dangerous' microscopic cracks on the crystal surface as a result of cavitation effects, particularly when a frequency of 717 kc, where cavitation effects with the power used are much less pronounced, makes little difference to the values obtained for the strength, as compared with the strength in water without the action of ultrasound.

TABLE 2

Mean values of salt strength, g/mm	From A.F. Ioffe	From M.V. Klassen-Neklíudova	From our measurements
Dry salt	400—500	294.0	399.0
In still water	—	—	2380
In flowing water	4000—5000	2486	4880
Under ultrasound of frequency 717 kc	—	—	4040
Under ultrasound of frequency 22 kc	—	—	310

Hence, the etched figures forming on the crystal surface when it is irradiated by ultrasound of frequency 22 kc and which are absent at the given intensity for a frequency 717 kc, are also connected with the formation on the crystal surface of microscopic cracks produced by cavitation and serving as 'nuclei' for the etched figures.

The authors thank Academician A. V. Shubnikov for his interest in this work.

LITERATURE CITED

[1] Kh. S. Bagdasarov and A. P. Kapustin, "Obtaining of etched figures by the use of ultrasonic vibrations," Crystallography 1, 1, 139-140 (1956).

[2] M. V. Klassen-Neklíudova, Plastic Properties and Strength of Crystals [in Russian] (1933).

[3] M. A. Levitskaia, "Bending of rock salt in air and water," J. Russ. Phys.-Chem. Soc. 58, 41 (1926).

Institute of Crystallography
AN SSSR

Received December 3, 1956

(Translation of the Journal "Crystallography" of the USSR, Vol. 2, No. 2, published by the American Institute of Physics, October, 1958)

CONTENTS

	Page	Russ. Page
Memorial to Viktor Ivanovich Mikheev. I. I. Shafranovskii and N. N. Stulov	199	203
Symmetry of Scalars, Vectors, and Tensors of Second Rank. I. S. Zheludev	202	207
X-Ray Diffraction Study of Sodium and Potassium Oxygen Vanadium Bronzes $Me_{0.33}V_2O_5$. R. P. Ozerov, G. A. Gol'der and G. S. Zhdanov	211	217
Crystal Chemistry of the Oxygen Vanadium Bronzes. R. P. Ozerov	219	226
X-Ray Study of the System $PbTiO_3$–$BaSnO_3$. Iu. N. Venevtsev, A. G. Kapyshev, and Iu. V. Shumov	225	233
The Crystal Structures of Trans-Diisothiocyanotetrammine-Nickel. E. K. Iukhno and M. A. Porai-Koshits	230	239
Electron Diffraction Study of the Structure of Thin Films of Molten Tin. A. I. Bublik	240	249
Determination of the Radial-Distribution Function for Atoms in a Liquid Metallic Alloy from Electron-Diffraction Data. A. I. Bublik and A. G. Buntar'	246	255
Electron Diffraction Study of Amorphous Antimony Sulfide. L. I. Tatarinova	251	260
Refractometric Determination of the Structure of Complex Cobalt Compounds. S. S. Batsanov	259	268
Study of Slip Lines in Silver Chloride Crystals. V. E. Kochnov and M. P. Shaskol'skaia	265	274
Brief Communications		
Crystalline Structure of Cis-$[Pt(NH_3)_2(SCN)_2]$. Ia. Ia. Bleidelis	270	278
The Crystalline Structure of the Trans-Diamminedithiocyanide of Divalent Platinum. Ia. Ia. Bleidelis and G. B. Bokii	274	281
Crystal Structure of the Metastable Phase Formed During the Tempering of Cu – Sn Alloys Containing 24-27 % Sn. Iu. A. Bagariatskii	277	283
Electron Diffraction Study of InSb Films. S. A. Semiletov and M. Rozsíbal	281	287
Crystal Chemistry of the Metal Hexaborides. G. S. Zhdanov, N. N. Zhuravlev, A. A. Stepanova and M. M. Umanskii	284	289
Photoelectric Multiplier for Scintillation Gamma-Spectrometers. L. G. Leiteizen, B. M. Glukhovskoi and I. Ia. Breido	286	290

(continued)

CONTENTS (continued)

	Page	Russ. Page
The Nature of Polarization in Crystals of Impure Rochelle Salt. V. P. Konstantinova and V. A. Iurin	290	294
Some Alterations in the Dielectric Properties of Rochelle Salt Crystals Exposed to X-Rays. I. Ia. Eisner	293	296
Excitation of Ultrasonic Vibrations in Quartz. K. N. Baranskii	296	299
Inhomogeneity of Stress Distribution in the Grain of a Polycrystal in the Initial Stage of Plastic Deformation. V. E. Kochnov	301	303
Determination of Temperature-Conductivity Coefficients in Crystals of Ethylene Diamine Tartrate. I. M. Sil'vestrova	303	304
Some New Simple Forms of Pyrite. G. K. Abdullaev	307	307
Some Experimental Data on the Nature of the Formation of Etched Figures in an Ultrasonic Field. Kh. S. Bagdasarov and V. Ia. Khaimov-Mal'kov	309	309

SIGNIFICANCE OF ABBREVIATIONS MOST FREQUENTLY ENCOUNTERED IN SOVIET CRYSTALLOGRAPHY LITERATURE

AN SSSR	*Academy of Sciences, USSR*
FIAN	*Physics Institute, Academy of Sciences USSR*
GITI	*State Scientific and Technical Press*
GITTL	*State Press for Technical and Theoretical Literature*
GOI	*State Optical Institute*
GONTI	*State United Scientific and Technical Press*
Gosfizkhimizdat	*State Physical Chemistry Press*
Gozkhimizdat	*State Chemistry Press*
GOST	*All-Union State Standard*
Goztekhizdat	*State Technical Press*
GTTI	*State Technical and Theoretical Press*
GUPIAE	*State Office for Utilization of Atomic Energy*
IF KhI	*Institute of Physical Chemistry Research*
IFP	*Institute of Physical Problems*
IK	*Institute of Crystallography*
IL	*Foreign Literature Press*
IPF	*Institute of Applied Physics*
IPM	*Institute of Applied Mathematics*
IREA	*Institute of Chemical Reagents*
ISN (Izd. Sov. Nauk)	*Soviet Science Press*
IIaP	*Institute of Nuclear Studies*
Izd	*Press (publishing house)*
KISO	*Solar Research Commission*
LETI	*Leningrad Electrotechnical Institute*
LFTI	*Leningrad Institute of Physics and Technology*
LIM	*Leningrad Institute of Metals*
LITMiO	*Leningrad Institute of Precision Instruments and Optics*
MATI	*Moscow Aviation Technology Institute*
MGU	*Moscow State University*
Metallurgizdat	*Metallurgy Press*
MOPI	*Moscow Regional Pedagogical Institute*
NIAFIZ	*Scientific Research Association for Physics*
NIFI	*Scientific Research Institute of Physics*
NIIMM	*Scientific Research Institute of Mathematics and Mechanics*
NII ZVUKSZAPIOI	*Scientific Research Institute of Sound Recording*
NIKFI	*Scientific Institute of Motion Picture Photography*
OIIaI	*Joint Institute of Nuclear Studies*
ONTI	*United Scientific and Technical Press*
OTI	*Division of Technical Information*
OTN	*Division of Technical Science*
RIAN	*Radium Institute, Academy of Sciences of the USSR*
SPB	*All-Union Special Planning Office*
Stroiizdat	*Construction Press*
TsNIIChERMET	*Central Scientific Research Institute for Ferrous Metallurgy*
URALFTI	*Ural Institute of Physics and Technology*

NOTE: Abbreviations not on this list and not explained in the translation have been transliterated, no further information about their significance being available to us.—*Publisher*

The expanded program of the American Institute of Physics comprises translation of six leading Soviet physics journals, as listed below. These translations, by competent, qualified scientists, provide all research laboratories and libraries with accurate and up-to-date information of the results of research in the U.S.S.R.

Soviet Physics—Technical Physics

A translation of the "Journal of Technical Physics" of the Academy of Sciences of the U.S.S.R. The translation began with the 1956 issues. Twelve issues per year, approximately 3,000 Russian pages. Annually $75.00 domestic, $79.00 foreign. Libraries* $35.00 domestic, $39.00 foreign. Back numbers, all issues $8.00.

Soviet Physics—Acoustics

A translation of the "Journal of Acoustics" of the Academy of Sciences of the U.S.S.R. The translation began with the 1955 issues. Four issues per year, approximately 400 Russian pages. Annually $12.00 domestic, $14.00 foreign. (No library discounts.) Back numbers, all issues $4.00.

Soviet Physics—Doklady

A translation of all of the "Physics Sections" of the Proceedings of the Academy of Sciences of the U.S.S.R. The translation began with the 1956 issues. Six issues per year, approximately 1,500 Russian pages. Annually $35.00 domestic, $38.00 foreign. Libraries* $15.00 domestic, $18.00 foreign. Back numbers for Volumes 1 and 2, $5.00 per issue; Volume 3 and subsequent, $7.00 per issue.

Soviet Physics—JETP

A translation of the "Journal of Experimental and Theoretical Physics" of the Academy of Sciences of the U.S.S.R. The translation began with the 1955 issues. Twelve issues per year, approximately 4,000 Russian pages. Annually $75.00 domestic, $79.00 foreign. Libraries* $35.00 domestic, $39.00 foreign. Back numbers, all issues $8.00.

Soviet Physics—Crystallography

A translation of the journal "Crystallography" of the Academy of Sciences of the U.S.S.R. The translation began with the 1957 issues. Six issues per year, approximately 1,000 Russian pages. Annually $25.00 domestic, $27.00 foreign. Libraries* $10.00 domestic, $12.00 foreign. Back numbers, all issues $5.00.

Soviet Astronomy—AJ

A translation of the "Astronomical Journal" of the Academy of Sciences of the U.S.S.R. The translation began with the 1957 issues. Six issues per year, approximately 1,100 Russian pages. Annually $25.00 domestic, $27.00 foreign. Libraries* $10.00 domestic, $12.00 foreign. Back numbers, all issues $5.00.

Subscriptions should be addressed to the American Institute of Physics, 335 East 45th Street, New York 17, N. Y.

* For libraries of non-profit academic institutions.